2012

Assessment Of Molecular Interactions Via Magnetic Relaxation: A Quest For Inhibitors Of The Anthrax Toxin

Oscar Santiesteban
University of Central Florida

ASSESSMENT OF MOLECULAR INTERACTIONS VIA MAGNETIC RELAXATION: A QUEST FOR INHIBITORS OF THE ANTHRAX TOXIN

by

OSCAR JULIAN SANTIESTEBAN
B.S. University of Central Florida, 2007

A dissertation submitted in partial fulfillment of the requirements
for the degree of Doctor of Philosophy
in the Department of Chemistry
in the College of Sciences
at the University of Central Florida
Orlando, Florida

Fall Term
2012

Major Professor: J. Manuel Perez

ABSTRACT

Anthrax is severe disease caused by the gram-positive *Bacillus anthracis* that can affect humans with deadly consequences. The disease propagates via the release of bacterial spores that can be naturally found in animals or can be weaponized and intentionally released into the atmosphere in a terrorist attack. Once inhaled, the spores become activated and the anthrax bacterium starts to reproduce and damage healthy macrophages by the release of the anthrax toxin. The anthrax toxin is composed of three virulent factors: (i) anthrax protective antigen (APA), (ii) anthrax lethal factor (ALF), and (iii) anthrax edema factor (AEF) that work in harmony to effectuate the lethality associated with the disease. Out of the two internalized factors, ALF has been identified to play a critical role in cell death. Studies in animals have shown that mice infected with an anthrax strain lacking ALF survive the infection whereas when ALF is present the survivability of the mice is eliminated.

Although the current therapy for anthrax is antibiotic treatment, modern medicine faces some critical limitations when combating infections. Antibiotics have proven very efficient in eliminating the bacterial infection but they lack the ability to destroy or inhibit the toxins released by the bacteria. This is a significant problem since ALF can remain active in the body for days after the infection is eliminated with no way of inhibiting its destructive effects. The use of inhibitors of ALF is an attractive method to treat the pathogenesis of anthrax infections. Over the last decade several inhibitors of the enzymatic activity of ALF have been identified. In order to identify inhibitors of ALF a variety of screening approaches such as library screenings, Mass Spectroscopy- based screenings and scaffold-based NMR screening have been used. Results from these

screening have yielded mainly small molecules that can inhibit ALF in low micromolar to nanomolar concentrations. Yet, although valuable, these results have very little significance with regards to treating ALF in a real-life scenario since pharmaceutical companies are not willing to invest in further developing these inhibitors. Furthermore, the low incidence of inhalation anthrax, the lack of a market for an ALF inhibitor, and the expenses associated with the approval process of the FDA, have hindered the motivation of pharmaceutical companies to pursuit these kind of drugs. Therefore we have screened a small-molecule library of FDA approved drugs and common molecules in order to identify currently approved FDA drugs that can also inhibit ALF (Chapter III). The screening revealed that five molecules: sulindac, fusaric acid, naproxen, ketoprofen and ibuprofen bound to either ALF or APA with sulindac binding both.

Additionally, we have developed a nanoparticle-based screening method that assesses molecular interactions by magnetic relaxation changes (Chapter II). Using this assay, we were able to accurately measure the dissociation constants of different interactions between several ligands and macromolecules. Moreover, we have used computational docking studies to predict the binding site of the identified molecules on the ALF or APA (Chapter IV). These studies predicted that two molecules sulindac and fusaric acid could be potential inhibitors of ALF since they bind at the enzymatic pocket. As a result, we tested the inhibitory potential of these molecules as well as that of the metabolic derivatives of sulindac (Chapter V). Results from these studies provided conclusive evidence that fusaric acid and sulindac were both strong inhibitors of ALF. Furthermore, the metabolic derivatives of sulindac, sulindac sulfide and sulindac sulfone

also inhibited ALF. Overall, taking together these results we have discovered the alternate use of a currently used drug for the treatment of ALF pathogenesis.

Dedicated to

Magda and Oscar – my parents

the ones with never-ending motivation and encouragement

and who sacrificed their careers and way of life

to bring my sister and I to this country.

Jennifer Santiesteban – my wife

for her constant support and understanding

in the days with the longest hours.

Mercedes and Amador – my parents-in-law

for always giving me a place at their dinner table

ACKNOWLEDGMENTS

The last five years have been a quest not only of scientific proportion but also of personal development. This journey has had its mountains to climb and deep rivers to cross, and yet along the way I have met remarkable individuals who walked with me even through the toughest obstacles.

First and foremost, I would like to thank my advisor Dr. J. Manuel Perez. His guidance, help, support and encouragement never faltered. His true dedication to his students and myself is worthy of praise and the least I can do is to sincerely thank him.

I would like to thank my committee members Dr. Cherie Yestrebsky, Dr. Yi Liao, Dr. Michael Hampton, and Dr. Stephen Lambert for their willingness to discuss my progress and for their time to oversee my development. Most especially, I would like to thank Dr. Michael Hampton for letting me work in his laboratory as an undergraduate student which opened my eyes to sensors.

I also thank my lab and office mates Dr. Charalambos Kaittanis who was always ready to jump into a new venture with me. Dr. Atul Asati whose advice and encouragement was always positive and welcoming. Dr. Santimukul Santra who taught me how to be a better organic chemist. Sincerely, I thank Mr. Hamza Boukiss for his hard work and patience. Lastly, I would like to acknowledge David Lehmkuhl and Everett Sutherland whose good humor and enthusiasm made everyday enjoyable.

I would like to thank Mrs. Mercedes Sommerhage for introducing me to the facilities at the Nanoscience Technology Center and allowing me to discover Dr. Perez's lab.

I also thank the staff at both the Chemistry Department and the Nanoscience Technology Center for their help throughout this journey.

TABLE OF CONTENTS

LIST OF FIGURES

LIST OF TABLES

LIST OF ACRONYMS/ABBREVIATIONS

AEF	anthrax edema factor
Ag-NP	silver nanoparticles
ALF	anthrax lethal factor
APA	anthrax protective antigen
Au-NP	gold nanoparticles
bMR	binding-magnetic relaxation nanosensors.
bp	boiling point
CDI	1,1'-carbonyldiimidazole
$CHCl_3$	chloroform
CH_2Cl_2	dichloromethane
CFU	colony forming units
Con A	concanavalin A
CTB	cholera toxin B subunit
DCM	dichloromethane
dH2O	deionized water
DI	deionized
DLS	dynamic light scattering
DMF	dimethyl formamide
DMSO	dimethylsulfoxide
DNA	deoxyribonucleic acid
EDC	1-ethyl-3-(3-dimethylaminopropyl) carbodiimide
EF	anthrax edema factor
ELISA	enzyme-linked immunosorbent assay
FDA	Food and Drug Administration
FR	folate receptor
FR ab	anti-Folate receptor antibody
FT-IR	Fourier-transform infrared spectroscopy
HEPES	4-(2-hydroxyethyl)-1-piperazineethanesulfonic acid
HCl	hydrochloric acid
IC_{50}	inhibitory concentration at 50 %
IONP	iron oxide nanoparticles
K_D	dissociation constant
KOH	potassium hydroxide
LF	anthrax lethal factor
LT	lethal toxin (ALF and APA mixed)
MAPKK	Mitogen-activated protein kinase kinase
MeOH	methanol
MES	2-(N-morpholino)ethanesulfonic acid
MRI	magnetic resonance imaging
MRnS	magnetic relaxation nanosensors
MRSA	methicillin-resistant Staphylococcus aureus
N_3	azide functional group
N-Hippuryl	N-Hippuryl-His-Leu Hydrate (N-Benzoyl-Gly-His-Leu)

NHS	N-hydroxysuccinimide
PA	anthrax protective antigen
PAA	polyacrylic acid
PBS	phosphate buffered saline
PCR	polymerase chain reaction
Qdots	quantum dots
R_1	spin-lattice relaxivity
R_2	spin-spin relaxivity
RNA	ribonucleic acid
SPR	surface plasmon resonance
T_2	spin-spin relaxation time
TEM	transmission electron microscopy
THF	tetrahydrofuran
UV-vis	ultraviolet-visible
ΔT2	change in spin-spin relaxation time

CHAPTER I: GENERAL INTRODUCTION PAVING THE ROAD AHEAD.

Bacterial infections are among the most devastating diseases throughout the world[1]. These type of infections can produce a broad range of symptoms that can manifest anywhere from a couple of minutes to years after infection. Although the majority of these pathogens cause mild symptoms and can be successfully treated with modern antibiotics. The emergence of antibacterial resistance bacteria represents a challenge for such successful treatments, with infections often leading to death[2, 3]. Among these lethal bacteria we find methicillin-resistant *Staphylococcus areus* (MRSA), which is responsible for several difficult to treat infections and owes its lethality to commonly used antibiotics[4]. *Clostridium tetani* and *Clostridium botulinum*, which cause tetanus and botulism respectively, are also of major concerns[5]. More deadly still, *Bacillus anthracis*, is the bacteria that produces Anthrax, a disease that can potentially be used as a biological weapon[6]. Spreading through the release of bacterial spores, Anthrax is capable of infecting different areas of the body depending on the methods of contact[7]. Commonly, spores contaminate an open wound creating a mild to severe infection that is know as subcutaneous anthrax[8]. More deadly still, Inhalation Anthrax occurs when the spores are inhaled and the bacterium reproduces in the lungs, leading to a severe infection with a very high mortality rate[9]. With the exception of some multidrug-resistant strains, most bacterial infections are treatable with modern antibiotics. However the problem still remains with the fact that although antibiotics are effective at killing the bacterium, they

fail at stopping the tissue damaging effect that the toxins released by the bacteria have on the infected host[10].

The majority of bacterial pathogens synthesize toxins as primary virulent factors that affect several physiological processes[11]. Whether used as a defensive mechanism as a way to inhibit the immune response, or as food scavengers by destroying nutrient-rich neighboring cells, bacterial toxins, not the bacteria themselves are the cause of lethality in most bacterial infections[12]. Bacterial toxins have been defined as "soluble substances" that alter the normal metabolism of host cells with deleterious effects on the host. These deleterious effects manifest via different modes of action depending on the toxin and the microorganism that it comes from[13]. There are two general types of toxins, endotoxins and exotoxins. Endotoxins form part of the outer portion of the cell wall and are released once the bacteria dies and the cell wall breaks apart. Exotoxins are otherwise produced inside the bacterium and can be secreted or released following lysis onto the surrounding medium.

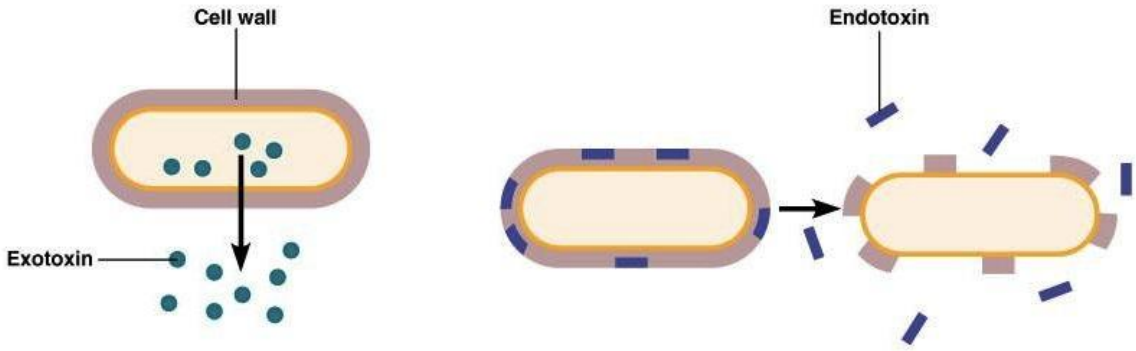

Figure 1. Exotoxins vs. Endotoxins.
Produced inside the bacterium, exotoxins are secreted or released after lysis into the surrounding environment. Endotoxins form on the outer cell membrane of bacterium and are released in the surrounding environment after the bacterium dies and the cell membrane breaks up.

Overview of different bacterial toxins and their characteristics by mode of damage to the host cell.[11]

- Pore-forming toxins: Numerous bacterial exotoxins are capable of inflicting damage to the plasma membrane of eukaryotic cells. In the majority of cases the damage is mediated by pore formation, which causes an imbalance in the intracellular homeostasis by disturbing the selective influx and efflux of ions across the cell membrane of healthy cells. Among the mild pore-forming toxins we find alerolysin, which is released from *Aeromonas hydrophila* and targets glycophorin to cause diarrhea. Another mild exotoxin is hemolysin, which comes from *Escherichia coli* and attacks the cell membrane of red blood cells. Some of the more moderate pore-forming toxins include streptolysin O released by *Streptococcus pyogenes* and pneumolysin released by *Streptococcus pneumoniae*, which respectively cause strep throat and pneumonia. Other pore-forming toxins that produce more severe diseases include perfringolysin O (*Clostridium perfringens*) and listeriolysin O (*Listeria monocytogenes*). The latter two toxins cause gas gangrene and meningitis respectively, both very deadly and devastating diseases.
- Protein synthesis inhibitors: Another class of bacterial toxins is those that damage the host cell by inhibiting protein synthesis. These toxins traditionally attack ribosomal RNA or factors that are necessary for protein synthesis within the cells. Within this category we find the Shiga toxins (*Shigella dysentariae*), which acts as a N-glycosidase that modifies a RNA subunit of the ribosome. This causes the ribosome to become faulty, which leads to the inhibition of protein synthesis.

- Second Messenger Activators: A class of toxins that specializes in the activation or modification of second messengers. Second messengers are molecules that transfer signals from extracellular receptors to molecules inside the cell. This class of toxins works on activating or modifying these signal transduction pathways that are essential in maintaining a variety of key cellular functions. Examples of these toxins include the edema factor (*Bacillus Anthracis*) one of the key components of Anthrax, and the cholera toxin (*Vibrio Cholerae*) the main cause of Cholera.
- Immune System Activators: These are bacterial toxins that directly stimulate or disturb T-cells and other immune system cells. The majority of toxins in this category are know as superantigens which are a class of antigens that cause the non-specific activation of T-cells and as a result a massive response of the immune system. These superantigen exotoxins are a common cause of toxic shock syndrome a devastating and potentially fatal illness. *Staphylococcus Areus* and *Streptococcus pyogenes* are among the bacteria that produce superantigen toxins.
- Proteases: Toxins in this category are those that have enzymatic activity. Good examples of these kinds of toxins are the botulinum toxins (*Clostridium Botulinum*), which cause botulism, a serious and life-threatening disease in humans. Particularly, this toxin destroys fusion proteins at a neuromuscular junction resulting in the inhibition of acetylcholine release and consequently an interference in nerve impulses. The lack of nerve impulses causes paralysis of muscles such as the diaphragm often leading to suffocation. Another protease toxin that causes paralysis is the tetanus toxin (*Clostridium Tetani*), which causes

muscles to overreact and contract due to a lack of inhibitory neurotransmitters. Both the botulinum and tetanus toxins are considered the deadliest toxins in the world with LD_{50} in the ng/kg range. Within this category, we also find the lethal factor toxin (*Bacillus anthracis*) another deadly toxin that is the main cause of pathogenesis in anthrax. The Lethal factor toxin acts as a Zn^{2+}-dependent endopeptidase that cleaves the N-terminus of mitogen-activated protein kinase kinases (MAPKK), altering the signal pathway used by the cell to recruit immune system cells. This alteration of the signal pathway ultimately leads to apoptosis.

The challenge faced with bacterial toxins.

Although with modern medicine and antibiotics most bacterial infections can be stopped before they become fatal, significant pathogenesis still occurs after antibiotic therapy. The keystone of an antibiotic is that they are designed to kill the bacteria that is causing the infection, but therein lays the problem as well. These antibiotics are made to target the bacteria and not the toxins they produce, which are the main cause of damage to a healthy organism. Even after the bacterial infection has been subdued, the toxins they released continue to circulate through the body for hours and even days causing havoc to healthy tissue[14-17]. Therefore, it is essential to be able to detect and inhibit toxins after the organism that secreted them has been eradicated.

Currently there are no therapies that focus on inhibiting bacterial toxins. Some successful attempts have been made with antibodies and small molecules to inhibit bacterial toxins, but these therapies are still a long way from potential clinical uses.[18, 19] In animal models, mice immunized with an antibody against alpha-hemolysin a toxin

released by USA300 a strain of MRSA, reduced the severity of skin and soft tissue damage cause by the toxin[20]. Other researchers have focused on identifying small molecule inhibitors that either inhibits the toxin itself or the cellular receptors necessary for them to enter healthy cells[17, 21]. These small molecules have proven very effective in cell studies showing a dramatic decrease in cell death when used as an inhibitor of the toxins.

Since toxins in circulation cause damage long after the bacteria is eliminated, it is important to be able to detect them as well. Existing toxin detection methods rely on antibody-antigen interactions in ELISA[22], antibody microarrays[23], surface plasmon resonance biosensors[24], Western blots[25], and antibody-coated polystyrene microbeads[26]. Although sensitive, these methods have a major drawback in that they need highly purified samples. These purification procedures are usually time-consuming and traditionally required complex and expensive reagents imposing a major limitation on the usefulness of these methods. Additionally, on low abundant samples, these purification methods reduce the amount of toxins that can be detected. Other techniques employ the use of Multidimensional Protein Identification (MudPIT)[27] and Liquid Chromatography Mass Spectrometry (LC-MS)[28], that while they do not face the limitations observed with the previous methods and can achieve limits of detection in the fM range, they require expensive and specialized instrumentation not commonly available.

Nanoparticles as a suitable molecular probe.

In 1959, Nobel laureate Richard Freyman introduced the field of nanotechnology with his famous words “there is plenty of room at the bottom”. Since then, and

particularly in the last decade researchers have found more than "room at the bottom" by developing complex and novel nanomaterials with a vast range of applications[29, 30]. Nanotechnology is the study and manipulation of matter at the nanoscale, usually focusing at the 1-100 nm range. At this scale matter exhibits increased surface area and reactivity, increased electrical conductivity, quantum confinement effects, tunable electrical properties, and improved magnetic properties, among other properties[31].

Nanoparticles in particular, are colloidal suspensions of different materials that exhibit one or several of these properties. Some of the traditionally used nanoparticles include gold nanoparticles, quantum dots, polymeric nanoparticles, and iron oxide nanoparticles. Specifically when used as sensors, these nanoparticles provide a reliable, sensitive, and cost effective method to detect different targets. In the case of gold nanoparticles a surface plasmon band change can be observed in its absorption spectra when different biomolecules are absorbed at their surface[32]. Similarly, quantum dots have been extensively used to detect a wide range of biological targets[33]. Quantum dots are nano-sized semiconductors with tunable optical properties that can emit light well into the infrared region. Depending on their size or ratio of semiconducting material used, researchers can vary their band-gap, essentially tuning their fluorescence emission[31]. Polymeric nanoparticles on the other hand do not tend to have optical properties of their own, but by engineering the composition of the polymer, the assembly of the nanoparticle can be controlled in such way that hydrophobic pockets are created[34]. These hydrophobic pockets can carry fluorophores that are used to detect biomolecules. In addition, iron oxide nanoparticles have been used not for their optical capability, but because of their

magnetic properties and their ability to alter the magnetic spins of neighboring water atoms, a property utilized in Magnetic resonance Imaging (MRI).[31, 35]

Iron Oxide Nanoparticles, the path to the better sensor.

Superparamagnetic iron oxide nanoparticles (IONPs) have the capability of affecting neighboring water proton relaxation times, thus allowing for a sensitive and robust detection method that do not depend on optical properties as other nanomaterials do. Iron oxide nanoparticles owe their superparamagnetic properties to their Fe_3O_4/Fe_2O_3 core, which is usually covered with polymer coating for added stability. Although most modern synthetic procedures require the stabilizing polymer coating, some preparations can be prepared without the coating. Due to their superparamagnetic state, IONPs posses an induced magnetic field which directly disturbs the spin-spin relaxation of neighboring water protons.[36] This shortens the time it takes from the water protons to relax to their original state thus reducing the spin-spin relaxation times T_2 (**Figure 1A**). The change in T_2 can be accurately observed using a magnetic relaxometer (a miniaturized MRI), allowing iron oxide nanoparticles to become Magnetic Relaxation nano-Sensors (MRnS).

The development of new synthetic techniques and protocols in the production of MRnS has allowed for a nanoparticle design with a controllable surface. Especially the use of polymers such as dextran and polyacrylic acid provide surface functional groups that can be manipulated when adding different ligands to yield nanoparticles with controlled valencies.[37] High-valency MRnS that carry several targeting ligands offer the benefit of a surface-mediated multivalent affinity, resulting from multiple and strong interactions between the high local concentration of binding ligands on the nanoparticle's

surface and receptors on the corresponding target[38]. Due to the larger number of surface ligands, high-valency MRnS have the capability to interact with multiple target units at the same time, thus driving the formation of a cluster made of target units and several nanoparticles. The formation of these nano-sized clusters causes a decrease in the overall T_2 of the solution due to permanent localization of water molecules locked within the clusters in the induced magnetic field (**Figure 1D**). High-valency MRnS have been extensively used to detect and quantify numerous targets, including DNA, mRNA, viruses, proteins and cells.

It is not until recently that low-valency MRnS have been studied for the detection various targets[39]. Low-valency MRnS have a low number of targeting ligands on their surface and as opposed to high-valency systems, generally tend to be weak binders due to the absence of increased multivalent affinity. In the case of magnetic nanoparticles, the use of low-valency MRnS has traditionally not been encouraged because the low-density of targeting ligands on the surface of the nanoparticles will not induce the formation of clusters. In a recent study published by our group, we have reported a newly discovered interaction mechanism that uses low-valency MRnS as a binding magnetic relaxation (bMR) nanosensor, to produces substantial changes in the magnetic relaxation signal while taking advantage of faster binding kinetics and minimal amounts of target compounds. With lower amount of surface ligands, bMRs do not induce the formation of clustering, but instead bind a low amount of target to the surface of the nanoparticles. The presence of the targets on the surface of the bMR obstructs the access of the water molecule to the induced magnetic field causing the T_2 of the solution to increase (**Figure 1B-C**). This low valency assay has been used to detect peptides, DNA, and proteins with

high sensitivity and reproducibility. Similarly, this technique can be used to detect toxins by using an anti-toxin antibody or a small molecule as a ligand[40]. Furthermore, because the formation of a cluster is not necessary and the binding of targets to surface ligands is a fast process, this bMR detection method provides faster kinetics, thus reducing the length of the assay.

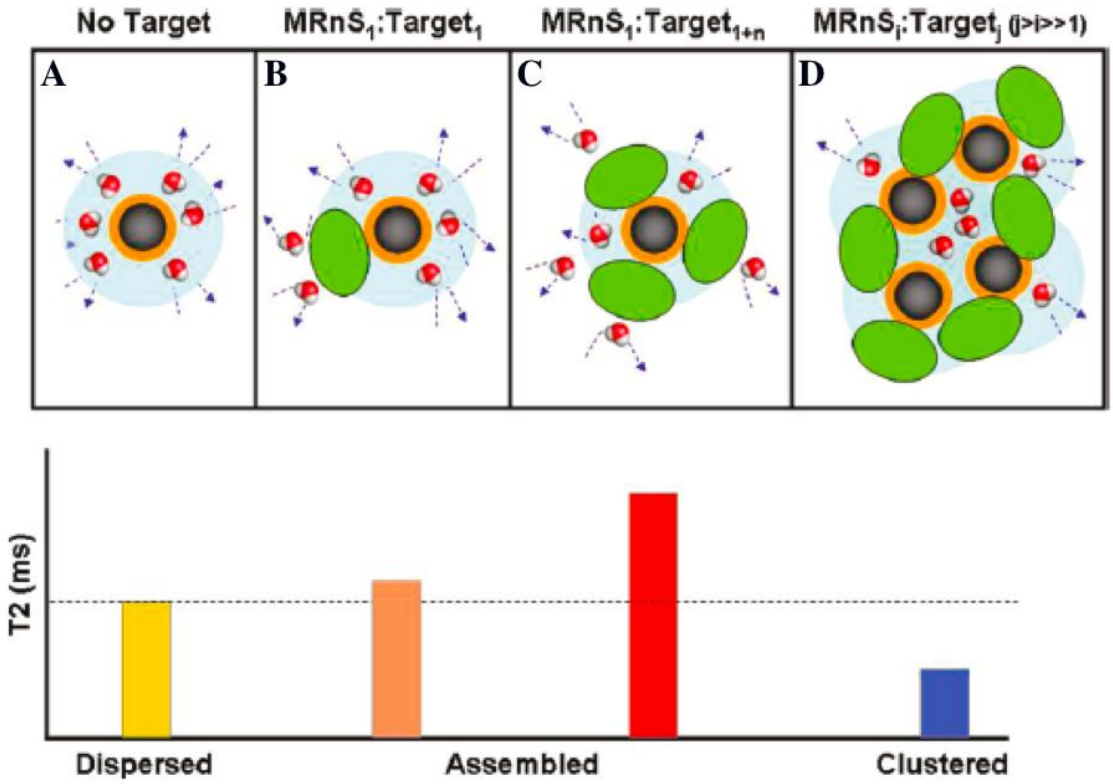

Figure 2. Visual representation of nanoparticle states as targets bind to their surface.[39]
A: In the absence of targets bound to the surface water protons are able to feely move in and out of the induced magnetic field. B-C: As the concentration of target bound on the surface increases, the intercation between the water molecules and the induced magnetic field is disrupted, resulting in an increase in the T_2 signal. D: When enough target is added to cause a cluster, the water molecules are locked into the induced magnetic field, resulting in a large decrease of the T_2.

Small Molecule Libraries, a pool of targeting ligands.

Although highly specific, the use of antibodies as capturing ligands has a series of issues such as instability at higher temperatures, antibody denaturation and slow kinetics. These issues are of great concern in any antibody-based diagnostics assay, in particular if its intended use is in the field or remote locations where a controlled lab setting is not available. Specifically, when antibodies are used as surface ligands for nanoparticles, their disadvantages become more noticeable. Size-induced precipitation, steric interactions, nanoparticle instability, and reduced target affinity are among the drawbacks of conjugating antibodies to the surface of nanoparticles. For these reasons, it would be ideal to conjugate more stable targeting ligands, such as small molecules to the nanoparticles. Small molecules are low molecular weight organic compounds that by definition are not polymers. They come in every size and reactivity and traditionally have been implicated in several important molecular interactions such as that of pharmaceuticals and their respective targets.

Small molecules that can be used in pharmaceutical applications are traditionally identified out of small molecule libraries (SML). SMLs are pools of molecules that are screened for binding to biological receptors or targets of interest[41]. Traditionally, SMLs contain anywhere from tens to hundred of thousands molecules, and can be focused to specific functional groups or provide a wide range of functionalities and molecular functions. These libraries can be synthesized either in solid supports or solution, and are commercially available for purchase. Small molecules selected from SMLs screenings have provided many of the currently know therapeutics[41]. Specifically, in recent years, the screening of SMLs has yielded various molecules with the capability to inhibit

bacterial toxins. Among these, are several anthrax toxins inhibitors that can be used to arrest the pathogenesis of the toxin.[42, 43] It will be years before one of these molecules is able to pass through the regulatory agencies and become available to patients. This is in part due to the lack of incentive from pharmaceutical companies due to the large expense that is associated with bringing new drugs to market as well as putting a new drug through the long review process imposed by the Food and Drug Administration (FDA). Additionally, the low occurrence of anthrax infections adds to the lethargic interest exhibited by pharmaceutical companies.

The roadmap ahead, an organizational overview of this study.

Therefore, the primary objective of this dissertation is to assemble a SML of commonly available FDA-approved small molecule drugs that is to be screened against binding to the anthrax toxins. By using drugs that are already available to patients, they can be readily used if they are found to inhibit the toxins. The screening will be performed via magnetic relaxation by conjugating these small molecules to the surface of bMRs. Furthermore, computational binding studies and inhibition assays will shed light into the usefulness of the screened small molecules as potential inhibitors of the anthrax toxins.

This dissertation will be divided into four major chapters that will address the objectives of this work. In Chapter 2 a new method that measure the affinities of molecular interactions via magnetic relaxation is described. The described methods can be applied to a broad range of interactions including those between small molecules and toxins. In Chapter 3, a Small Molecule Library (SML) will be selected and screened for

binding to the anthrax toxins. The protective antigen and lethal factor will be selected as a model system for the screening due to their pivotal role in the pathogenesis of the disease and because it will be beneficial to discover a known drug that inhibits these proteins. Within this section of the work the small molecules will be chemically attached to the surface of bMRs and used to detect and measure the interaction between each molecule and the targets. After some molecules are identified to bind the anthrax toxins, in Chapter 4, they will be studied computationally in order to assess the location of the binding on the toxin. Concluding, in Chapter 5, the results from the studies in chapter three will be taken into consideration and the inhibition potential of the identified molecules will be evaluated against the protease activity of the anthrax lethal factor.

CHAPTER II: DETERMINATION OF DISSOCIATION CONSTANT K_D VIA MAGNETIC RELAXATION.

Introduction

Molecular interactions, particularly those involving a ligand and a protein, play a vital role in multiple biological processes.[44-48] For example, the association between an antibody and its target or the binding of a small molecule drug to a cellular receptor is an important example of these interactions. The study of these interactions, notably those associated with disease, is important for the development of novel therapeutics and sensing technologies. These interactions are typically evaluated by a dissociation constant; an equilibrium constant that describes how strongly a ligand binds to a particular target protein by measuring the propensity of the ligand to dissociate from the protein. Denoted as K_D, the dissociation constant is the inverse of the association constant and it is expressed in the following equation where complex A_xB_y breaks into xA and yB subunits:

$$A_xB_y \text{ É } xA + yB$$

$$K_D = \frac{[A]^x \times [B]^y}{[A_xB_y]}$$

The smaller the K_D, the higher the affinity between the ligand and protein thus the stronger the interaction between the two.

Several techniques have been developed to assess these molecular interactions and measure K_D values. However, as most reported K_D values have been determined using different methods, comparative studies are difficult as variations in K_D values can

be seen using different techniques.[49] The most commonly used techniques to measure K_D include:

- Surface plasmon resonance (SPR)[44] is a technique that uses specialized instrumentation to sensitively measure the association and dissociation between ligands and a stationary target. This method involves the use of a metal plate, traditionally gold, to which proteins are attached. This metal support has an specific surface plasmon band, that changes as the ligands associate or dissociate with the anchored protein. Some of the drawbacks of SPR is that it requires the binding of either the ligand or the protein on a solid support, which affect the binding kinetics and it is not representative of the binding affinity in solution. Additionally, purified proteins are needed for the experiment, making it a labor intensive and expensive technique.
- Isothermal titration calorimetry[50, 51] is a physical technique used to determine the thermodynamic parameters of interactions in solution. It uses a calorimeter that has a sample and reference cell within an adiabatic jacket. This instrument uses a set of very sensitive thermocouples to detect temperature differences between the sample and reference cells. The protein/macromolecule is placed in solution in the sample cell and the ligand is titrated into it allowing the instrument to detect a change in temperature as the macromolecule and ligand bind. The major drawback with this technique is that it requires expensive instrumentation that is not commonly available. Additionally, the nature of the instrument does not allow for measurements directly on live cells.

- Radioligand binding assays[52] uses a radioactively-labeled ligand to asses the biding between that ligand and a protein/macromolecule. Using a competitive assay a single concentration of radioligand competes against different amount of unlabeled-ligand for binding to the macromolecule. Measurements are usually made using a scintillation counter. The drawbacks to this technique is that it uses expensive radioactive materials that can pose a hazard to the user.

The conjugation of targeting ligands to iron oxide nanoparticles has been extensively utilized to fabricate nanosensors and targeting imaging agents for the detection of various molecular targets.[30, 37, 53, 54] In particular, we recently reported that binding of a protein target to a ligand attached to magnetic iron oxide nanoparticle in solution resulted in an increase in the spin-spin relaxation times (T_2) of the water protons in solution.[39] This observation facilitated the development of magnetic relaxation nanosensors that can quantitatively sense the presence of a target by measuring the increase in the water T_2 upon target binding. To differentiate our nanosensors from previously described magnetic nanosensors that cluster upon target addition resulting in a decrease (not an increase) in T_2, we herein denote our nanosensors as binding magnetic relaxation (bMR) nanosensors and explore their utility as sensors to interrogate molecular interactions. Specifically, we hypothesized that a targeting bMR nanosensor can be used in a competition assay format to determine the K_D of a particular molecular interaction as it occurs on the surface of a nanoparticle.

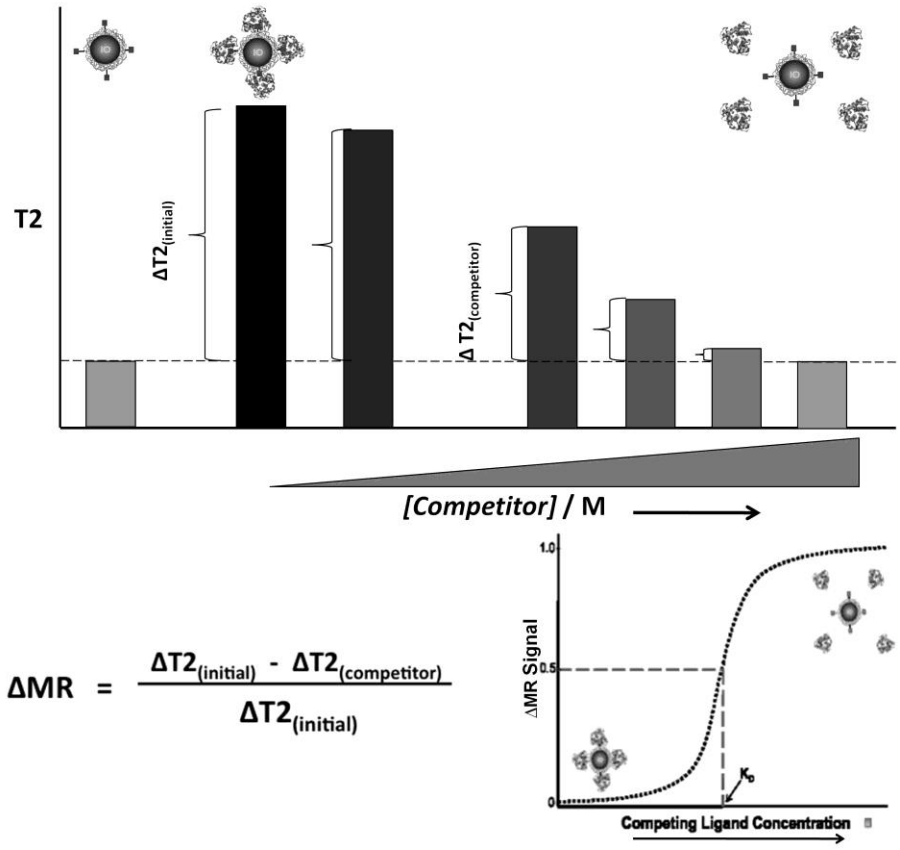

Figure 3. Approach for the determination of the dissociation constant (K_D) via changes in magnetic relaxation.
In the absence of a competing ligand, the target protein interacts with ligands on the bMR nanosensors, resulting in a low ΔMR signal. As the concentration of competing ligand increases, the intercation between the protein and the nanosensor is disrupted, resulting in an increase in the ΔMR signal.

Assay Design

In our magnetic-relaxation-based competition assay, a constant amount of bMR nanosensors in a series of aqueous solutions containing increasing amounts of free competing ligand is mixed with the targeting protein. In the absence of free ligand, the target protein binds to ligands on the bMR nanosensors, causing an increase in the T_2 of the solution. This change in T_2 represents the initial state of our assay and herein we

denote it as $\Delta T_{2\ (initial)}$. The addition of increasing amounts of free ligand (competitor) in the sample lowers the observed change in T_2, as the added free ligands in solution compete with the bMR nanosensors for binding to the target protein. We denote this change in T_2 in the presence of a competitor as $\Delta T_{2\ (competitor)}$. As the amount of free ligand increases, the magnetic relaxation signal change (ΔMR signal) defined herein as the $[\Delta T_{2\ (initial)} - \Delta T_{2\ (competitor)}]/\Delta T_{2\ (initial)}$ increases, reaching a plateau when ΔMR-signal approaches a value of one (**Figure 3**). The initial ΔMR signal in the absence of a competitor will be zero, since there is no competing ligand present in the sample to compete for binding to the target protein. Thus, low competitor concentrations will yield low ΔMR signals while high competitor concentrations will cause a disruption in the interaction between the target protein and the bMR nanosensors causing larger ΔMR signal values.

Therefore as the concentration of the competitor increases in the system, the ΔMR-signal values are expected to increase, reflecting the competition that the free and competing ligand is effecting on the system. The concentration of free ligand at which a 50% change in the MR value is observed is then defined as the dissociation constant. Specifically at this concentration, an equilibrium is achieved, where 50% of the target protein interacts with a free ligand and the remaining portion associates with the nanosensors, inducing quantifiable MR changes.

Materials and Methods

Reagents.

All reagents were of analytical reagent grade. Iron salts ($Fe_2Cl_3 \bullet 4H_2O$ and $Fe_3Cl_3 \bullet 6H_2O$) were obtained from Fluka. Polyacrylic acid (PAA, MW 1.8 kDa), ammonium hydroxide, hydrochloric acid, N-hydroxysuccinimide (NHS), the CTB pentamer, Avidin, Biotin, Rhein, Glucose, Galactose, Lactose, β-Cyclodextrin and Concanavalin A were purchased from Sigma-Aldrich, whereas Dextran (MW 10 kDa) was received from Pharmacosmos. EDC (1-ethyl-3- [3-dimethylaminopropyl]carbodiimide hydrochloride) and Protein G were obtained from Pierce Biotechnology, and the Tetanus toxin C fragment (TTC) was from Roche Biomedical. Doxorubicin and PBS buffer were purchased from Fisher Scientific. Anti-FR antibody and EpCAM antibody were received from Santa Cruz Biotechnology. MCF-7 and HeLa cell lines were established from ATCC.

Synthesis of protein-carrying bMRs.

For the conjugation of proteins to the iron oxide nanoparticles, we utilized EDC/NHS chemistry as previously described[39]. Specifically, poly(acrylic acid)-coated nanoparticles ([Fe] = 0.25 mg/mL) were mixed with 2 mL of MES buffer (pH 6), followed by the drop wise addition of EDC (1 mg, 0.11 mmol) and NHS (0.8 mg, 0.15 mmol). The reaction mixture was incubated for 3 min before the drop wise addition of Protein G (0.1 mg) or Avidin (0.15 mg) in DI water (0.1 mL). The reaction continued for 30 min at room temperature under continuous mixing, before overnight incubation at 4 °C. To obtain the protein-carrying bMRs, we magnetically separated the reaction mixture

through a 1X-PBS-equilibrated LS25 column (Miltenyi). Conjugation of antibodies to Protein G-carrying bMRs (250 μL) was performed as previously reported,[39] by using 0.5 ng of EpCAM Ab (Santa Cruz Biotechnology) or 0.5ng of FR Ab (Santa Cruz Biotechnology), which resulted in low valency bMRs. The nanoparticle valency was evaluated as previously reported[37], through quantification of the nanoparticle's antibody amount using the BCA assay (Pierce Biotechnology).

Preparation of small-molecule-carrying bMRs.

Folic acid and doxorubicin- carrying bMRs were prepared as described in the literature[39]. To synthesize Rhein-conjugated bMRs a similar approach was followed. Briefly, propargylated poly(acrylic acid)-coated nanoparticles (3 mg, 2 mg/mL) were added to a low stoichiometric ratio of azide-functionalized Rhein (0.5 μg Rhein-N3, 10 μg/ml DMSO). The reaction was initiated at room temperature in the presence of catalytic amount of CuI (0.01 μg in 500 μL of bicarbonate buffer, pH 8.5), and further incubated for 12 h at room temperature. The final reaction mixture was purified with a magnetic column (LS25, Miltenyi) using DMSO as the elutant. The rhein – nanoparticle preparation was stored at room temperature until further use. Confirmation of the successful conjugation of Rhein to the nanoparticles was achieved through UV-Vis absorption spectroscopy, by recording rhein's absorbance at 443 nm using Cary 300 spectrophotometer.

Dextran-coated Nanoparticle.

Dextran-coated bMR nanoparticles were synthesized using a previously described method. Briefly, An acidic solution of iron salts containing 0.203 g $FeCl_2$. $4H_2O$ and 0.488 g $FeCl_3$. $6H_2O$ in HCl solution (88.7 μl 12 N HCl in 2 ml water) was

mixed with ammonium hydroxide solution (830 µl NH_4OH in 15 ml DI water) under stirring. The reaction mixture was stirred for 25 seconds before a solution of dextran (5 g in 10 ml DI water) was added. The resultant solution was continued to stir for 1 hr and then centrifuged at 4,000 rpm for 30 minutes to get rid off large particles. The resulting dextran-coated iron oxide nanoparticles in the supernatant were collected and washed and several times with distilled water and concentrated using a KrosFlow filtration system.

Assay for the Determination of Dissociation (K_D) Constant via Magnetic Relaxation:

Avidin – Biotin K_D Measurement: For this interaction we utilized Avidin-carrying bMRs (0.015 mg Fe/mL), which had a diameter of 76 nm and a *r*2 relaxivity of 116 $mM^{-1}s^{-1}$. The bMR analyzing solution consisted of 4.5 µL Avidin-carrying bMRs and 2,000 µL of de-ionized water. Samples containing 10 µL of different concentrations of free Avidin (competing ligand, 0.1 fM to 1 pM, in DI water) and 200 µL of the bMR analyzing solution (bMR nanosensor) were prepared followed by the addition of 10 µL Biotin (target small molecule, 205 nM). A negative control sample was prepared in the same fashion, adding 10 µL fresh 1X PBS buffer instead of Biotin (0 M Biotin control sample). Magnetic relaxation measurements were performed after 15 minutes of incubation at room temperature. Dynamic light scattering (DLS) studies were done using a PDDLS/CoolBatch 40T instrument using Precision Deconvolve 32 software. Transverse (T_2) proton relaxation times measurements were done using a Bruker Minispec mq20 NMR analyzer operating at a magnetic field of 0.47 T and at 37 °C.

Protein G – IgG magnetic-relaxation-based K_D determination: Following a similar approach as the Avidin – Biotin assay, the Protein G – IgG dissociation constant was measured. An analyzing solution of Protein G-carrying bMRs (0.007 mg Fe/ mL) was

incubated with various amounts of free Protein G (0.43 fM – 0.43 pM) in 1X PBS buffer. After the addition of IgG (50 nM, 1X PBS buffer) in the form of IgG-EpCAM antibody (Santa Cruz Biotechnology) as the target protein a 15-minute incubation period at room temperature was allowed before magnetic relaxation measurements were performed.

Concanavalin A – Dextran K_D determination: Dextran-coated iron oxide nanoparticles (0.012 mg Fe/mL, 115 nm and a *r*2 relaxivity of 175 $mM^{-1}s^{-1}$, in DI water) were used as bMR sensors and introduced into a solution containing various amounts of free dextran (1.25 nM – 62.5 nM). The samples were then incubated with Concanavalin A (50 nM) for 15 minutes at room temperature, followed by magnetic relaxation measurements.\

Folic Acid – Folate receptor expressed on the plasma membrane of HeLa cells: Various samples of 200 µL of an analyzing solution containing folic acid-carrying bMRs (0.01 mg Fe/mL, in 1X PBS) were incubated with varying concentrations of free folic acid (competitor, 1.1 nM – 0.56 µM, 1X PBS). Folate-receptor-expressing HeLa cells in 1X PBS (10 µL , 10,000 cells quantified with a hemocytometer) were added to each sample followed by an incubation period of 30 minutes at room temperature. Magnetic relaxation measurements were then performed.

Anti-folate-receptor Antibody – folate-receptor-expressing HeLa cells: Anti-folate-receptor antibody-carrying bMRs (0.008 mg Fe/mL) were incubated with various concentrations of free anti-folate receptor antibody (competitor, 0.45 pM – 4.5 nM, 1X PBS). The samples were then incubated with FR-expressing HeLa cells (10 µL, 10,000 cells in 1X PBS) for 30 minutes at room temperature before performing magnetic relaxation measurements.

EpCAM Antibody – EpCAM-expressing MCF-7 cells: Samples containing EpCAM antibody-conjugated bMRs (0.008 mg Fe/mL) were incubated with various concentrations of free EpCAM antibody (competing protein, 45 fM – 45 nM, 1X PBS). The samples were then incubated with EpCAM-expressing MCF-7 cells (10 µL, 8,000 cells in 1X PBS,) for 30 minutes at room temperature followed by magnetic relaxation measurements.

TTC – Doxorubicin: Samples consisting 200 µL of an analyzing solution containing Doxorubicin-conjugated bMR nanosensors (0.01 mg Fe/mL) and increasing amounts of free doxorubicin (0.9 µM – 12 µM, in 1X PBS) were prepared. The target protein TTC (4 nM) was added to each sample followed by a 15- minute incubation at room temperature and magnetic relaxation measurements.

TTC – Rhein: Following the same protocol as with the previous assays, rhein-conjugated bMR were introduced into a solution containing various amounts of free Rhein (0.5 µM – 500 µM, 1X PBS). The samples were then incubated with TTC (4 nM) for 15 minutes at room temperature, before performing magnetic relaxation measurements.

CTB – Carbohydrates: A nanoparticle analyzing solution was made out of 4.5 µL dextran-coated nanoparticles (5 mg Fe/ mL) and 2,000 µL de-ionized water. Samples containing of different concentrations of the carbohydrates of interest (concentration range provided below) and 200 µL of the nanoparticle analyzing solution were prepared, followed by the addition of CTB (10 µL 1.7 µM DI water). The samples were incubated for 15 minutes before performing magnetic relaxation measurements. *Carbohydrates of Interest (DI water)*: Dextran (0.1 µM – 50 µM), Glucose (2.4 µM – 470 µM), Galactose (0.2 µM – 94 µM), Lactose (3.8 µM – 380 µM), β-Cyclodextrin (0.4 µM – 200 µM)

Results

In order to test our assay, we measured the K_D via magnetic relaxation of a broad range of protein-ligand interactions with different degrees of affinities. As a model system, we first used the avidin - biotin interaction, a well-studied strong interaction, with reported K_D values in the femtomolar range.[55] For these studies, we designed a bMR nanosensor consisting of avidin-conjugated iron oxide nanoparticles (76 nm and an *r*2 relaxivity of 116 $mM^{-1}s^{-1}$ at 0.47T). Samples containing the bMR nanosensor (0.015 mg Fe/mL) in a solution containing different concentrations (10 fM – 1 pM) of free avidin (competitor) were prepared, followed by the addition of biotin (200 nM). Within 15 minutes, T_2 measurements and calculation of the ΔMR signal values at various concentrations of inhibitor revealed a concentration-dependent trend (**Figure 4A**). A 50% change in the ΔMR signal values was observed at an avidin concentration of 3 fM, indicating that the avidin-biotin K_D was equal to this value. This K_D value is in close agreement with a reported K_D value of 1fM, determined via titration calorimetry studies.[55] In control studies with bovine serum albumin, the bMR nanosensors yielded nominal changes, suggesting that the observed changes in magnetic relaxation were target-specific.

Next, we investigated the affinity between Protein G and IgG (**Figure 4B**), as well as Concanavalin A and dextran (**Figure 4C**), as model interactions for protein-protein and protein-carbohydrate interactions. For the Protein G – IgG interaction, a bMR nanosensor composed of Protein G-carrying iron oxide nanoparticles was incubated with various amounts of free Protein G (0.43 fM – 0.43 pM), before addition of mouse IgG (50 nM) as target protein. Our magnetic relaxation results indicated that the K_D of this

interaction was in the picomolar range (0.4 pM). The reported K_D value for a similar interaction, using a rabbit IgG in a fluorescence binding assay, is also in the picomolar range (50 pM), although slightly higher.[56] This is expected as the interaction with Protein G and IgG has been reported to be different depending on the source of IgG used (rabbit vs mouse).[57] Meanwhile, for the interaction between dextran and the carbohydrate-binding protein Concanavalin A (**Figure 4C**), dextran-coated iron oxide nanoparticles were used as bMR sensors and introduced to a solution containing various amounts of free dextran (1.25 nM – 62.5 nM), before addition of Concanavalin A (50 nM). Our measurements indicated that a K_D value for this interaction was is in the nanomolar range (18.8 nM), within the same range of the reported value in the literature (90 nM).[58] The use of different sources and batches of Concanavalin A (a lectin) and dextran (a complex carbohydrate) might affect the interaction between these two macromolecules, resulting in different K_D values. Furthermore, control experiments using bovine serum albumin (BSA) do not reveal a concentration-dependent signal change confirming the specificity of our assays **(Figure 5, A-B)**. Taken together, these results indicate that our bMR-based method can rapidly measure the dissociation constant of different protein–ligand interactions within a wide range of affinities.

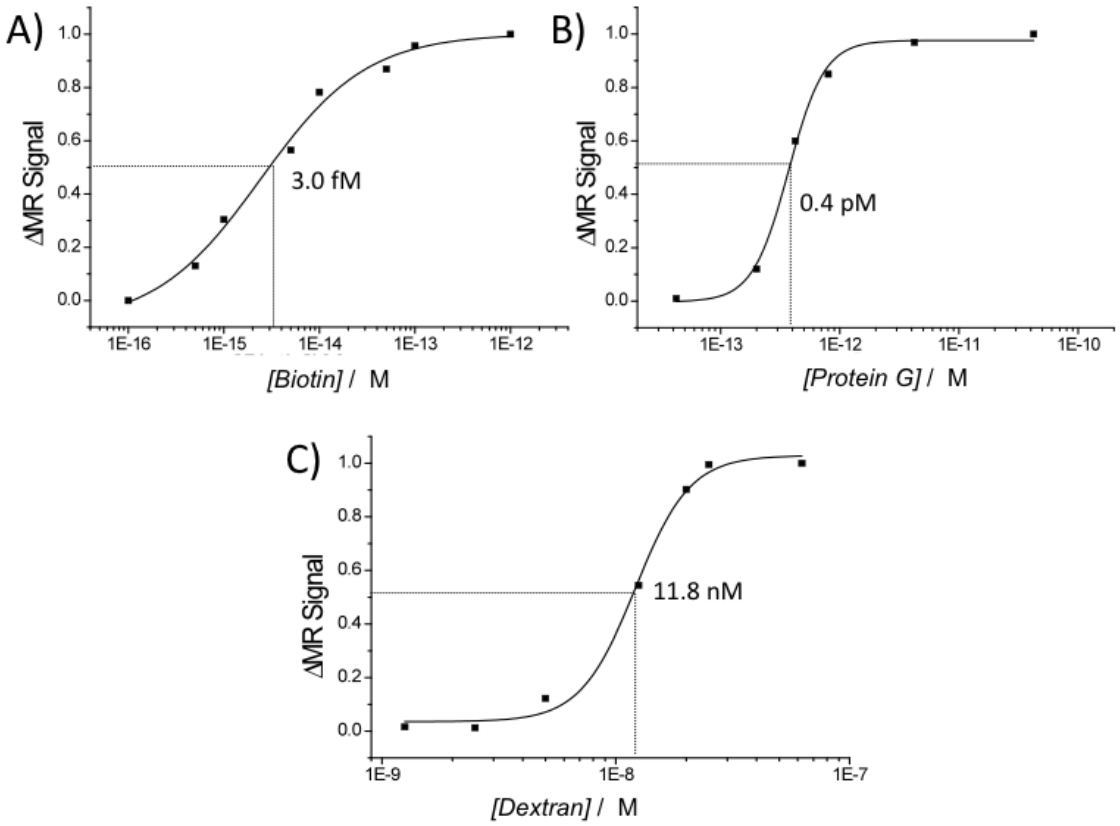

Figure 4. Determination of the dissociation constant for protein-protein interactions via magnetic relaxation and bMR nanosensors.

A) Avidin – Biotin, B) Protein G – IgG, C) Dextran – Concanavalin A. (Errors were within 1-2%, which are too small to depict).

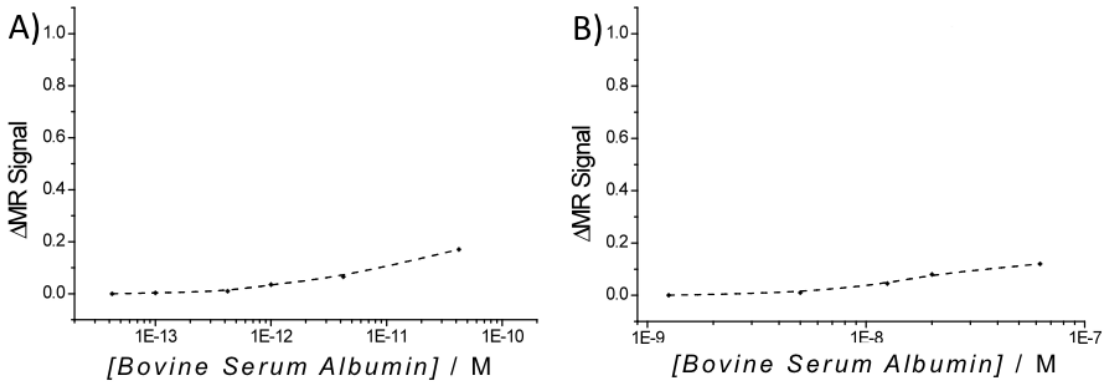

Figure 5. Control experiments using different competitors.
In this set of experiments the protein used as the competitor was different from that being used in the surface of the nanoparticles. These competitors were chosen specifically so that they would not specifically bind the target in order to establish the selectivity of our method. A) Protein G coated nanoparticles targeting IgG with Bovine Serum Albumin (BSA) as a competitor. B) Detxran coated nanoparticles targeting Concanavalin A with BSA as a competitor.

After validating the ability of our magnetic relaxation method to measure K_D values of molecular interactions in solution, we investigated whether our method can be applied to study interactions with transmembrane proteins in intact cells. Membrane proteins and cellular receptors control key biological processes within the cell and are the target for a wide variety of therapeutics.[59-61] Most of the current methods to determine Kd values use purified membrane receptors in solution or attached to a flat surface.[49, 62-64] Therefore, we reasoned whether one could use the bMR assay to determine the K_D between a ligand and a cell receptor using cells in suspension. To validate our hypothesis, we used the folate receptor (FR) as a model system and investigated the affinity of this receptor to its natural targeting ligand, folic acid, using HeLa cells as the source of FR.[65] For these studies, a folic-acid-conjugated iron oxide nanoparticle was used as the bMR nanosensor. Following a 30-minute incubation of the HeLa cells with the bMR

nanosensors and increasing amounts of free folic acid (1.1 nM – 0.56 μM), a similar behavior to that observed with the soluble protein targets was observed (**Figure 6A**). At low amount of competitor, a low ΔMRS-signal was observed that increased at higher concentrations and eventually reached a plateau, allowing us to calculate the K_D as 16 nM for this particular interaction. This value compares with the reported values of 0.1 nM[66] and 30 nM[65] for folate receptor/folic acid interactions. However, these values were obtained using the solubilized receptor in a radioligand-binding assay, instead of using HeLa cells in suspension. It is worth noticing the different K_D values reported in the literature for the same molecular interaction, suggesting that these values depend on the nature of the assay and experimental conditions. [49]

The interaction between the folate receptor and an anti folate receptor antibody (Santa Cruz Biotechnology, sc-28997) was also studied (**Figure 6B**). For this study, anti folate antibody conjugated nanoparticles were used as bMR sensors. Results revealed a K_D value in the low nanomolar range (0.19 nM), while the reported value in the literature for a system using a recombinant solubilized receptor and a totally different antibody was 2.23 nM.[62] In control studies, substituting the FR antibody with the EpCAM antibody (Santa Cruz Biotechnology, sc-73491) resulted in no significant increase in the ΔMR signal value with increasing concentration of EpCAM antibody. Similarly, no response was observed when MCF-7 cells were used, as this cell line does not express the folate receptor assays **(Figure 7 A-B)**. These results indicate that the observed changes in ΔMR signal are specific to a folate receptor/anti-folate antibody interaction and not to a non-specific interaction between the designed bMR nanosensors and the HeLa cells. In additional experiments, we used the anti EpCAM antibody conjugated iron oxide

nanoparticles as bMR nanosensors to measure the K_D between the EpCAM antibody and EpCAM receptors in MCF-7 cells (**Figure 6C**). Our results indicated a K_D of 73 pM while the reported value in the literature is 550 pM.[63] Again, these studies were performed using the extracellular domain of EpCAM (expressed and purified from yeast) and attached to a solid support for SPR studies. Taken together, these results indicate that our magnetic relaxation method can be used to study the interaction of small molecule ligand and proteins with cell surface receptors using intact cells with comparable accuracy to current methods, yet at a higher speed and potentially lower cost. As these experiments are performed within 30 minutes with cells in suspension, any endocytosis of the nanoparticles is minimized.

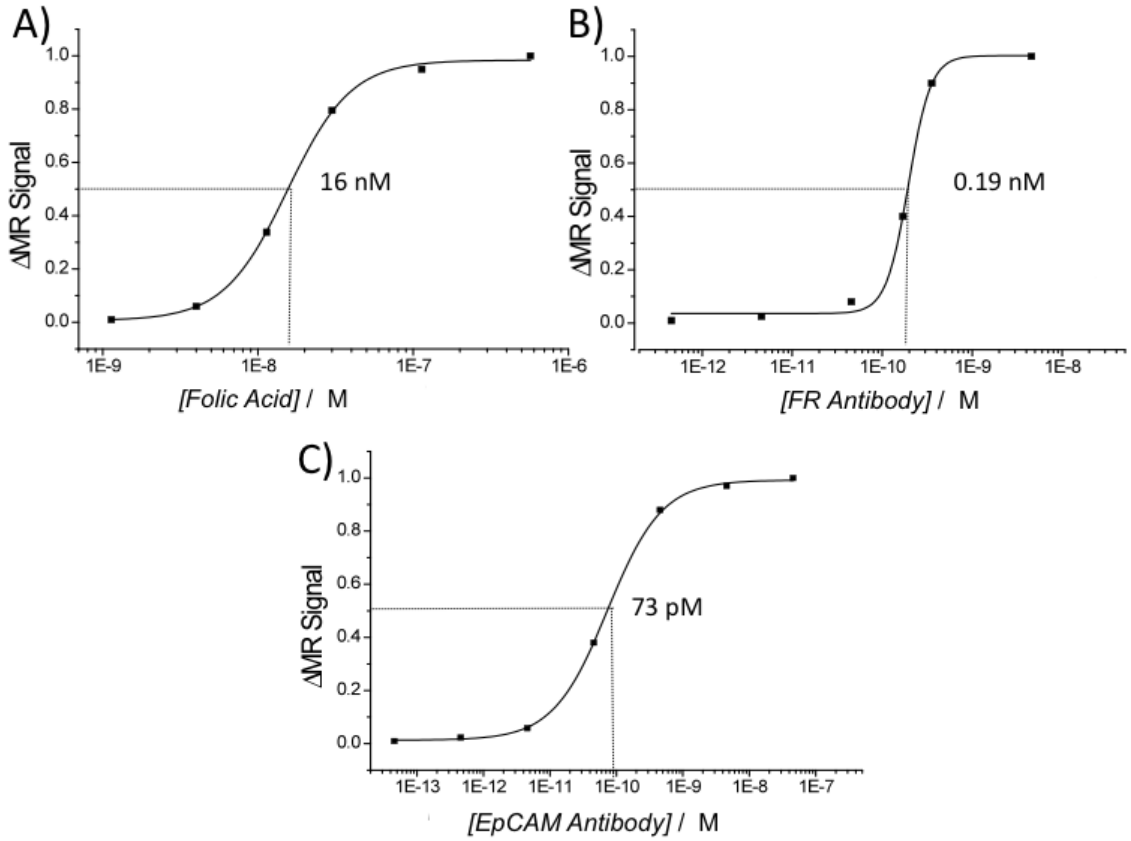

Figure 6. Determination of the dissociation constant for protein-cells interactions via magnetic relaxation and bMR nanosensors.

A) Folic acid – Folate receptor (FR) expressed on HeLa cells, B) anti-folate-receptor antibody – Folate receptor on HeLa cells), C) anti-EpCAM antibody – EpCAM Receptor (MCF-7 Cells). (Errors were within 1-2%, which are too small to depict).

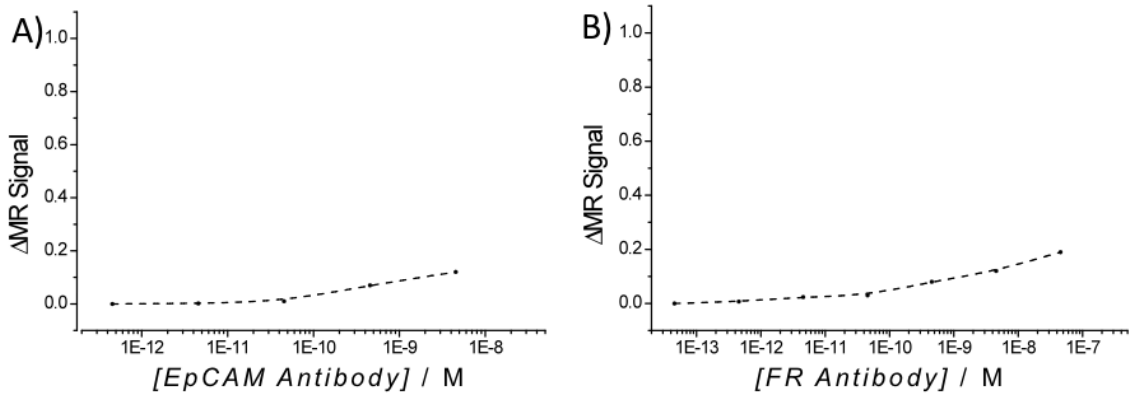

Figure 7. Control experiments using different competitors.
In this set of experiments the protein used as the competitor was different from that being used in the surface of the nanoparticles. These competitors were chosen specifically so that they would not specifically bind the target in order to establish the selectivity of our method. A) FR Antibody coated nanoparticles targeting FR receptor on HeLa cells with EpCAM antibody as a competitor. B) EpCAM Antibody coated nanoparticles targeting EpCAM receptor on MCF-7 cells with FR antibody as a competitor.

Next, we utilized the bMR nanosensor based competition assay to study the interaction between toxins and small molecules. Recent reports describe the interaction of doxorubicin with the tetanus toxin C fragment (TTC)[67] and galactose or dextran with cholera toxin B subunit (CTB).[40] The study of these interactions is important for the development of small-molecule-based therapeutics. For the TTC-doxorubicin interaction, a doxorubicin-carrying iron oxide nanoparticle was designed. Within 15 minutes, we were able to observe a sigmoidal response with increasing ΔMR-signal value upon incubation of the bMR nanosensors with TTC (4 nM) in the presence of increasing amounts (0.9 μM – 12 μM) of doxorubicin (**Figure 8A**). Using this data a K_D of 4.1 μM was calculated, which is close to the reported value of 9.4 μM determined using a similar competition assay to ours with a fluorescence readout instead of magnetic relaxation.[68]

Next, we tested if rhein, an anthracycline antibiotic structurally similar to doxorubicin, binds to TTC. Results show that indeed rhein interacts with TTC with a Kd value of 33.6 μM, which is slightly higher (weaker affinity) to the interaction with doxorubicin (**Figure 8B**). To our knowledge this is the first time that rhein has been reported to bind TTC. This interaction can be atributed to the fact that both molecules posess an anthraquinone group, which in the case of doxorubicin has been reported to play a key role in TTC binding.[25] This observation points toward the use of our bMR nanosensor-based competition assay in structure activity relationship (SAR) studies, where the competition of structurally similar compounds toward binding to a particular protein or cellular receptor is studied by magnetic relaxation.

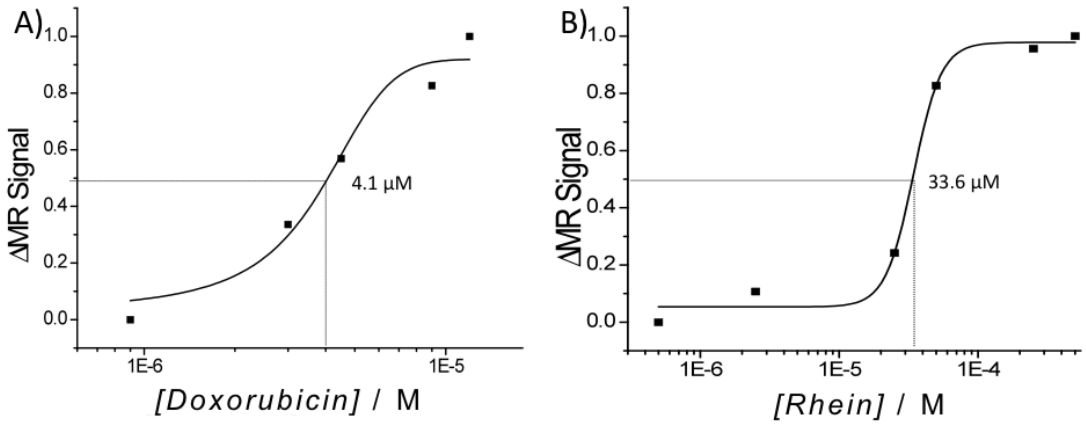

Figure 8. Determination of the dissociation constant of small molecules (doxorubicin and rhein) and TTC, via bMR nanosensors and magnetic relaxation.
A) Doxorubicin – TTC. B) Rhein – TTC. (Errors were within 1-2%, which were too small to depict.)

Meanwhile, the interaction of the cholera toxin B subunit (CTB) with dextran was studied using dextran-coated iron oxide nanoparticles as bMR nanosensors (**Figure 9**).

Using our competition method, we found that the K_D of the dextran – CTB interaction to be 4.9 μM. This value is substantially lower that the value we have previously reported using SPR (14 mM).[40] In that report, CTB was immobilized to the SPR gold plate, using a ganglioside as a linker. Likely, this approach may block sites where dextran binds to, therefore affecting the interaction between CTB and dextran. Hence as the spatial orientation of these entities is constrained by the adhering mechanism, this may affect the K_D values. Our magnetic relaxation method using bMR sensors in solution is a homogeneous assay and therefore more sensitive than those involving the attachment of the target protein to a solid support.[69, 70]

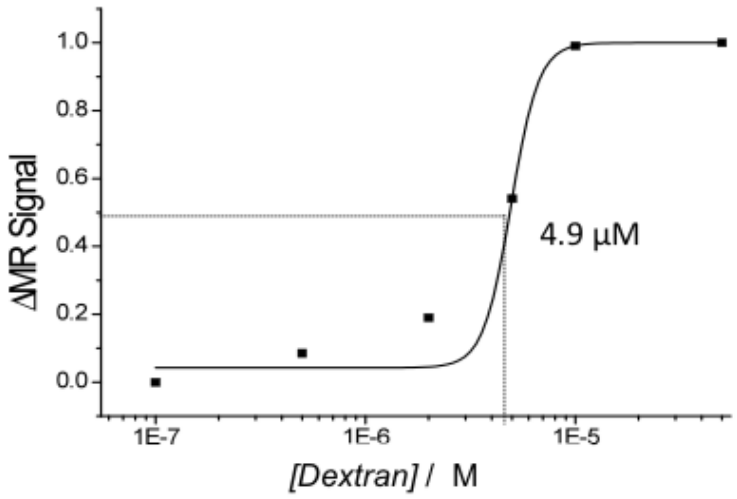

Figure 9. Determination of the dissociation constant of Dextran and CTB via magnetic relaxation and bMR nanosensors.

Finally, we investigated whether the dextran-coated iron oxide nanoparticles can be used as bMR nanosensors to study the interaction of CTB with other carbohydrates. We reasoned that this bMR nanosensor may be able to identify the K_D of similar molecules, due to their structural resemblance and chemical composition (i.e. functional groups) between the nanoparticles' coating and the screened molecules. These studies revealed that increasing concentrations of glucose, galactose, lactose and β-cyclodextrin disrupted the association between dextran-coated iron oxide nanoparticles and CTB **(Figure 10A-D)**. Hence, we determined that glucose had a K_D of 36 μM, whereas the K_D of galactose, lactose, and β-cyclodextrin were 3.5 μM, 88 μM, and 5.6 μM respectively. Summarizing, we observed that dextran has a lower affinity towards CTB than galactose and β-cyclodextrin, while lactose has the least affinity followed by glucose ($K_{DGal} < K_{DCyclo} < K_{DDex} < K_{DGlu} < K_{DLac}$). To our knowledge, the interaction of these carbohydrates with CTB has not been previously reported. Overall, this study's findings are summarized in **Table 1**.

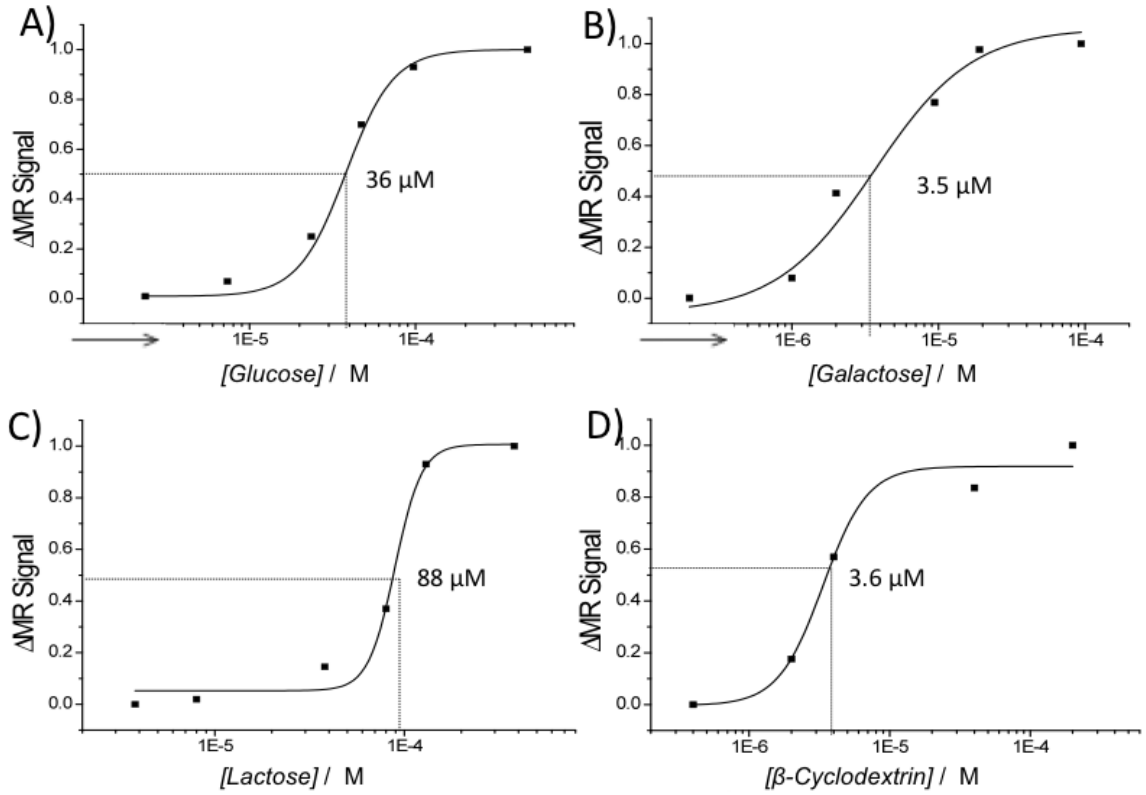

Figure 10. Determination of the dissociation constant of carbohydrates and CTB via magnetic relaxation and bMR nanosensors.

A) Glucose – CTB. B) Galactose – CTB. C) Lactose – CTB. D) β-Cyclodextrin – CTB. (Errors were within 1-2%, which were too small to depict.)

Table 1. Comparison of dissociation constant (K_D) values determined in this study with those reported in the literature.

Interaction	K_D [a]	K_D [b] Reported
Avidin – Biotin	3 fM	1 fM [55]
Protein G – IgG	0.4 pM	50 pM [56]
Concanavalin A – Dextran	11.8 nM	90 nM [58]
Folate receptor – Folic Acid	16 nM	0.1 nM [66]
Folate receptor – anti-FR Ab	0.19 nm	2.2 nM [62]
EpCAM receptor – anti-EpCAM Ab	73 pM	550 pM [63]
TTC – Doxorubicin	4.1 μM	9.4 μM [68]
TTC – Rhein	33.6 μM	N/A
CTB – Dextran	4.9 μM	14 mM [40]
CTB – Glucose	36 μM	N/A
CTB – Galactose	3.5 μM	N/A
CTB – Lactose	88 μM	N/A
CTB – β-Cyclodextrin	3.6 μM	N/A

[a] Values determined using bMR nanosensor competition assay

[b] Values reported in the literature, corresponding reference in bracket

Conclusion

- We have developed a new method to measure the dissociation constants K_D of molecular interactions based on magnetic relaxation.
- Our system has the ability to work over a wide range of affinities and conditions.
- This is a unique method as it measures the interaction between ligands on the surface of a nanoparticle with either solubilized proteins or a cell surface receptor on intact cells.
- Due to the multivalent nature of the interactions between ligand on a nanoparticle and receptors on the surface of a cell, our assay is able to give a more realistic K_D measurement as it takes into account the role that avidity plays in these interactions.
- We discovered the interaction between a Rhein and TTC and reported its dissociation constant.
- New interactions between galactose, β-cyclodextrin, lactose and CTB were discovered and reported.

Discussion

The use of Magnetic Relaxation Nanosensors (MRnS) for the detection of pathogens has become a powerful biodiagnostic tool capable of producing rapid and accurate results. For instance, MRNs avoid the downfall of commonly used technologies that rely in the use of expensive reagents and/or sensitive reporting modalities (fluorophores), by taking advantage of their intrinsic and robust magnetic properties to

report changes of macromolecular aggregation with a high degree of sensitivity. In recent years this technology has been extensively used to investigate the detection of different targets such as bacteria, cancer cells and toxins. Also throughout this time, along with the ongoing development of these MRnS-based biodiagnostics, the molecular dynamics associated nanoparticle – target interaction was further studied. This led to the understanding of the binding versus clustering effect in which nanoparticle valency and target concentration play a vital role in dictating the behavior of nanoparticles in solution.

Based on this knowledge, we created an assay capable of measuring the dissociation constant K_D of different interactions using bMRs (binding Magnetic Relaxation sensors). This assay takes advantage of the sensitive response observed when low amount of targets interact with low-valency nanoparticles. By controlling the amount of target that binds to the surface of the nanoparticle, we were able to developed a competitive assay that accurately measured the dissociation constant of protein – protein, protein – live-cell receptors, and small molecule – toxin interactions.

Our bMRs assay provided various advantages over the currently used techniques such as surface plasmon resonance (SPR), titration calorimetry, and radioligand binding assay. For instance, the bMRs assay does not need the binding of either the ligand or the protein onto a solid support, a requirement for SPR that neglects the effect a real conditions such as avidity that may be found on a cell's surface. Also, as opposed to titration calorimetry and radioligand binding assay, our system does not require expensive instrumentation or the use of radioactive materials.

Overall, we introduced a novel method to measure the dissociation constants of molecular interactions over a wide range of affinities using magnetic relaxation.

Experiments with different categories of interactions showed that significant accuracy can be achieved when using this methodology as compared to traditionally established methods. Furthermore we established a method that is capable of measuring dissociation constants on the cellular surface while the cells are suspended in solution. Also the previously unknown K_D values of different carbohydrate-CTB interactions as well as two newly discovered interactions between small molecules and Tetanus toxin C fragment were reported. Lastly, it is likely that the reported method could facilitate the study of K_D values by taking advantage of the robustness and stability that MRnS possesses.

Taking the merits of our method into consideration, this study is important because it uses a platform technology, based on magnetic nanoparticles, that can be used to study multiple kinds of molecular interactions including those between toxins and small molecules. Since the surface of bMRs can be easily modified to carry any ligand of choice, the applications of this technique can be expanded to just about any kind of molecular interaction. This can facilitate and accelerate the discovery of new interactions in the field of therapeutics, specifically when identifying new inhibitors for toxins. The discovery of small molecules that bind and inhibit toxins is of great importance due to the prevalent damage associated with toxins. Using the magnetic relaxation method we could easily identify and measure new interactions between small molecules and toxins, without the need of special instrumentation or radioactive regents. Furthermore, this method will allow for quick and effective measurements that can be performed in solution, without the need of having the toxin attached to a metal support.

CHAPTER III: SCREENING OF A SMALL-MOLECULE LIBRARY AGAINST THE ANTHRAX TOXIN VIA MAGNETIC RELAXATION.

Introduction

An Anthrax infection usually has a deadly and devastating effect on the host before it can be correctly detected and successfully treated. Anthrax is a bacterial infection from the gram-positive *Bacillus anthracis* that propagates through the release of bacterial spores. Historically, Anthrax infections have been of little danger to humans since they typically occur in animals that eat or inhale spores while grazing[22]. Yet, the weaponization of the bacterial spores has made this disease a potential danger to humans[71]. There are two types of anthrax, subcutaneous[8] which occurs when the spores enter a surface wound and inhalation, which occurs when the spores are directly inhaled. Subcutaneous anthrax is a mild disease treatable with antibiotics while inhalation anthrax, the weaponized type, tends to be fatal in 90% of cases[72]. Once the spores are inhaled, the bacteria is able to reproduce and starts to damage healthy cells by the release of the anthrax toxin. The anthrax toxin is composed of three proteins: (i) anthrax protective antigen (APA), (ii) anthrax lethal factor (ALF), and (iii) anthrax edema factor (AEF) that work in combination to effectuate the lethality associated with the disease. Out of the three proteins the first two are of greater importance due to the indispensable role that the protective antigen plays in internalizing the two factors into healthy cells, and the rapid and devastating effect that the lethal factor has on host cells[73-75].

After infection, the disease progresses in different stages (**Table 2**).[76] The common development of the disease starts with the incubation period, a time in which the spores settle into the body, usually lasting less than one week but can extend up to two months and culminates with the initial onset of symptoms. These symptoms manifest in the form of low-grade fever, nonproductive cough, malaise, profound sweats and chest discomfort. This followed by a subsequent phase that starts with a 1-5 days period in which the patient experiences an abrupt onset of high fever and severe respiratory distress due to the release of the anthrax toxins into the blood stream. Sometimes the subsequent phase is delayed by 1-3 day period of improvement in the symptoms. The subsequent phase ends with the patient going in to shock, which lasts 24-36 hours and culminates in death. Experiments in mice have revealed that death occurs within a couple of hours after signs of infection are observed. In humans, the subsequent phase lasts up to 10 days after the initial symptom onset due to the slower progressing of the disease. Therefore the subsequent phase is crucial for the treatment of anthrax in humans as this is the period in which the disease can be detected and treated.

Table 2. Progression of anthrax in humans.

Stage	Duration	Symptoms
Incubation period	<1 week, my last up to 2 months	None
Onset of Symptoms	1-5 days	Low-grade fever, nonproductive cough, malaise, profound sweats and chest discomfort
Subsequent Phase	1-5 days	High fever, severe respiratory distress.
Shock	24-36 hours	Death

Current diagnostic technologies lack the speed needed to identify the disease on time, and modern antibiotics are effective at killing the bacterium but have no effect on the destructive toxins left behind long after the bacteria is eliminated[77]. With symptoms similar to those of other diseases, faster diagnostic systems are needed to quickly treat the infection in the early stages of the disease.[76] Furthermore, not only the bacterium needs to be eradicated from the body, but the toxins that are left behind also need to be inhibited in order to arrest further damage to healthy tissue. Therefore, there is need for fast and reliable detection methods as well as more effective therapeutic approaches that focus on detecting and inhibiting the bacterial toxins instead of just killing the bacterium. In particular, nanoparticle-based diagnostics can offer a sensitive, robust, portable, and low-cost detection system while also potentially being used to inhibit the anthrax bacterial toxins.

Existing treatment options for anthrax are limited to a few antibiotics such as ciprofloxacin, doxycycline and penicillin that target and eliminate the bacterium but have no effect on the destructive toxins that can stay in the circulation a couple of days after the infection is eliminated[78]. On the other hand there are various detection methods that can successfully identify the bacterium, yet none of these methods are fast enough to improve the prognosis of an infected patient[77]. Currently available detection methods include traditional microscopy studies in which the bacteria is grown for 1-2 days and then stained and observed via microscopy. Further confirmatory tests are usually required and tend to prolong the time for diagnosis by several days. More recent methods use nucleic acid-based detection assays, which rely on PCR amplification and require the use of specialized primers or probes that have to be carefully selected to avoid any cross-

reaction with other related species during the amplification. Although this method can provide a faster diagnosis, a bacterial culture is still required to isolate the nucleic acids adding a couple of days to obtain results. Due to the rapid progress of the disease, a detection method with a faster turn around time is needed. This was particularly observed during the 2001 U.S anthrax attacks in which 5 out of the 11 cases of inhalation anthrax ended in death with a subsequent phase lasting approximately 5 days.[72] During this time, only 1 of the 5 anthrax infections was confirmed before the death of the patients, making the need for a fast detection method that does not rely in bacterial culture of outmost importance.

One alternative is to directly detect the anthrax toxin in the blood stream. This will bypass the need for a bacterial culture as well as significantly reduce the time needed for an efficient diagnosis. Additionally, a detection method that directly targets the toxin can also be used to inhibit its activity without the need of additional therapeutics. A nanoparticle that selectively binds to a toxin and the binding results in a detectable signal that is sensitive and quantifiable can be used as a detection assay. Furthermore, if the binding event occurs at or near the catalytic site of the toxin, therefore affecting the pathogenic tissue damaging of the toxin, then it can also be used as a therapeutic. With the expansion of nanotechnology, systems that offer theranostic (therapeutic and diagnostic) capabilities have been more widely used due to the multi-platform approach inherent of nanotechnology. The development of polymeric coated nanoparticles have allowed for theranostics with fast detection times as well as therapeutic cargoes usually stored within the polymeric coating. Specifically, superparamagnetic iron oxide nanoparticles (IONP) theranostics have been used to successfully treat and detect cancer

cells.[37] As a detection method, IONP based systems have been used as Magnetic relaxation nanosensors (MRnS) that have the capability of analyzing and detecting different pathogens within a couple of hours. Recently, MRnS have been used to detect several biological agents such as cells, toxins and DNA fragments in complex samples.[30, 38, 40, 79, 80] Detection occurs after the specific binding of a target to the surface of the MRnS produces a change in the water proton spin-spin relaxation time (T_2) of the sample.[36] MRnS can be tailored to detect a range of multiple targets by engineering the ligands in the surface of the nanoparticle. These ligands can be small peptides, antibodies, DNA fragments or small molecules. Specifically, antibodies and small molecules have been identified to bind and inhibit the anthrax toxins, particularly the APA and ALF, allowing for the opportunity to use MRnS to detect and inhibit the anthrax toxins. There are various commercially available antibodies that target the APA as well as several small molecules inhibitors of the ALF.[19, 81, 82] The drawback with the identified ligands is that they tend to be expensive to produce, in the case of antibodies, or are complex to synthesize, as it is the case for small molecules. Therefore there is a need for the identification of new anthrax toxins-binding ligands that have the capability to inhibit the toxin and are cost-efficient and readily available.

In order to achieve this undertaking an economic and readily available small-molecule library will be screened against the APA and ALF using MRnS as the detection method. Each candidate in the library will be chemically coupled to the surface of MRnS (**Figure 11**) and the change in magnetic relaxation as the small molecules interact with either toxin will be measured. If the small molecule that is attached to the MRnS binds to the toxins, a significant change in T_2 will be observed allowing the identification of a new

toxin binder. The affinity of the newly identified molecule to either anthrax toxin will then be evaluated by measuring the dissociation constant using the magnetic relaxation method used in the previous chapter. As these small molecule-carrying MRnS bind to the components of the anthrax toxin, they could be used not only to detect, but also potentially be used to treat the disease.

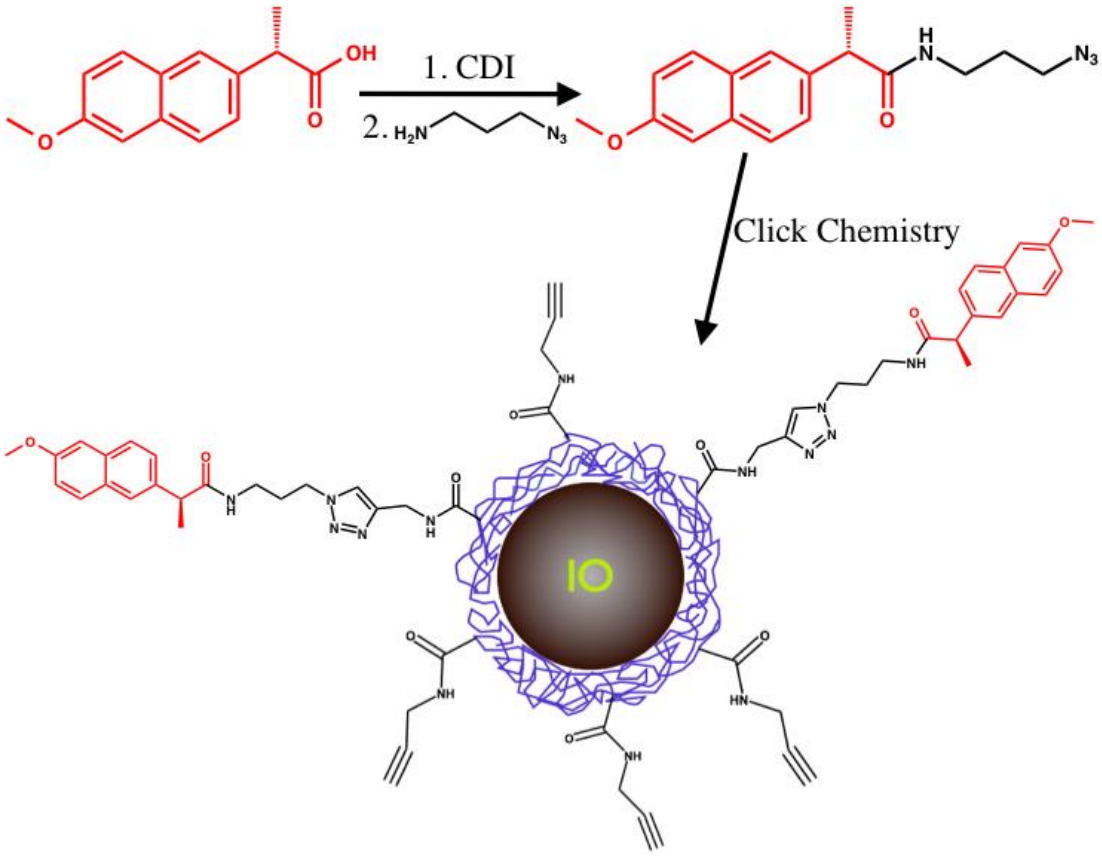

Figure 11. Synthetic procedure used to attach the small molecules to the nanoparticles.
Naproxen is the molecule shown in the diagram. Using a similar approach the small molecules of the library will be attached to iron oxide nanoparticles.

Selection of small-molecule library

The first step towards screening the small-molecule library for its binding to the anthrax toxins will be to assemble the library using the following criteria. In order to achieve this, a list of 1000 commonly available carboxylic acid-bearing small molecules was compiled from Sigma-Aldirch. Molecules with carboxylic acids were chosen because this functionality would later be used to attach the molecule to the surface of the nanoparticle. The list was then reduced to 43 molecules based on a comparison of structural similarity to that of know inhibitors of the target proteins. Out of the 43 molecules 34 were then selected based on price and availability. In order to ensure the biocompatibility of the small molecule library, all the compounds selected were common chemicals; most of them FDA approved drugs that are currently used in the field. By using small molecules that are already FDA approved, these small molecules could potentially be used to treat the effects of the anthrax toxin in the near future.

Materials and Methods

Reagents

All reagents were of analytical reagent grade. Iron salts ($Fe_2Cl_3 \bullet 4H_2O$ and $Fe_3Cl_3 \bullet 6H_2O$), Polyacrylic acid (PAA, MW 1.8 kDa), ammonium hydroxide, hydrochloric acid, propargylamine, N-hydroxysuccinimide (NHS), Bezafibrate, Sulindac, Ketoprofen, Indometacin, Ibuprofen, Retinoic Acid, (S)-(+)-6-Methoxy-α-methyl-2-naphthaleneacetic acid, Homovanillic Acid, (±)-α-Lipoic acid, Sodium Deoxycholate, Nalidixic Acid, L-Mimosine from Koa hoale seeds, N-Hippuryl-His-Leu Hydrate,

Acemetacin, Mefenamic Acid, Cetirizine dihydrochloride, Furosemide, Enoxacin, 3-Iodo-L-Tyrosine, Rebamipide Hydrate, Bumetanide, Aristolochic Acid I, Mycophenolic Acid, Etodolac, Fusaric Acid, R(+)-IAA-94, Tamibarotene, NS3694, Sivelestat sodium salt hydrate, Oxaprozin, GW9508, Raltitrexed monohydrate, Rhein, and Doxorubicin were obtained from Sigma Aldrich whereas EDC (1-ethyl-3- [3-dimethylaminopropyl]carbodiimide hydrochloride) was obtained from Pierce Biotechnology. The Anthrax Lethal Factor and Anthrax Protective Antigen were obtained from List Biological Laboratories, INC.

Synthesis of PAA coated Iron Oxide Nanoparticles.

Iron oxide nanoparticles (PAA-IONPs) were prepared using a water based step-wise synthetic procedure. Three solutions were prepared; an iron salt solution (0.62 g of $FeCl_3$. $6H_2O$ and 0.32 g of $FeCl_2$. $4H_2O$) in 2.0 mL of DI water and 100 µL HCl (100 µL of 12 N HCl; an alkaline solution containing 1.8 mL of 30% NH_4OH solution in 15 mL of DI water; and a stabilizing polymer solution containing 820 mg of polyacrylic acid in 5 mL of DI water. The step-wise synthesis of the PAA-IONP was started by the addition of the iron salt solution to the alkaline solution under vigorous stirring. The resulting dark suspension of iron oxide nanoparticles was then stirred for 30 seconds before addition of the stabilizing polymer solution. The mixture of the three solutions was stirred for 1 h. The resulting suspension of PAA-IONPs was then centrifuged at 4000 rpm for 30 minutes and the nanoparticle-containing supernatant was filtered 20 times its volume with DI water to get rid of free polyacrylic acid and other unreacted reagents using a KrosFlow filtration system from Spectrum Labs (filtration column: PS/10kD). Finally, the PAA-IONP suspension was purified using magnetic column, washed with phosphate

buffer saline (pH = 7.4) and concentrated using the KrosFlow system. The iron concentration and magnetic relaxation of the PAA-IONPs was determined as previously reported [Josephson et. al. Bioconjugate Chem. 1999, 10, 186–191]. The successful coating of the IONPs with PAA was confirmed by the presence of a negative zeta-potential ($\zeta = -98$ mV) as well as the appearance of the acid carbonyl band at 1690 cm^{-1} in the FTIR spectra of the nanoparticle.

Propargylation of PAA-coated Iron Oxide Nanoparticles.

To a suspension of PAA-IONP (50 mg Fe) in MES buffer (30 mL, pH = 6.5), a solution of EDC (115.2 mg, 0.6 mmol) and NHS (69 mg, 0.6 mmol) in MES buffer (2.5 mL) was added and incubated under stirring for 3 minutes. To the resulting reaction mixture, propargylamine (33 mg, 0.6 mmol) in DMSO (0.75 mL) was added drop-wise under medium stirring and incubated for 6 h at room temperature. The resulting reaction mixture was then purified using a magnetic column and concentrated using KrosFlow filtration system to approximately 5 mg/ml Propargylated-IONP in PBS. The nanoparticles were stored at 4 °C. FT-IR data analysis confirmed the completion and success of the conjugation by the appearance of the amide N-H bending (1550 cm^{-1}) and C=O stretching (1640 cm^{-1}) as well as the alkyne C≡C stretching at 2260 cm^{-1}.

Synthesis of the Azide linker.

A solution of 3-chloropropylamine hydrochloride (1 equiv., 54 mmol) and sodium azide (3 equiv, 162 mol) in DI water (40 mL) was heated at 80 °C for 15h. After removing most of the water by distillation under vacuum, the reaction mixture was cooled in an ice bath. The remaining solution was mixed with diethyl ether (75 mL) and KOH pellets (7 g) while keeping the temperature below 10 °C. After separation of the

organic phase, the aqueous layer was further extracted with diethyl ether (3 X 20 mL). The combined organic layers were dried over K_2CO_3 and concentrated and dried under vacuum to give an oily compound. The resulting compound 3-azidopropan-1-amine(85% yield) bp: 48-50 °C was characterized by 1 H NMR (300 MHz), δ 1.53 (s , 2H), 1.75 (quint, 2H, J = 6.81, 2.82 (t, 2H, J = 6.8), 3.38 (t, 2H, J = 6.7). FTIR: N_3 stretching band at 2100 cm^{-1}.

Coupling of the Azide linker to the small molecules.

A solution containing the small molecule (1 equiv.) and CDI (1.2 equiv) in the selected solvent (see table) was stirred for 3 hrs at 45 °C under a dried N_2 atmosphere. After the time expired, the Azide-linker (1 equiv.) was added and the resulting solution was then stirred for 10 hrs at room temperature. The solvent from the reaction mixture was then evaporated via rotator evaporation and the remaining compound was purified by silica column chromatography using a MeOH/$CHCl_3$ mixture (0-20% MeOH / 100-80 % $CHCl_3$). The coupling of the azide linker to the small molecule was confirmed by FTIR by the appearance of the stretching band at 2100 cm^{-1} that is characteristic of the N_3 functional group. **Table 2** describes the weights of each reagent used as well as the reaction conditions for each molecule. Three of the molecules proved to be insoluble in the solvents necessary for the reaction to be successful. These insoluble molecules are labeled as insoluble in **Table 2** and no reaction was performed with them. The reaction involving one of the molecules was unsuccessful after several attempts to optimize the conditions. This molecule is labeled as NO RXN (no reaction) in **Table 2**.

Table 3. Conditions for the coupling of the azide linker to the small molecules

Small Molecule	Solvent	Wt. SM	Wt. CDI	Wt. Azide Linker	N_3 IR Band
3-Iodo-L-tyrosine	Insoluble	Insoluble	Insoluble	Insoluble	Insoluble
Acetametacin	$CHCl_3$	92.3 mg	43.1 mg	22.2 mg	2096 cm^{-1}
Aristolochic Acid I	THF	25 mg	14.2 mg	7.32 mg	2097 cm^{-1}
Bezafibrate	THF	100 mg	53.7 mg	27.6 mg	2096 cm^{-1}
Butanemide	THF	87 mg	46.5 mg	23.8 mg	2098 cm^{-1}
Ceterizine HCl	THF	50 mg	21.0 mg	10.8 mg	2097 cm^{-1}
Deoxycholate	Insoluble	Insoluble	Insoluble	Insoluble	Insoluble
Doxorubicin	THF	10 mg	3.35 mg	1.72 mg*	2098 cm^{-1}
Enoxacin	Insoluble	Insoluble	Insoluble	Insoluble	Insoluble
Etodolac	CH_2Cl_2	10 mg	6.8 mg	3.5 mg	2093 cm^{-1}
Furosemide	THF	99.1 mg	58.2 mg	30.0 mg	2097 cm^{-1}
Fusaric Acid	$CHCl_3$	91.5 mg	99.3 mg	51.1 mg	2093 cm^{-1}
GW9508	CH_2Cl_2	5.0 mg	2.8 mg	1.7 mg	2097 cm^{-1}
Homovanilic Acid	THF	69 mg	73.7 mg	37.9 mg	2097 cm^{-1}
Ibuprofen	$CHCl_3$	98.3 mg	92.6 mg	47.6 mg	2093 cm^{-1}
Indometacin	$CHCl_3$	100 mg	54.3 mg	28.0 mg	2096 cm^{-1}
Ketoprofen	$CHCl_3$	100 mg	76.5 mg	39.4 mg	2093 cm^{-1}
L-Mimosine	THF	25 mg	24.5 mg	12.6 mg	2102 cm^{-1}
Lipoic Acid	CH_2Cl_2	100 mg	94.4 mg	48.5 mg	2092 cm^{-1}
Mefenamic Acid	$CHCl_3$	100 mg	80.7 mg	41.5 mg	2094 cm^{-1}
Mycophenolic acid	THF	50.0 mg	30.4 mg	15.63	NO RXN
N-Hippuryl-His-Leu	THF	25 mg	11.3 mg	7.0 mg	2097 cm^{-1}
Nalidixic Acid	$CHCl_3$	100 mg	83.8 mg	43.1 mg	2097 cm^{-1}
Naproxen	$CHCl_3$	100 mg	84.5 mg	43.5 mg	2096 cm^{-1}
NS3694	THF	5.0 mg	2.71 mg	1.39 mg	2095 cm^{-1}
Oxaprozin	THF	5.0 mg	3.31 mg	2.0 mg	2094 cm^{-1}
R(+)-IAA-94	$CHCl_3$	10 mg	5.4 mg	3.4 mg	2096 cm^{-1}
Raltiterexed	THF	10 mg	4.1 mg	2.0 mg	2099 cm^{-1}
Rebamipide	CH_2Cl_2	5.0 mg	2.62 mg	1.6 mg	2098cm^{-1}
Retinoic Acid	THF	50 mg	32.4 mg	16.7 mg	2099 cm^{-1}
Rhein	$CHCl_3$	50 mg	34.2 mg	17.6 mg	2096 cm^{-1}
Sivelestat	THF	5.0 mg	2.24 mg	1.15 mg	2101 cm^{-1}
Sulindac	CH_2Cl_2	100 mg	54.5 mg	28.1 mg	2094 cm^{-1}
Tamibarotene	$CHCl_3$	5.0 mg	2.8 mg	1.7 mg	2097 cm^{-1}

* A different azide-linker was used, 3-azidopropanoic acid.

Attaching the Small Molecules to the MRnS.

To synthesize Small molecules-carrying MRnS click chemistry was used to couple the propargyl groups on the nanoparticles to the azide on the small molecules. Briefly, propargylated poly(acrylic acid)-coated nanoparticles (3 mg, 2 mg/mL, 1 equiv.) were added to a low stoichiometric ratio of azide-functionalized small molecules (5 equiv.) with the purpose of attaching approximately 5 small molecule per nanoparticle. The reaction was initiated at room temperature in the presence of catalytic amount of CuI (0.01 µg in 500 µL of bicarbonate buffer, pH 8.5), and further incubated for 12 h at room temperature. The final reaction mixture was purified with a magnetic column (LS25, Miltenyi) using DMSO as the elutant. The small molecule-carrying nanoparticle preparations were stored at room temperature until further use. Confirmation of the successful conjugation of the small molecules to the nanoparticles was achieved through either UV-Vis absorption spectroscopy or Fluorescence spectroscopy, depending on the spectroscopic profile of each individual molecule.

Assay for the screening of the small molecule library against APA and ALF.

An analyzing solution consisting of 10 µL of the Small molecule-carrying MRnS and 2,000 µL DI water was prepared. Samples containing different concentrations of free toxin (APA or ALF, 2 pM to 20 nM, in 1X PBS buffer) were prepared and 2 µL of each sample was added to 200 µL of the MRnS analyzing solution (Small molecule-MRnS). A negative control sample was prepared in the same fashion, adding 2 µL fresh 1X PBS buffer instead of toxin (0 M APA or ALF control sample). Magnetic relaxation measurements were performed every 15 minutes of incubation at room temperature for 1 hour. Transverse (T_2) proton relaxation times measurements were obtained using a

Bruker Minispec mq20 NMR analyzer operating at a magnetic field of 0.47 T and at 37 °C.

Results

After choosing the molecules they were chemically coupled to an azide liker via carbonyldiimidazole chemistry by taking advantage of their carboxylic acid groups. Out of the 34 molecules selected, there were four molecules that either did not react or were insoluble in all of the available solvents for a successful reaction (**Table 2)**. The remaining 30 molecules were verified via FTIR for the appearance of the stretching band of the N_3 at 2100 cm^{-1} that is characteristic of the N_3 functional group in the azide linker (**Figure 12**).

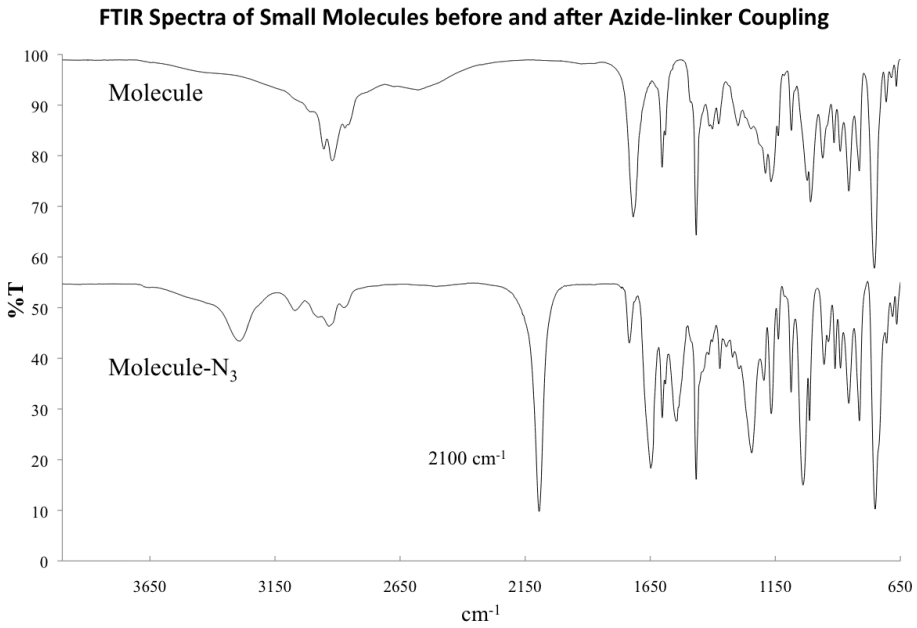

Figure 12. Representative FTIR spectra for the N_3 modification of the small-molecule library.
All of the selected molecules displayed the appearance of the 2100 cm^{-1} stretching band of the N_3 after the azide-linker was chemically coupled to the small molecule. This was indicative of the successful modification needed to attach the small molecule to the nanoparticle.

After the small-molecule library was selected and functionalized for click chemistry, the next step was to prepare the SM-MRnS conjugate. Briefly, polyacrylic acid coated iron oxide nanoparticles (75 nm, R_2: 230 mMs^{-1}) were synthesized and surface-functionalized with a small linker containing propargyl groups. The addition of propargyl groups to the surface of the IONPs was verified by observing a gain in the zeta potential (ζ) from – 98.8 mV to -57 mV. This increase is attributed to the addition of propargyl-linkers to the surface of the nanoparticle, which utilize carboxylic acid groups and consequently reduce the overall negative charge on the surface. Once the IONPs were ready for click chemistry the next step was to make them a MRNS by clicking the small molecules to their surface. This was achieved by reacting the propargyl-coated IONPs with the Azide-coupled small molecules in the presence of catalytic amounts of copper iodine. The successful addition of the small molecule to the surface of the nanoparticle was verified by either fluorescence or absorbance spectroscopy, depending on the spectroscopic characteristics of the small molecule in question. For small molecules with strong UV-VIS absorption, a UV-VIS spectrum of the small molecule and the SM-MRnS conjugate was collected and analyzed for the presence of the small molecule in the nanoparticle (**Figure 13B**). Similarly, if the small molecule exhibited a strong fluorescence at a particular wavelength, the small molecule and the SM-MRnS conjugate was analyzed by fluorescence spectroscopy using a fluorescence spectrophotometer (**Figure 13A**). The IONPs by themselves are not fluorescence and have a very low absorbance, therefore making it easy to distinguish the small molecule on the surface of the IONP (**Figure 13**).

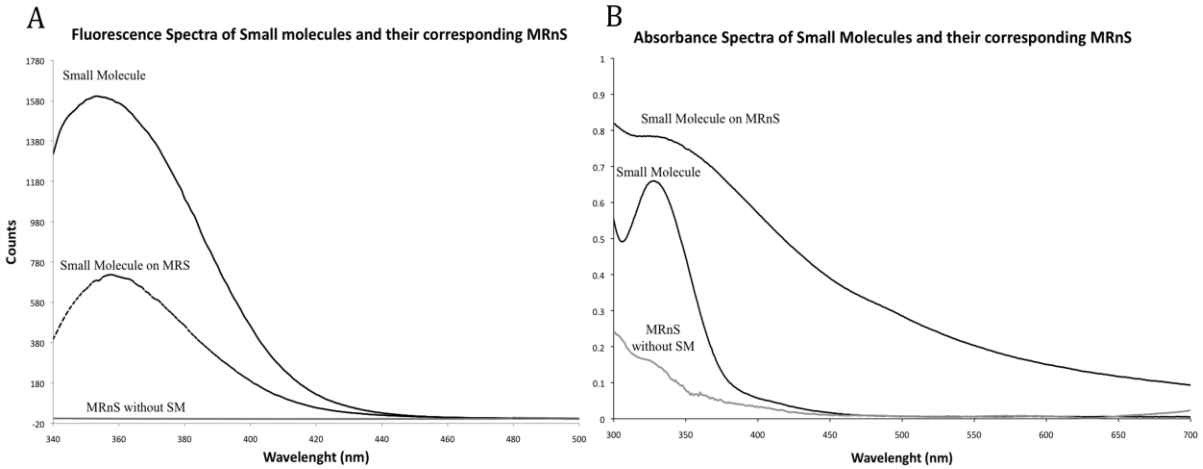

Figure 13. Spectral Characteristics of the Small Molecules before and after attachment to the nanoparticle.
The successful attachment of all the small molecules to the surface of the nanoparticle was verified by either fluorescence or absorbance emission depending on the spectral characteristic of the nanoparticle that was attached. A: Fluorescence spectra of a small-molecule and its corresponding MRnS. B: Absorbance spectra of a small molecule and it corresponding MRnS.

Binding detection of the small molecules to the toxin.

In order to detect which of the candidates bound to the APA and ALF the library of small-molecule MRnS was screened against both toxins. The screening was performed by measuring the ΔT_2 of the various MRnS as they interacted with either APA or ALF. A successful binding interaction was acknowledged after changes in T_2 were observed with increasing concentration of toxin. The changes in T_2 were attributed to the toxin binding to the SM-MRnS conjugate. A binding to the surface of the nanoparticle affects the time (T_2) that it takes for surrounding water protons to relax to their original state therefore allowing us to detect the interaction between the toxin and the SM-MRnS conjugate. A positive result was then further confirmed by measuring the dissociation constant K_D between the identified small molecule and the target toxin. The K_D measurements were

performed using magnetic relaxation as described in Chapter 2. A competitive assay with different concentrations of free small molecule (competitor) and fixed concentrations of toxin (target) and SM-MRnS conjugates (labeled ligands) was used to determine the dissociation constant. The competition between the free ligand and the label ligands for finding to the toxin provided us with a method for us to measure the K_D values of the studied interactions. The results of the screening (**Figures 14-44**) are displayed in the following section with information on each of the selected molecules as well as the results of the magnetic relaxation measurements. Molecules that were identified to bind the toxins will also include the results of the K_D measurements.

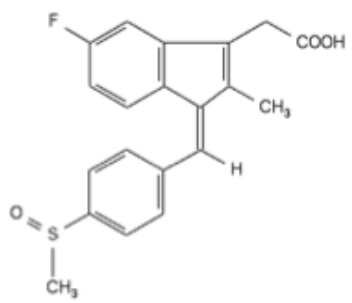

Sulindac

Molecule Info

- Drug
- FDA approved
- **Brand Name:** Clinoril
- **Uses:** NSAID, chronic inflammatory conditions.
- **Natural Target:** COX-1 and COX-2 nonselective.

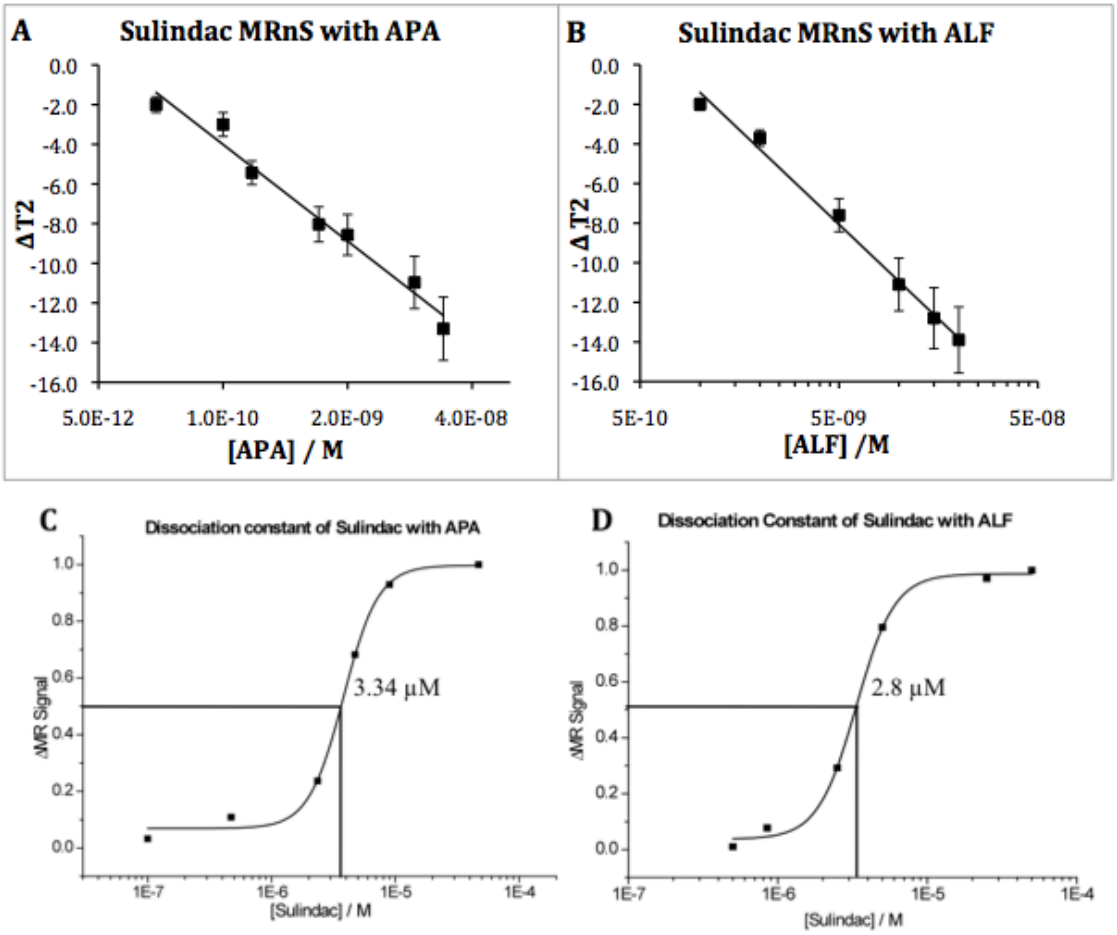

Figure 14. Studies with Sulindac.

Results of Sulindac-MRnS screening with APA and ALF (**Figure 14**):

The screening of sulindac-MRnS yielded positive results for both the Anthrax Protective Antigen and the Anthrax Lethal Factor. Upon binding to the APA we observed a limit of detection of 0.02 nM and a maximum change of -13.3 on the ΔT_2 (**Figure 14A**). For this interaction we measured a K_D of 3.34 uM (**Figure 14C**). Similarly, a strong interaction of sulindac with ALF was also detected with a maximum change of -13.9 in ΔT_2 and a limit of detection of 1 nM (**Figure 14B**). The ALF-Sulindac interaction yielded a K_D of 2.8 µM (**Figure 14D**). As seen in the previous figure, using Sulindac as a ligand on the surface of the MRnS provided a sensitive probe that allowed for the detection of both component of the anthrax toxin in the nanomolar range. These finding provide the opportunity to use a currently FDA approved drug for the fast detection (45 minutes) of APA and ALF. Furthermore, the inhibition potential towards the proteins, especially the enzymatic-active ALF needs to be evaluated in order to postulate Sulindac as a possible treatment for the anthrax toxin.

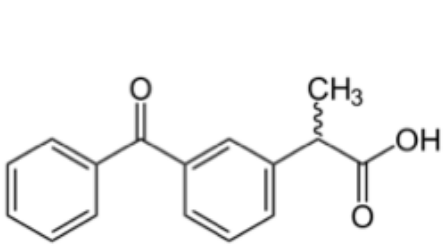

Ketoprofen

Molecule Info

- Drug
- FDA approved
- **Brand Name:** Orudis
- **Uses:** NSAID, fever, musculoskeletal pain.
- **Natural Target:** COX-1 and COX-2 nonselective.

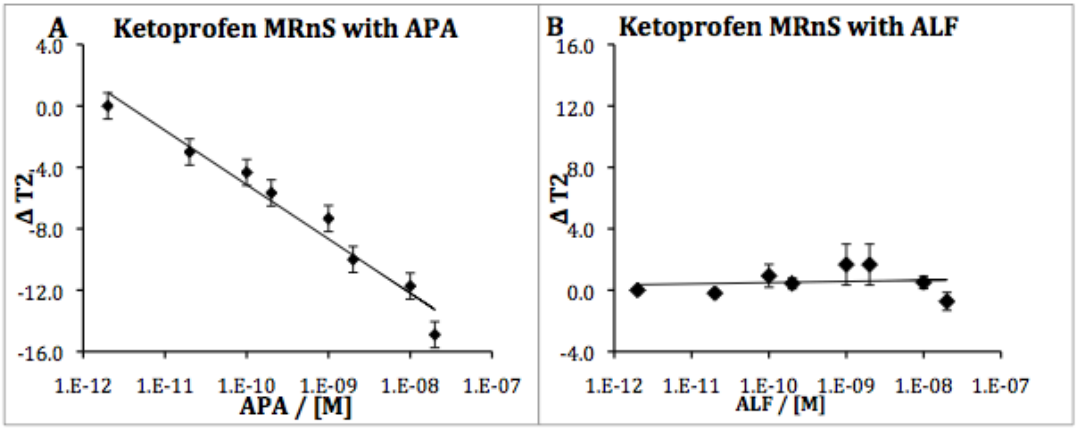

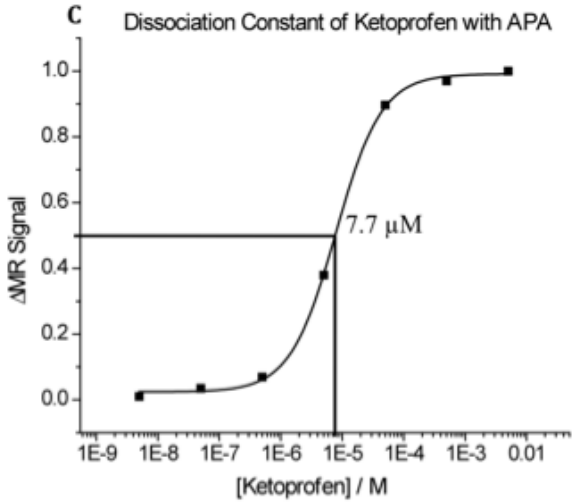

Figure 15. Studies with Ketoprofen.

Results of Ketoprofen-MRnS screening with APA and ALF (**Figure 15**):

The screening of the Ketoprofen-MRnS yielded positive results for Anthrax Protective Antigen. Upon binding to the APA a maximum change of -14.9 on the ΔT_2 was observed with a limit of detection in the 0.02 nN (**Figure 15A**). For this interaction we measured a K_D of 7.7 µM (**Figure 15C**). On the other hand, significant interaction of ketoprofen with ALF was observed (**Figure 15B**). The data in the previous figure suggests that Ketoprofen-MRnS can be used as a sensitive probe to detect APA below the nanomolar range.

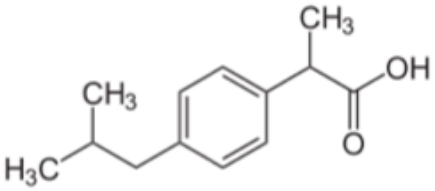

Ibuprofen

Molecule Info

- Drug
- FDA approved
- **Brand Name:** Advil
- **Uses:** NSAID, fever, pain relief.
- **Natural Target:** COX-1 and COX-2 nonselective.

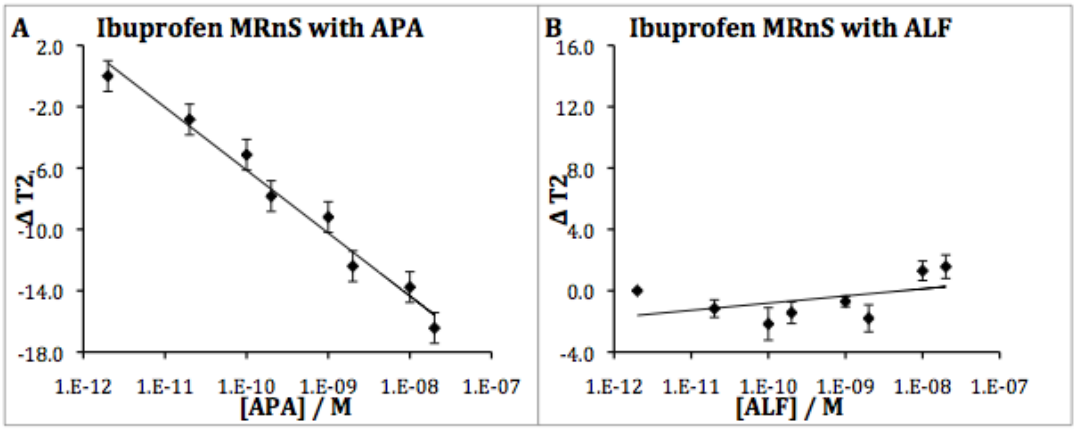

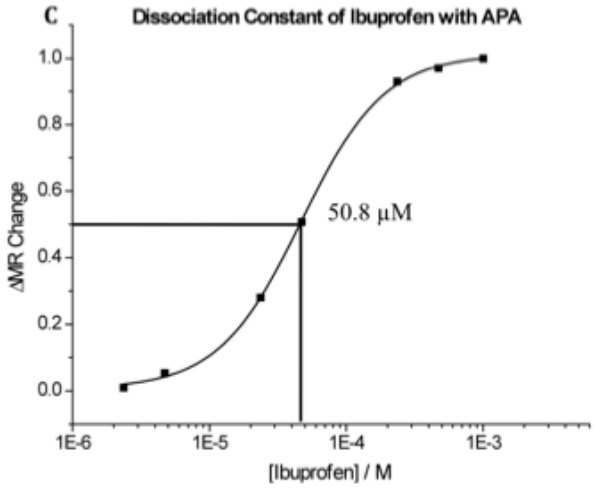

Figure 16. Studies with Ibuprofen.

Results of Ibuprofen-MRnS screening with APA and ALF (**Figure 16**):

The screening of the Ibuprofen-MRnS yielded positive results for the detection of the Anthrax Protective Antigen. Upon binding to the APA we observed a limit of detection of 2 nM and a maximum change of -16.9 on the ΔT_2 (**Figure 16A**). The negative change in ΔT_2 indicates the formation of clusters, which can be a result of multiple nanoparticles binding to either the same or different parts of the APA. For this interaction we measured a dissociation constant of 50.8 μM (**Figure 16C**). On the other hand, no significant interaction between Ibuprofen and ALF was observed (**Figure 16B**). The data in the previous figure suggests that Ibuprofen-MRnS can be used as a fast and sensitive probe to detect APA at the nanomolar range.

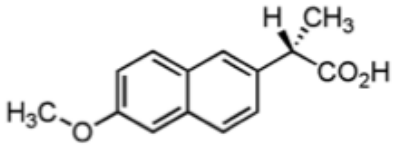

Naproxen

Molecule Info

- Drug
- FDA approved
- **Brand Name:** Aleve
- **Uses:** NSAID, Inflammation, Dysmenorrhea (menstrual cramps)
- **Natural Target:** COX-1 and COX-2 nonselective.

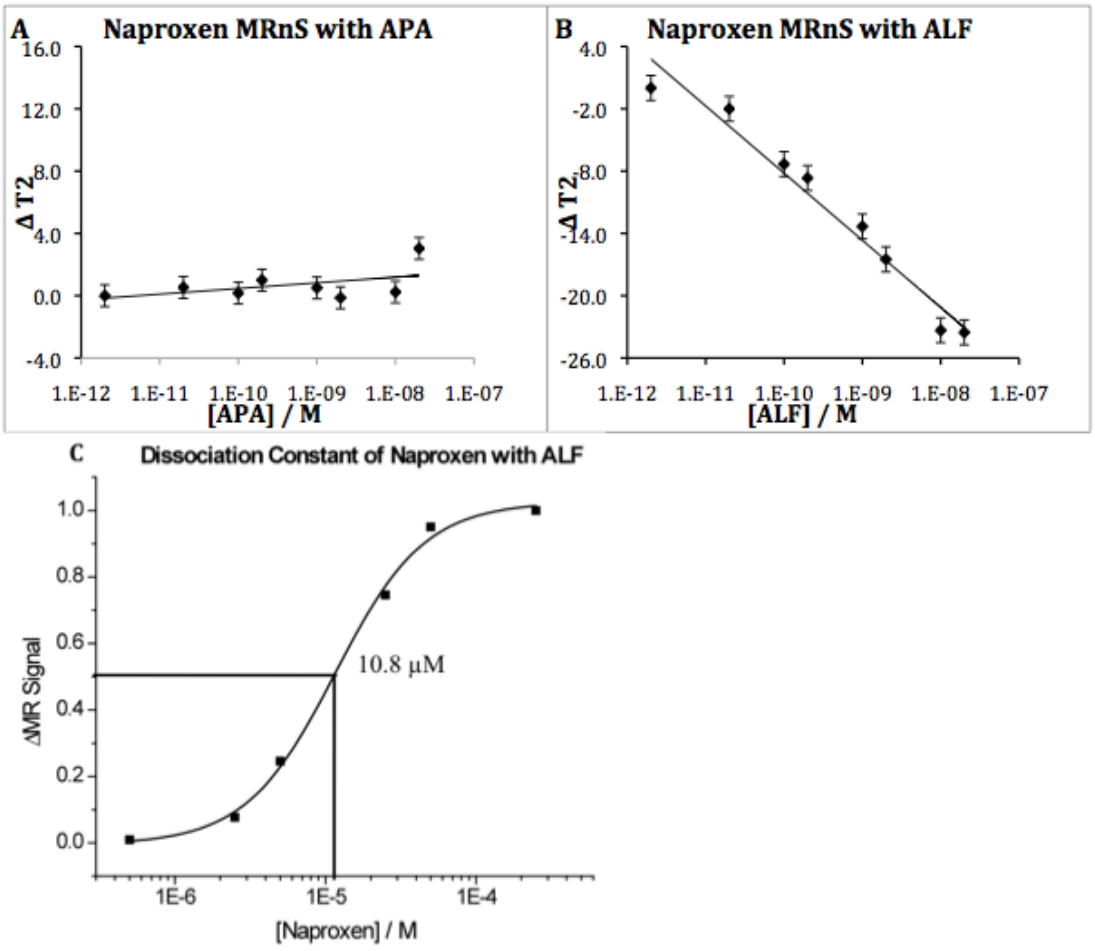

Figure 17. Studies with Naproxen.

Results of Naproxen-MRnS screening with APA and ALF (**Figure 17**):

The screening of the Naproxen-MRnS yielded positive results for the screening of Anthrax Lethal Factor. This positive result was confirmed by the binding of the Naproxen-MRnS to the ALF with a maximum change of -14.9 on the ΔT_2 and a limit of detection of 0.1 nN (**Figure 17B**). For this particular interaction we measured a K_D of 10.8 µM (**Figure 17C**). On the other hand, no significant interaction between Naproxen and APA was observed (**Figure 17A**). The data in the previous figure suggests that Naproxen-MRnS can be used as a sensitive probe to detect ALF below the nanomolar range. Additionally further experiments evaluating the potential of Naproxen to inhibit the enzymatic activity ALF need to be carried out in order assess the capability of Naproxen as a treatment for ALF.

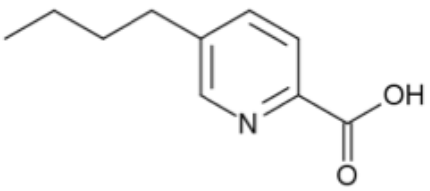

Fusaric acid

Molecule Info

- Inhibitor
- Not FDA approved
- **Brand Name:** None
- **Uses:** Prevents conversion of dopamine to norepinephrine.
- **Natural Target:** Dopamine beta-hydroxylase (DBH)

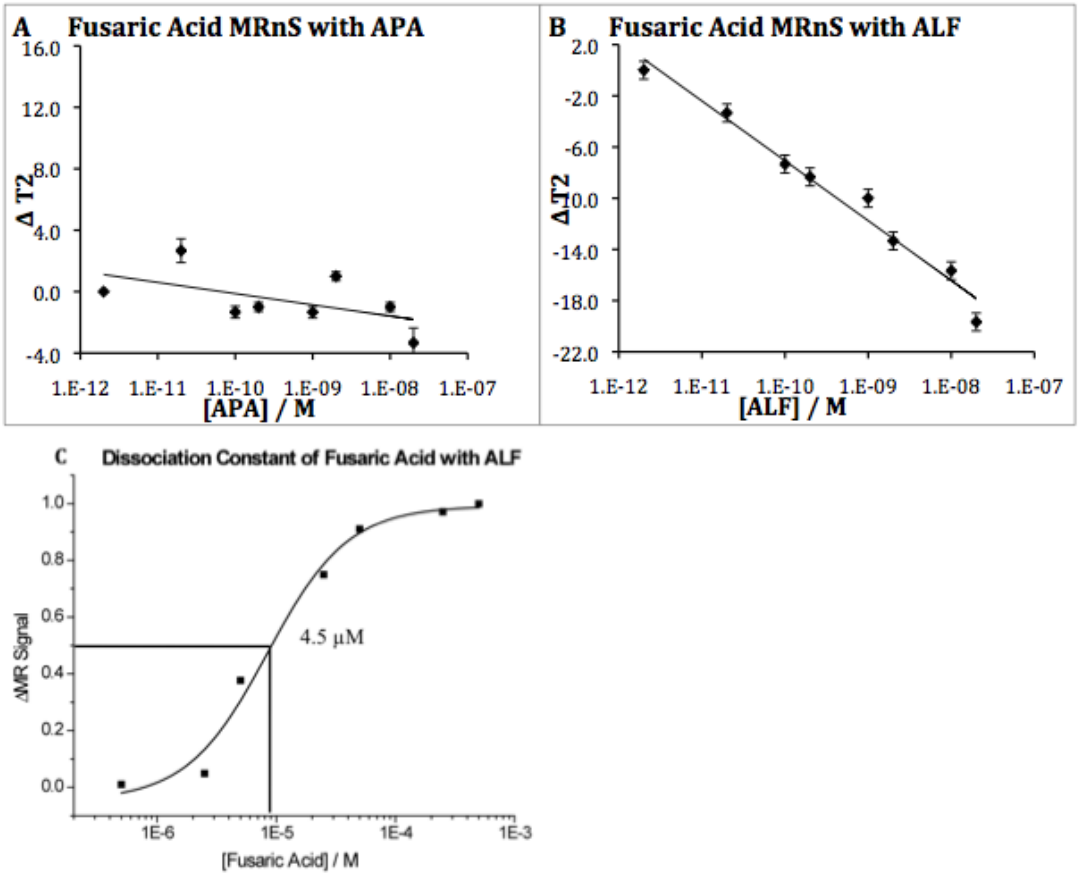

Figure 18. Studies with Fusaric Acid.

Results of Fusaric Acid-MRnS screening with APA and ALF (**Figure 18**):

The screening of the Fusaric Acid-MRnS yielded positive results for the screening Anthrax Lethal Factor. This positive result was confirmed by the binding of the Fusaric Acid-MRnS to the ALF with a maximum change of -19.7 on the ΔT_2 and a limit of detection of 0.02 nN (**Figure 18B**). For this particular interaction a K_D of 4.5 μM was measured (**Figure 18C**). Conversely, no significant interaction was observed between Fusaric Acid and APA (**Figure 18A**). The data in the previous figure suggests that Fusaric Acid-MRnS can be used to detect ALF with a sensitivity below the nanomolar range. Additionally further experiments evaluating the potential of Fusaric Acid to inhibit the enzymatic activity ALF need to be carried out in order assess its capability as a treatment for ALF.

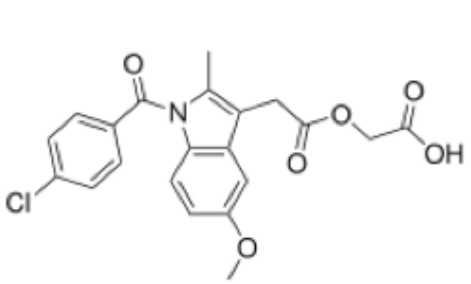

Acemetacin

Molecule Info

- Drug
- FDA approved
- **Brand Name:** Emflex
- **Uses:** NSAID, fever, arthritis and lower back pain.
- **Natural Target:** COX-1 and COX-2 nonselective.

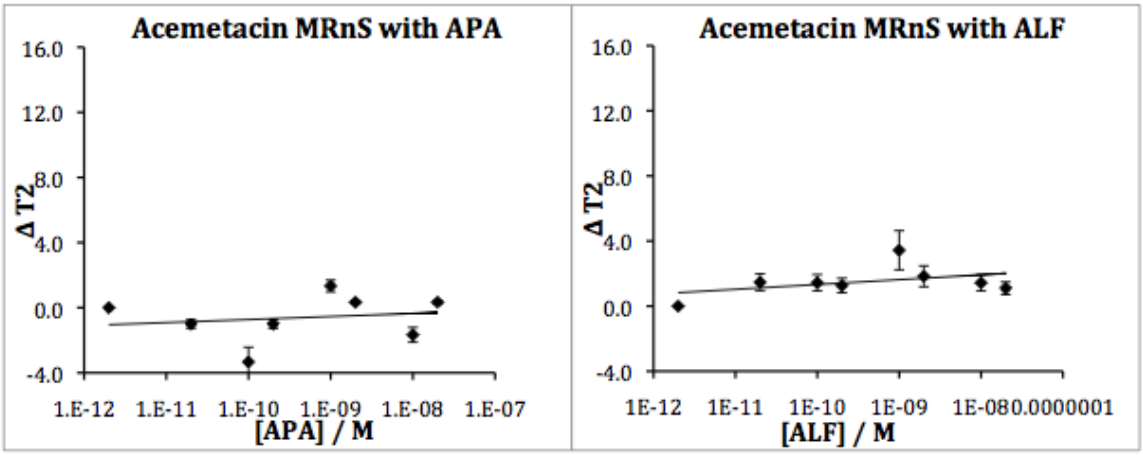

Figure 19. Studies with Acemetacin.
The screening of Acemetacin-MRnS provided negative results for both the APA and ALF. The lack of a MRnS signal with increasing concentration of either protein suggests that binding did not occur between Acemetacin and the components of the anthrax toxins.

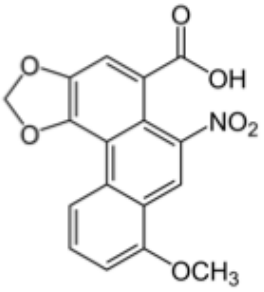

Aristolochic acid

Molecule Info

- Toxin
- Not FDA approved
- **Brand Name:** None
- **Uses:** herbal carcinogen, mutagen, and nephrotoxin.
- **Natural Target:** Bitter taste receptors

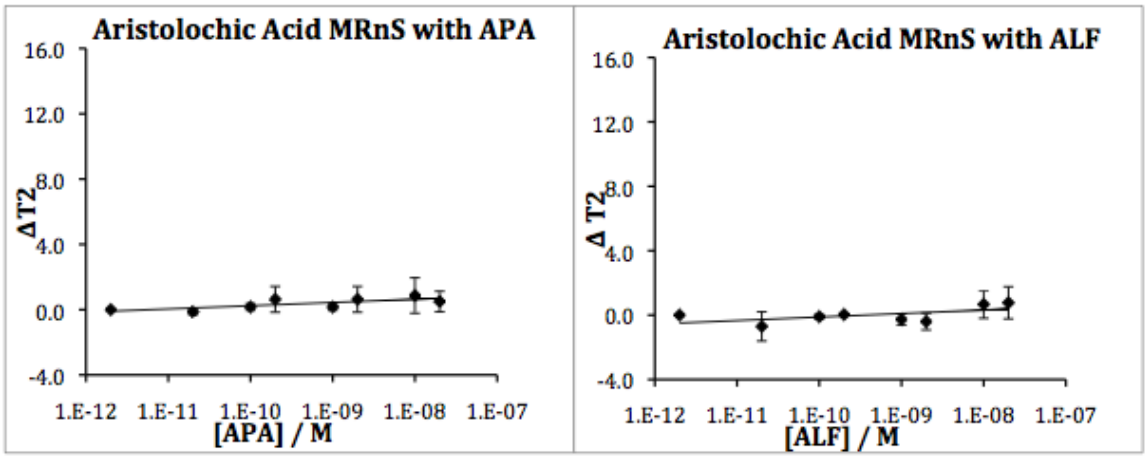

Figure 20. Studies with Aristolochic Acid.
The screening of Aristolochich Acid-MRnS provided negative results for both the APA and ALF. The lack of a MRnS signal with increasing concentration of either protein suggests that binding did not occur between Aristolochich acid and the components of the anthrax toxin.

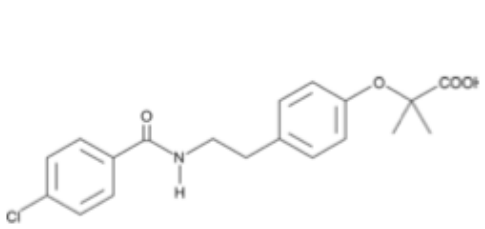

Bezafibrate

Molecule Info

- Drug
- FDA approved
- **Brand Name:** Bezalip
- **Uses:** Hyperlipidaemia
- **Natural Target:** Peroxisome proliferator-activated receptor alpha (PPARα)

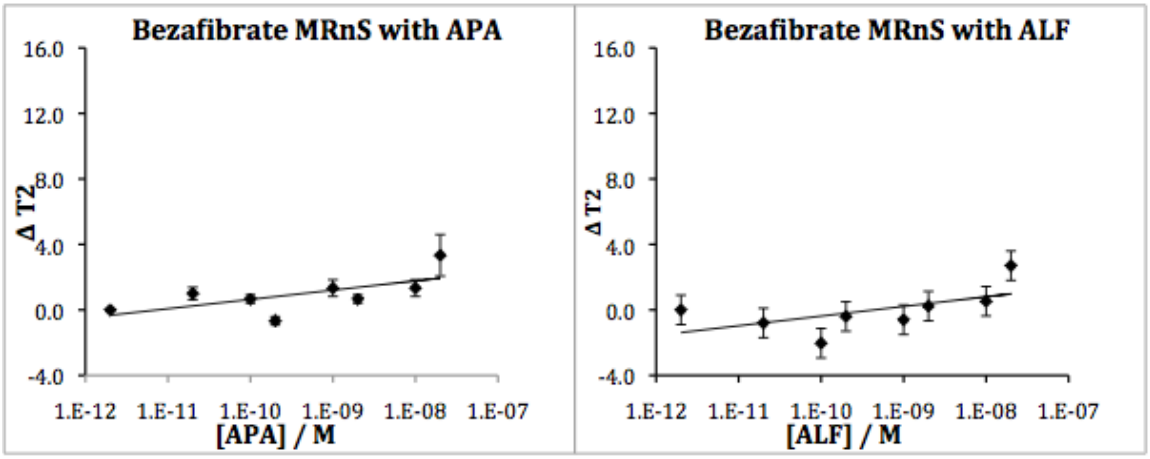

Figure 21. Studies with Bezafibrate.
The screening of Bezafibrate-MRnS provided negative results for both the APA and ALF. The lack of a MRnS signal with increasing concentration of either protein suggests that binding did not occur between Bezafibrate and the components of the anthrax toxin.

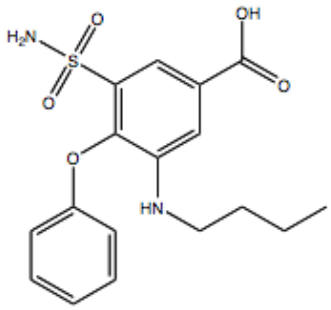

Bumetanide

Molecule Info

- Drug
- FDA approved
- **Brand Name:** Bumex
- **Uses:** Heart failure, Weight loss,
- **Natural Target:** NKCC1 cation-chloride cotransporter.

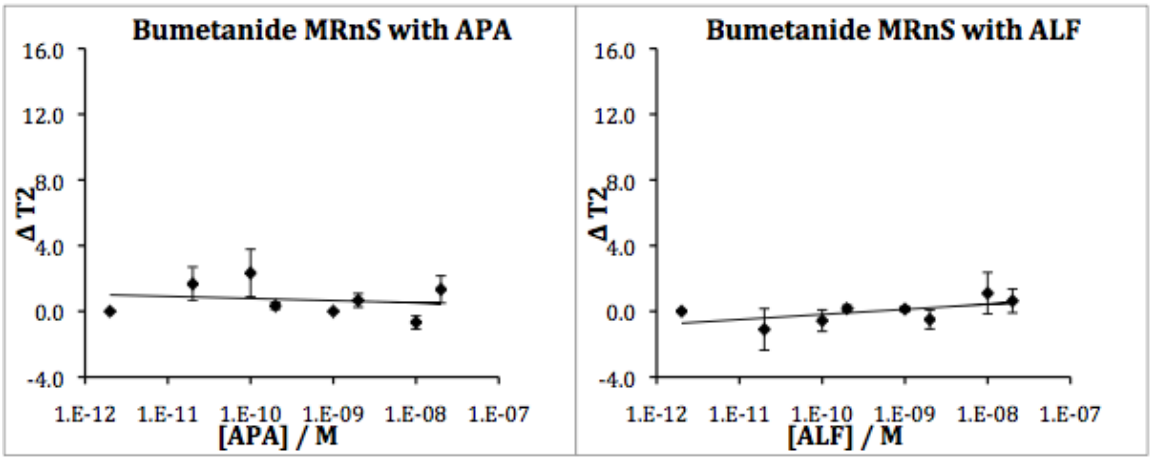

Figure 22. Studies with Bumetanide.
The screening of Bumetanide-MRnS provided negative results for both the APA and ALF. The lack of a MRnS signal with increasing concentration of either protein suggests that binding did not occur between Bumetanide and the components of the anthrax toxin.

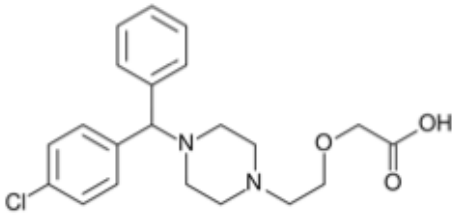

Ceterizine HCL

Molecule Info

- Drug
- FDA approved
- **Brand Name:** Zyrtec
- **Use:** Second-generation antihistamine
- **Natural Target:** Histamine H_1 receptor

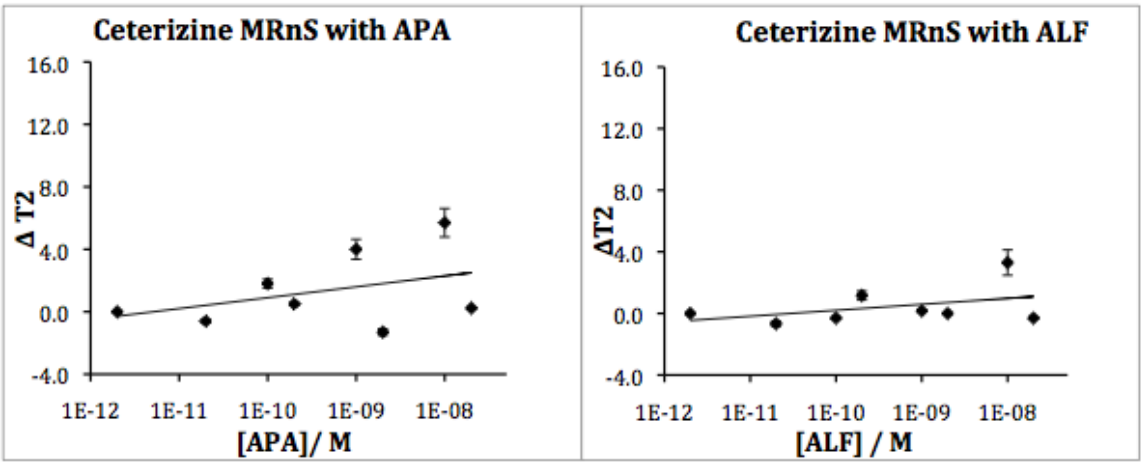

Figure 23. Studies with Ceterizine.
The screening of Ceterizine-MRnS provided negative results for both the APA and ALF. The lack of a MRnS signal with increasing concentration of either protein suggests that binding did not occur between Ceterizine and the components of the anthrax toxin.

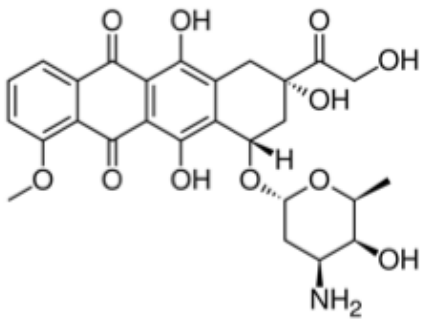

Doxorubicin

Molecule Info

- Drug
- FDA approved
- **Brand Name:** Andrimycin
- **Uses:** Wide-range chemotherapeutic, antibiotic.
- **Natural Target:** DNA Coils

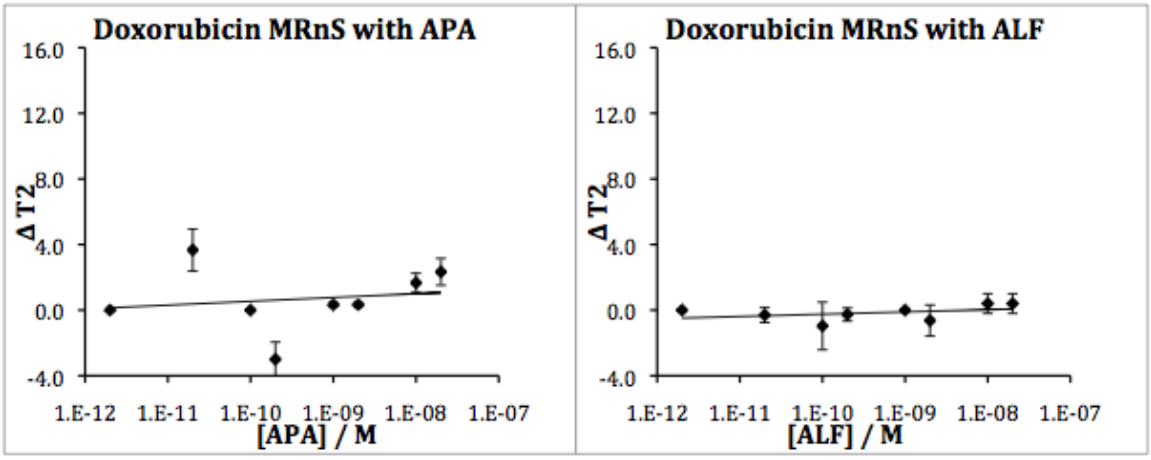

Figure 24. Studies with Doxorubicin.
The screening of Doxorubicin-MRnS provided negative results for both the APA and ALF. The lack of a MRnS signal with increasing concentration of either protein suggests that binding did not occur between Doxorubicin and the components of the anthrax toxin.

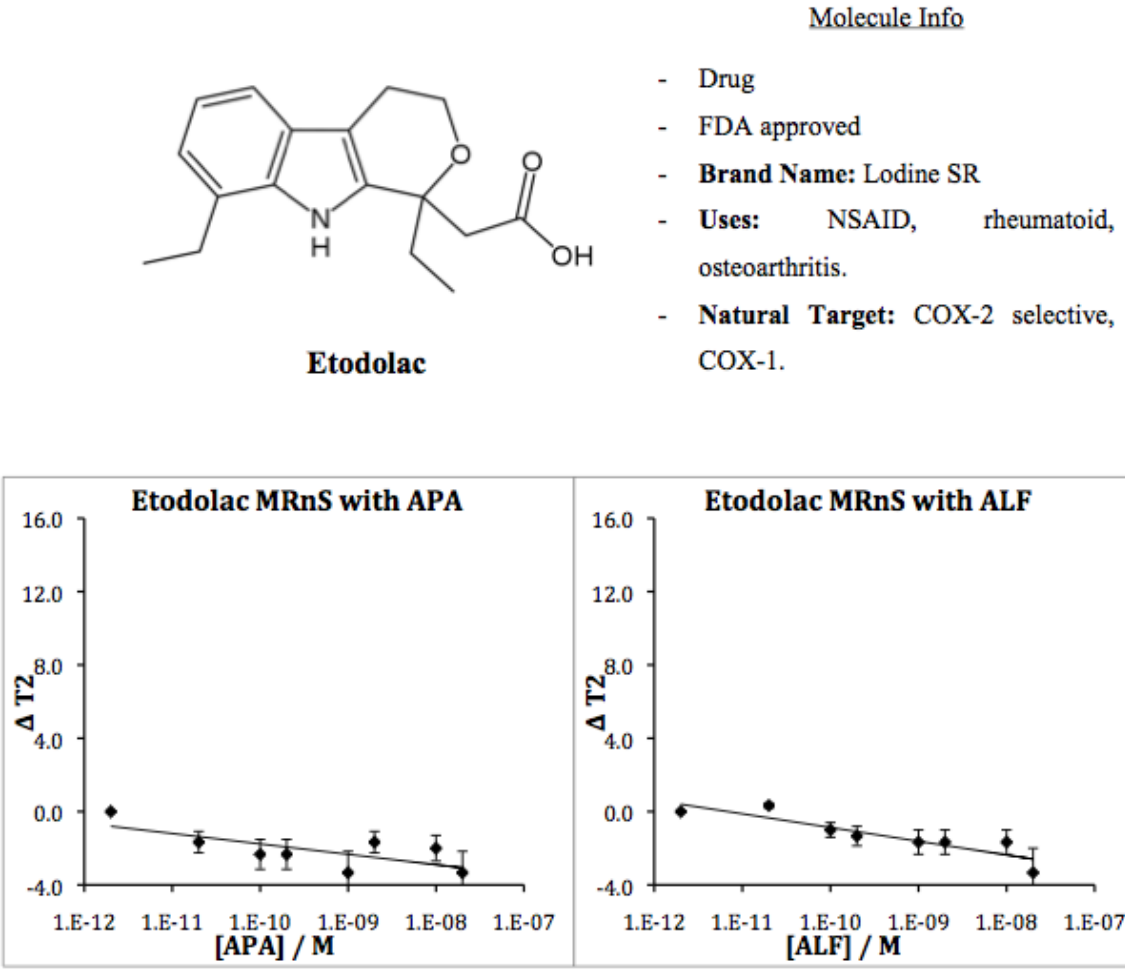

Figure 25. Studies with Etodolac.
The screening of Etodolac-MRnS provided negative results for both the APA and ALF. The lack of a MRnS signal with increasing concentration of either protein suggests that binding did not occur between Etodolac and the components of the anthrax toxins.

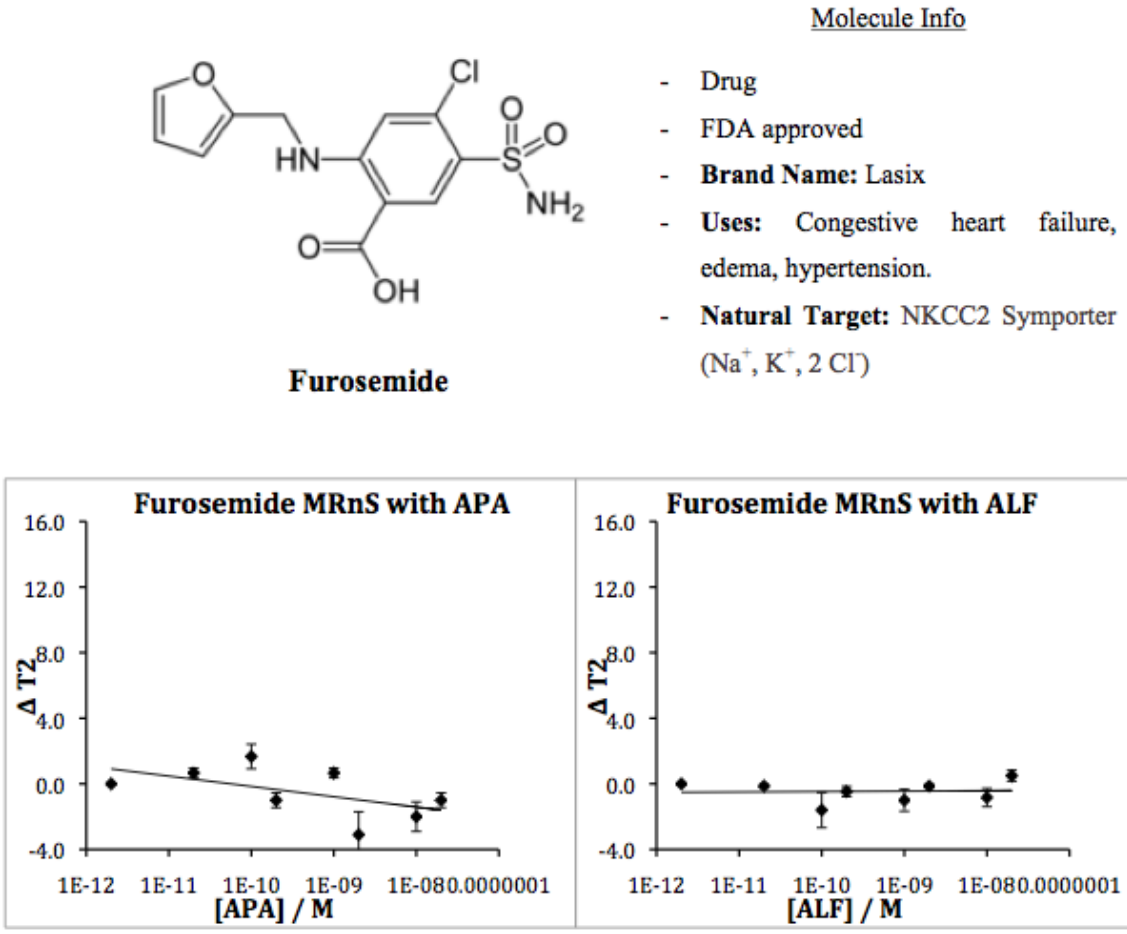

Figure 26. Studies with Furosemide.
The screening of Furosemide Acid-MRnS provided negative results for both the APA and ALF. The lack of a MRnS signal with increasing concentration of either protein suggests that binding did not occur between Furosemide acid and the components of the anthrax toxin.

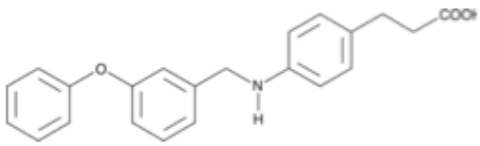

GW9508

Molecule Info

- Molecule
- Not FDA approved
- **Brand Name:** None
- **Uses:** Potentiates glucose stimulated insulin secretion.
- **Natural Target:** Agonist of GPR40 and GPR120 (G protein coupled) receptors

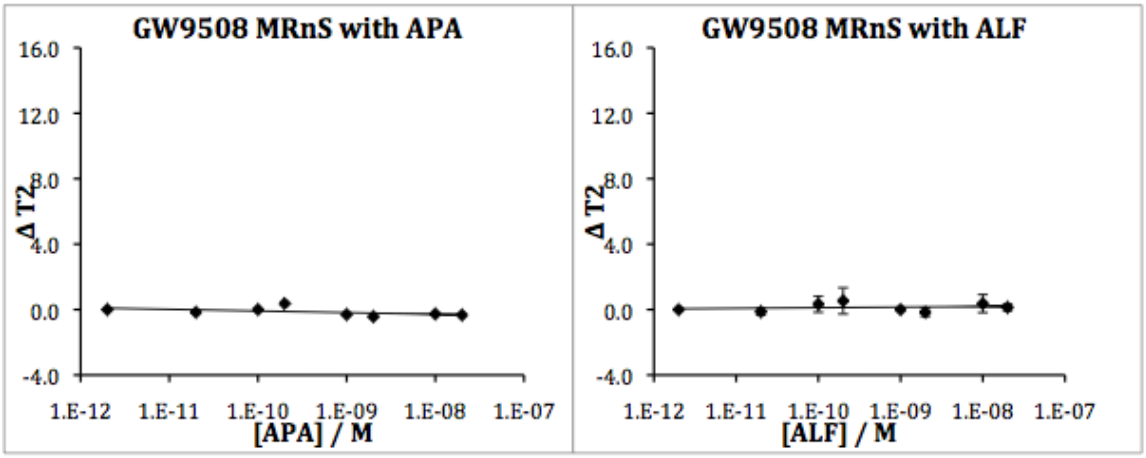

Figure 27. Studies with GW9508.
The screening of GW9508-MRnS provided negative results for both the APA and ALF. The lack of a MRnS signal with increasing concentration of either protein suggests that binding did not occur between GW9508 and the components of the anthrax toxin.

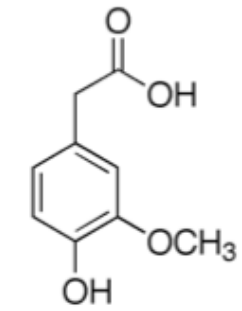

Homovanillic Acid

Molecule Info

- Metabolite
- Not FDA approved
- **Brand Name:** Indocin
- **Uses:** as a reagent to detect oxidative enzymes.
- **Natural Target:** None, it is a detectable metabolite.

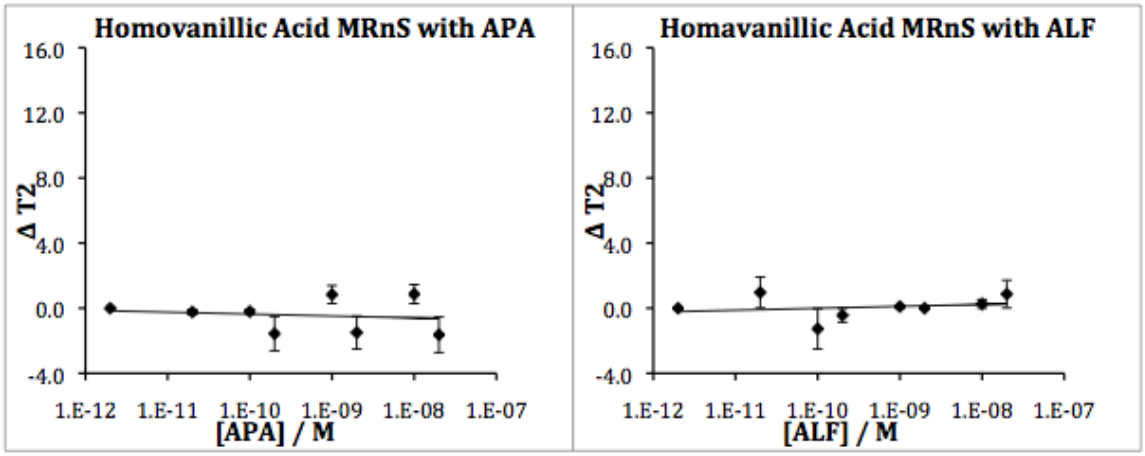

Figure 28. Studies with Homovanillic Acid.
The screening of Homovanillic Acid-MRnS provided negative results for both the APA and ALF. The lack of a MRnS signal with increasing concentration of either protein suggests that binding did not occur between Homovanillic Acid and the components of the anthrax toxin.

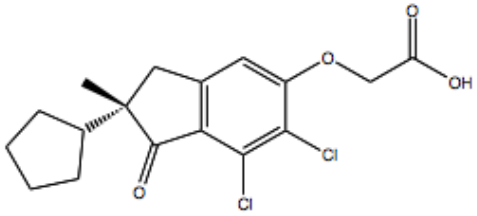

R(+)-IAA-94

Molecule Info

- Molecule
- Not FDA approved
- **Brand Name:** None
- **Uses:** Selective chloride channel inhibition.
- **Natural Target:** Skeletal/smooth muscle and epi/endothelial neuronal chloride channels.

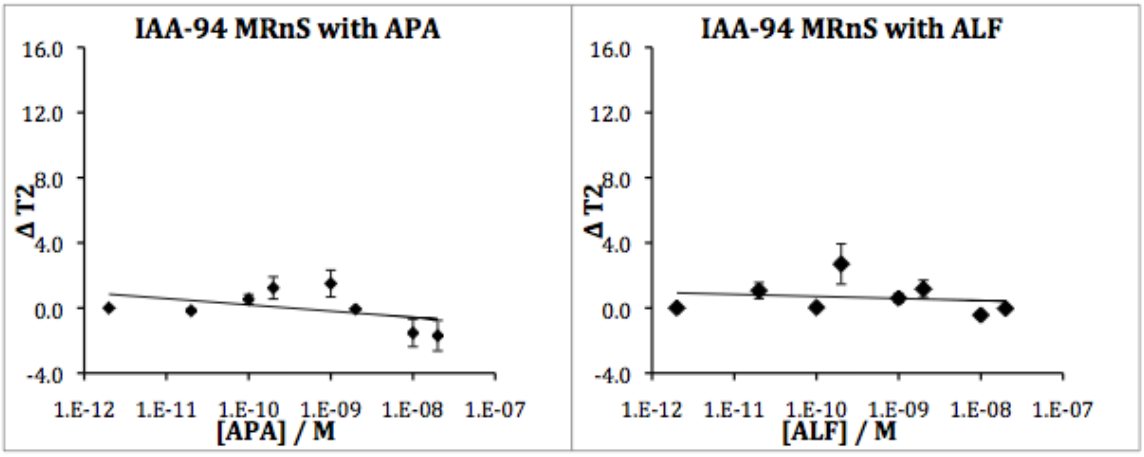

Figure 29. Studies with IAA-94.
The screening of IAA94-MRnS provided negative results for both the APA and ALF. The lack of a MRnS signal with increasing concentration of either protein suggests that binding did not occur between IAA-94 and the components of the anthrax toxin.

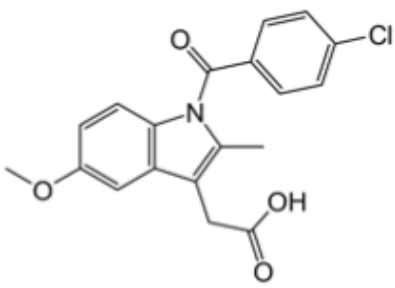

Indometacin

Molecule Info

- Drug
- FDA approved
- **Brand Name:** Indocin
- **Uses:** NSAID, pain relief, fever, stiffness.
- **Natural Target:** COX-1 and COX-2 nonselective.

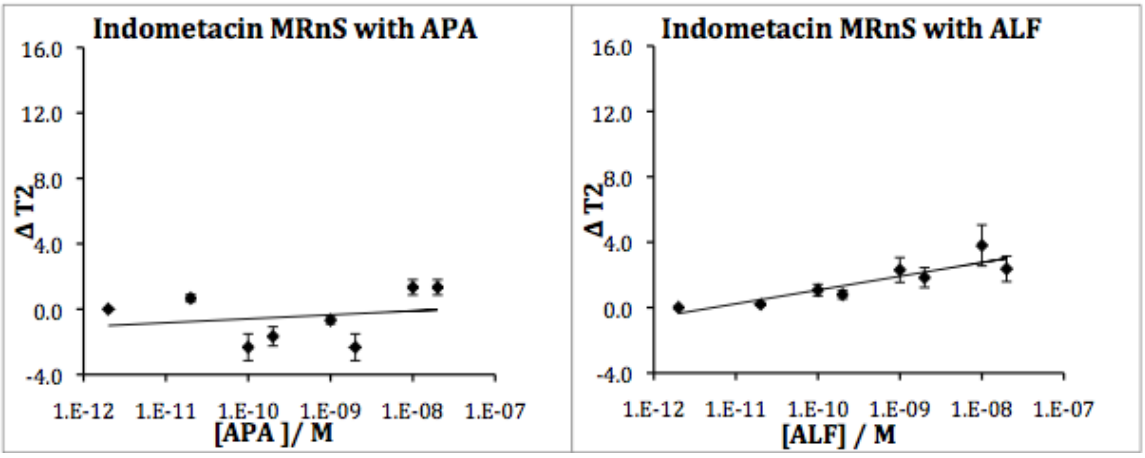

Figure 30. Studies with Indometacin.
The screening of Indometacin-MRnS provided negative results for both the APA and ALF. The lack of a MRnS signal with increasing concentration of either protein suggests that binding did not occur between Indometacin and the components of the anthrax toxin.

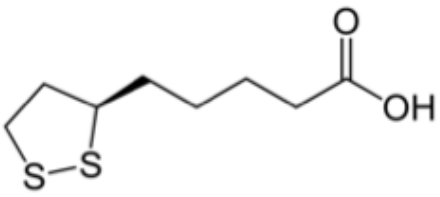

Lipoic Acid

Molecule Info

- Metabolite, Drug
- Not FDA approved
- **Brand Name:** None
- **Uses:** Polyneuropathies
- **Natural Target:** pyruvate dehydrogenase complex (PDC), acetoin dehydrogenase complex (ADh), 2-oxoglutarate dehydrogenase complex (OGDH), branched chain oxoacid dehydrogenase complex (BCDH).

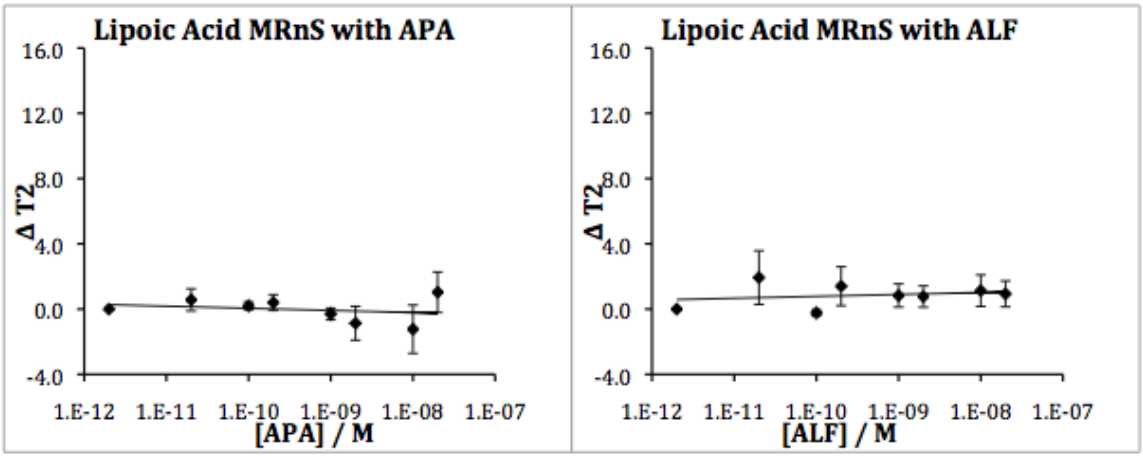

Figure 31. Studies with Lipoic Acid.
The screening of Lipoic Acid-MRnS provided negative results for both the APA and ALF. The lack of a MRnS signal with increasing concentration of either protein suggests that binding did not occur between Lipoic Acid and the components of the anthrax toxin.

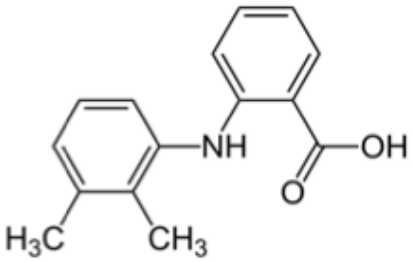

Mefenamic Acid

Molecule Info

- Drug
- FDA approved
- **Brand Name:** Ponstel
- **Uses:** NSAID, pain relief, Dysmenorrhea (menstrual cramps)
- **Natural Target:** COX-1 and COX-2 nonselective.

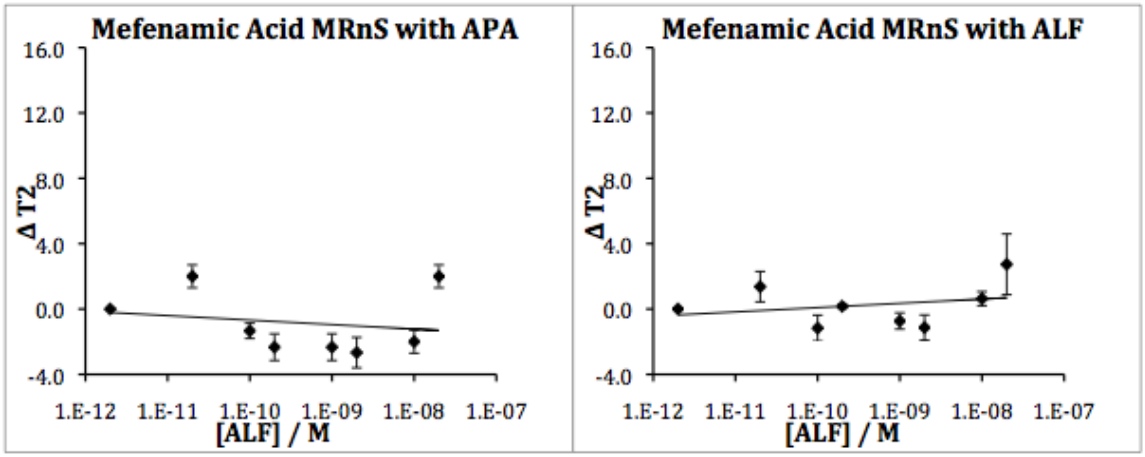

Figure 32. Studies with Mefenamic Acid.
The screening of Mefenamic Acid-MRnS provided negative results for both the APA and ALF. The lack of a MRnS signal with increasing concentration of either protein suggests that binding did not occur between Mefenamic Acid and the components of the anthrax toxin.

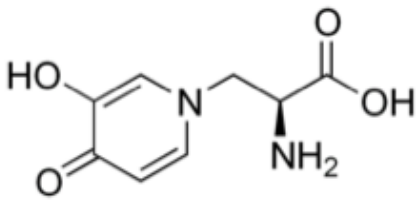

L-Mimosine

Molecule Info

- Non-protein free amino acid
- Not FDA approved
- **Brand Name:** None
- **Uses:** Anticancer properties, inhibits DNA replication initiation.
- **Natural Target:** Ribonucleotide Reductase (RNR), Hydroxylmethyltansferase (SHMT)

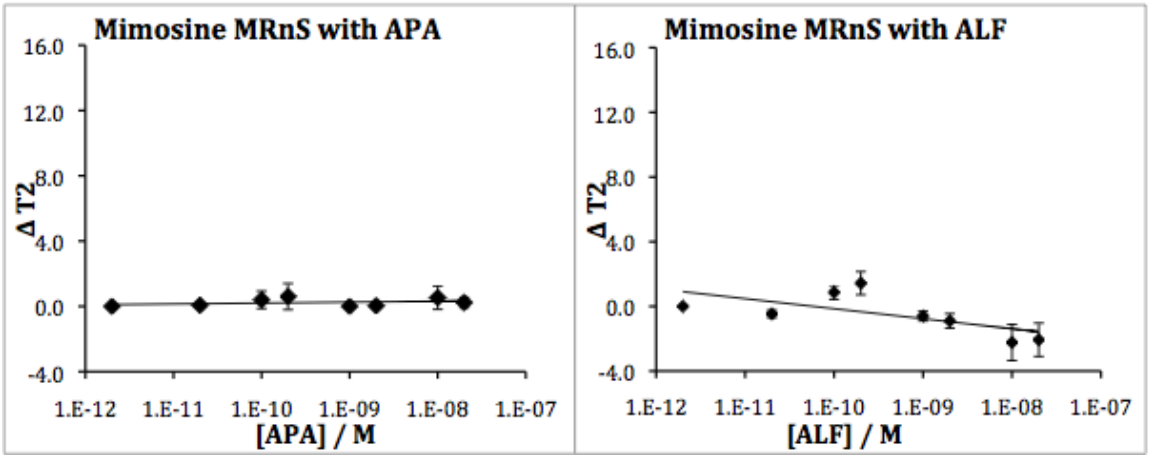

Figure 33. Studies with L-Mimosine.
The screening of Mimosine-MRnS provided negative results for both the APA and ALF. The lack of a MRnS signal with increasing concentration of either protein suggests that binding did not occur between Mimosine and the components of the anthrax toxin.

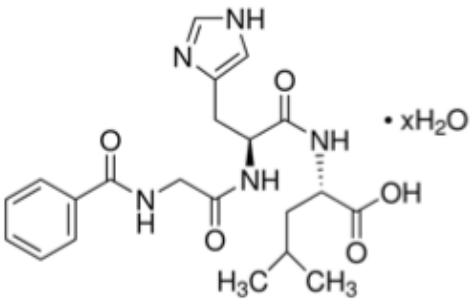

N-Hippuryl-His-Leu Hydrate (N-Benzoyl-Gly-His-Leu)

Molecule Info

- Substrate
- Not FDA approved
- **Brand Name:** None
- **Uses:** Angiotensin converting enzyme (ACE) assays
- **Natural Target:** Angiotensin converting enzyme (ACE)

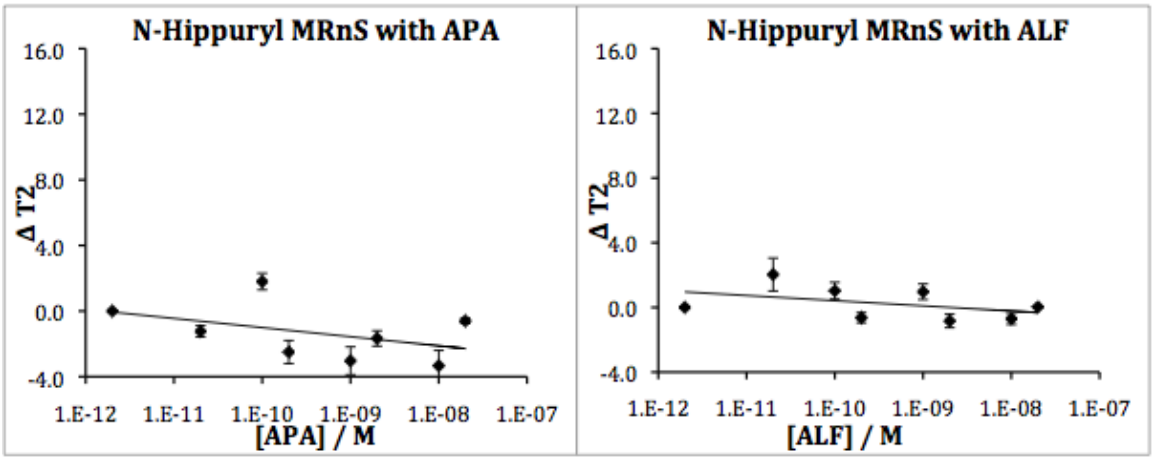

Figure 34. Studies with N-Hippuryl-His-Leu Hydrate (N-Benzoyl-Gly-His-Leu). The screening of N-Hippuryl-MRnS provided negative results for both the APA and ALF. The lack of a MRnS signal with increasing concentration of either protein suggests that binding did not occur between N-Hyppuryl and the components of the anthrax toxin.

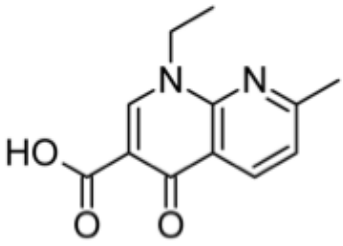

Nalidixic Acid

Molecule Info

- Drug
- FDA approved
- **Brand Name:** Nevigramon
- **Uses:** Antibiotic, gram (-) bacteria, Urinary tract infections.
- **Natural Target:** DNA gyrase.

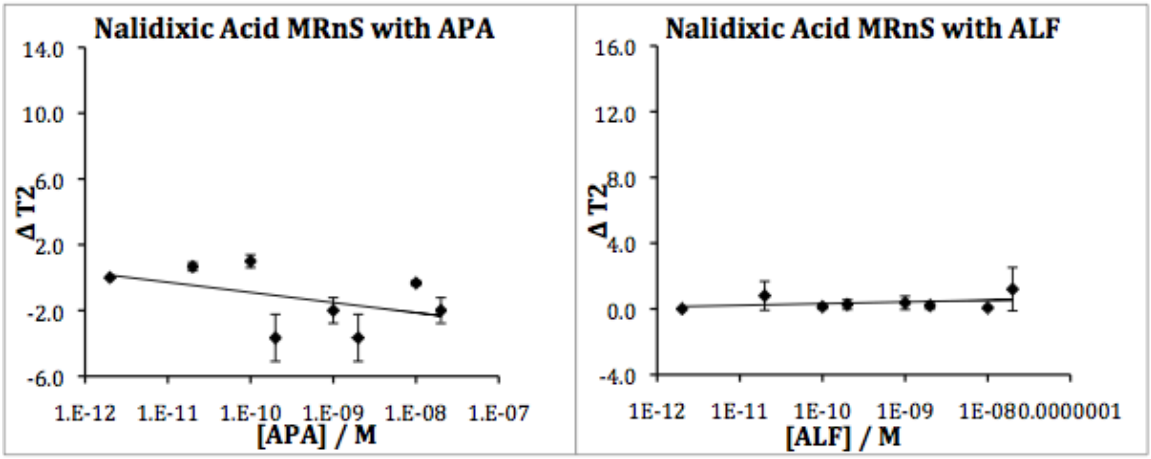

Figure 35. Studies with Nalidixic Acid.
The screening of Nalidixic Acid-MRnS provided negative results for both the APA and ALF. The lack of a MRnS signal with increasing concentration of either protein suggests that binding did not occur between Nalidixic Acid and the components of the anthrax toxin.

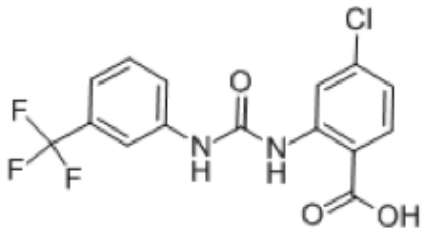

NS3694

Molecule Info

- Inhibitor
- Not FDA approved
- **Brand Name:** None
- **Uses:** inhibitor of apoptosome formation.
- **Natural Target:** the cytochrome *c*-induced formation of the active apoptosome.

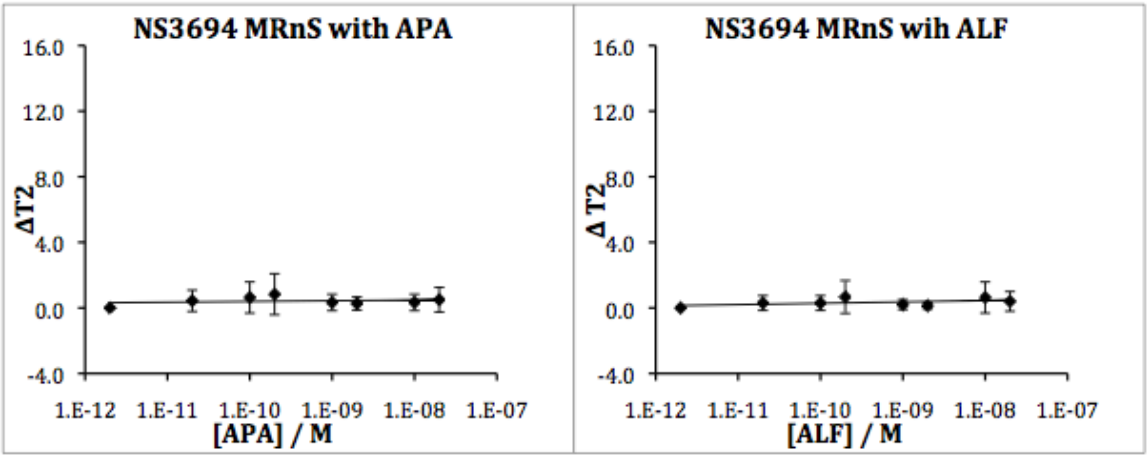

Figure 36. Studies with NS3694.
The screening of NS3694-MRnS provided negative results for both the APA and ALF. The lack of a MRnS signal with increasing concentration of either protein suggests that binding did not occur between NS3694 and the components of the anthrax toxin.

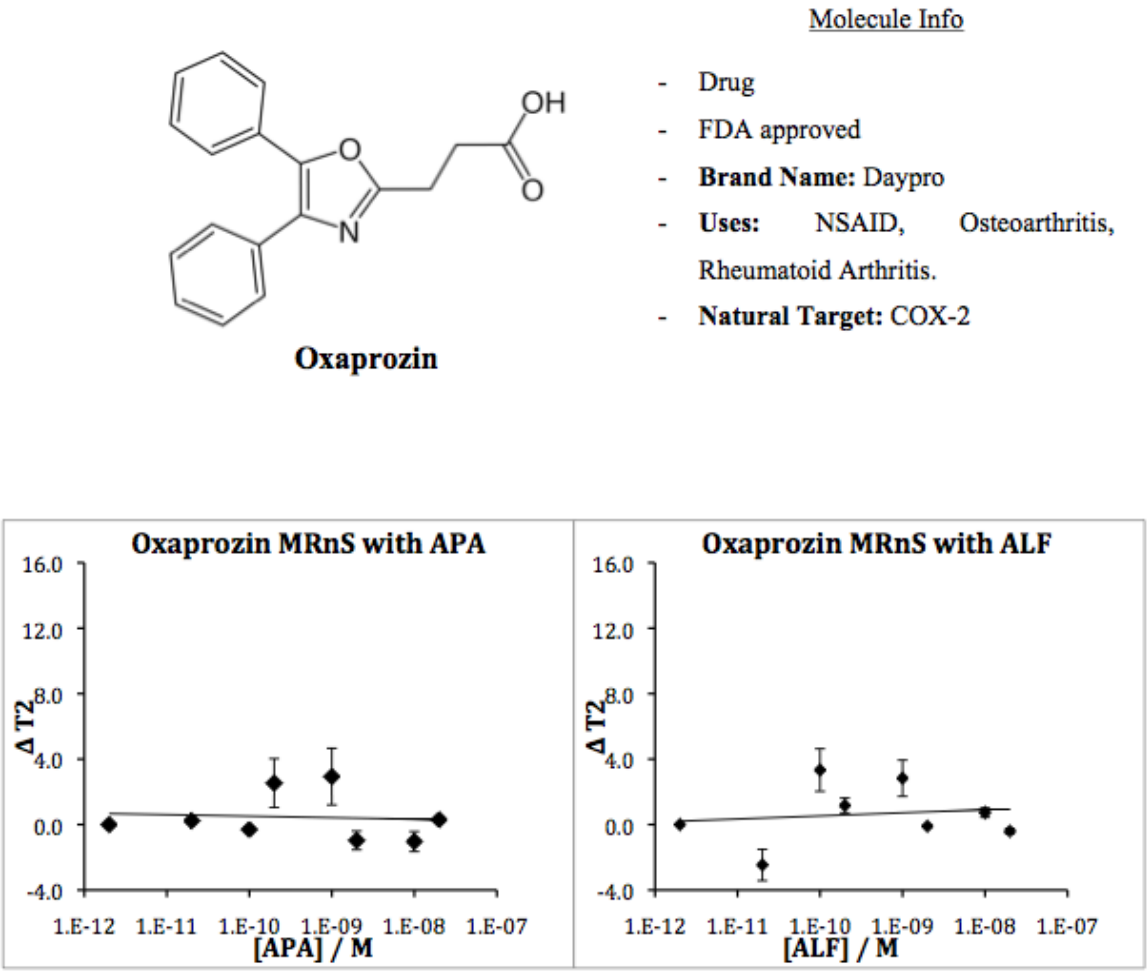

Figure 37. Studies with Oxaproxin.
The screening of Oxaprozin-MRnS provided negative results for both the APA and ALF. The lack of a MRnS signal with increasing concentration of either protein suggests that binding did not occur between Oxaprozin and the components of the anthrax toxin.

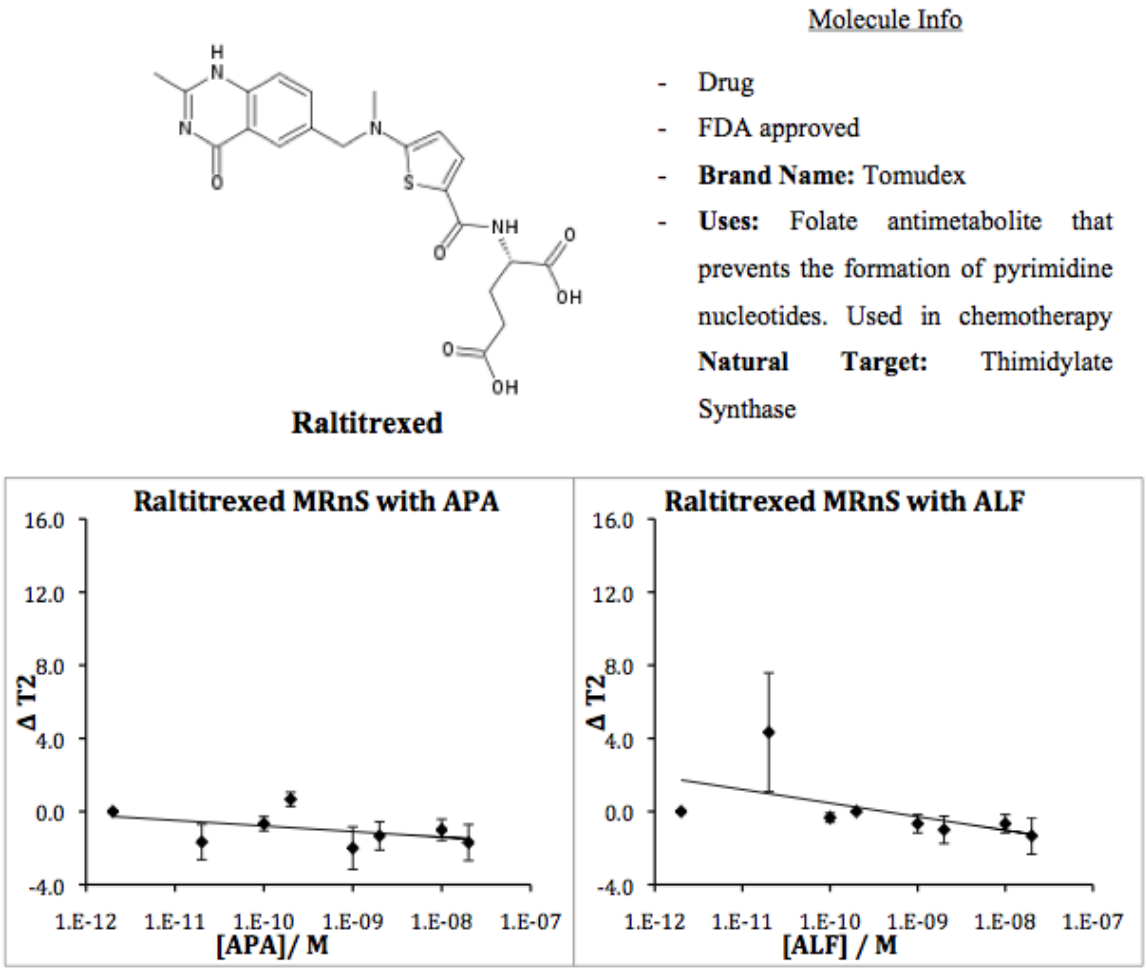

Figure 38. Studies with Raltitrexed.
The screening of Raltitrexed-MRnS provided negative results for both the APA and ALF. The lack of a MRnS signal with increasing concentration of either protein suggests that binding did not occur between Raltitrexed and the components of the anthrax toxin.

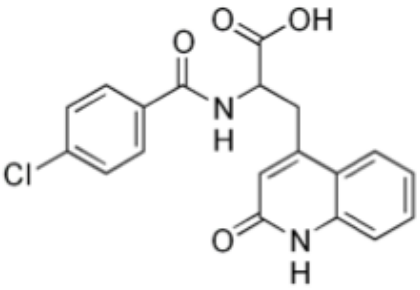

Rebamipide

Molecule Info

- Drug
- Clinical Trials Phase 3
- **Brand Name:** Mucosta
- **Uses:** Gastric Ulcers, Behcet's Disease.
- **Natural Target:** Mesenchymal cells of lamina propria mucosae, iNOS-immunoreactive cells.

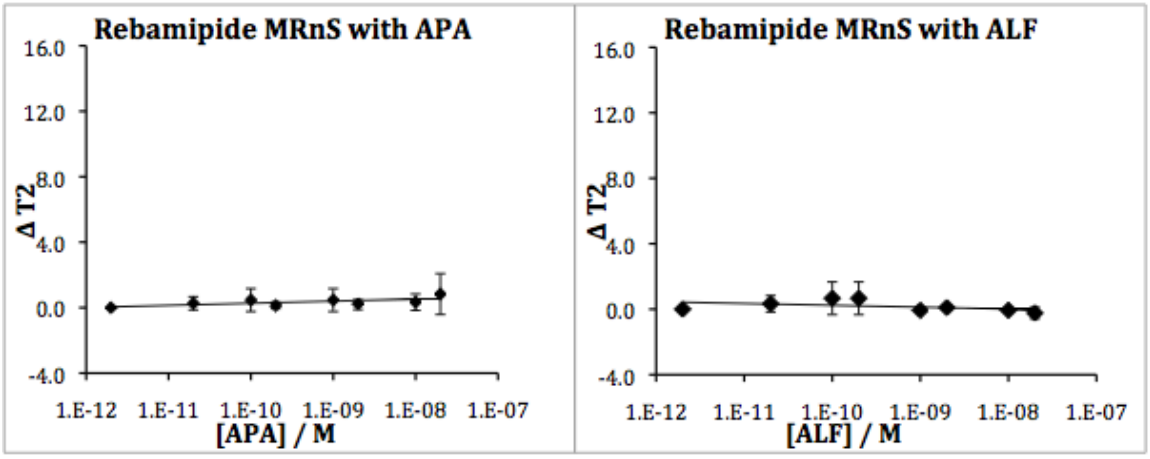

Figure 39. Studies with Rebamipide.
The screening of Rebamipide-MRnS provided negative results for both the APA and ALF. The lack of a MRnS signal with increasing concentration of either protein suggests that binding did not occur between Rebamipide and the components of the anthrax toxin.

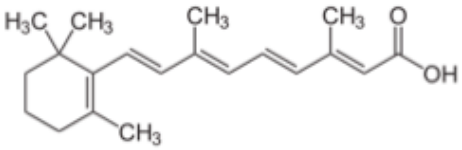

Retinoic Acid

Molecule Info

- Drug
- FDA approved
- **Brand Name:** Avita
- **Uses:** Acne, Acute Myeloid Leukemia
- **Natural Target:** Retinoic acid receptor (RAR)

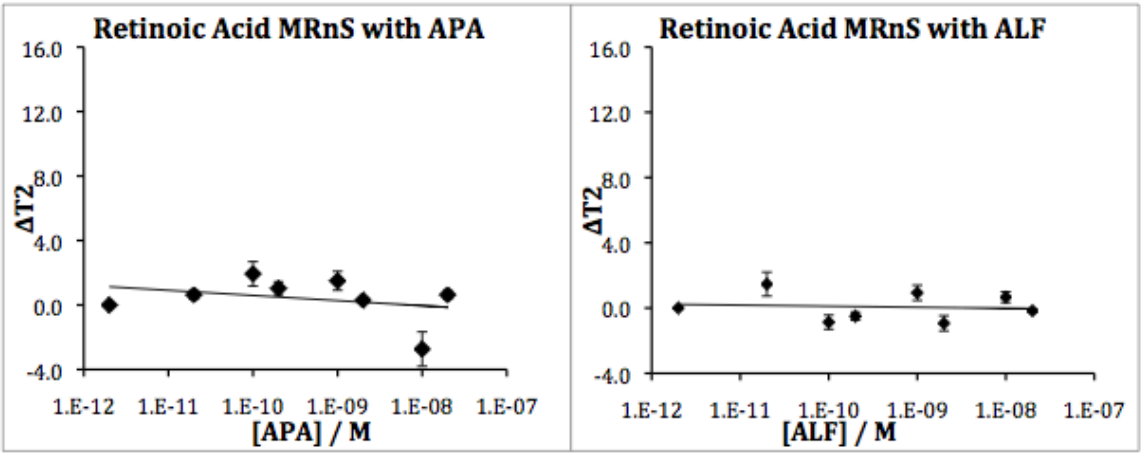

Figure 40. Studies with Retinoic Acid.
The screening of Retinoic Acid-MRnS provided negative results for both the APA and ALF. The lack of a MRnS signal with increasing concentration of either protein suggests that binding did not occur between Retinoic Acid and the components of the anthrax toxin.

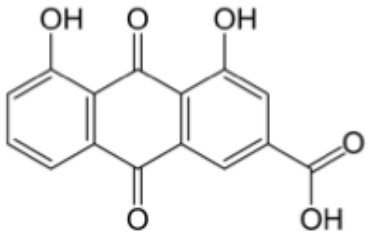

Rhein

Molecule Info

- Drug
- Not FDA approved
- **Brand Name:** none
- **Use:** proposed antibiotic
- **Natural Target:** Unknown

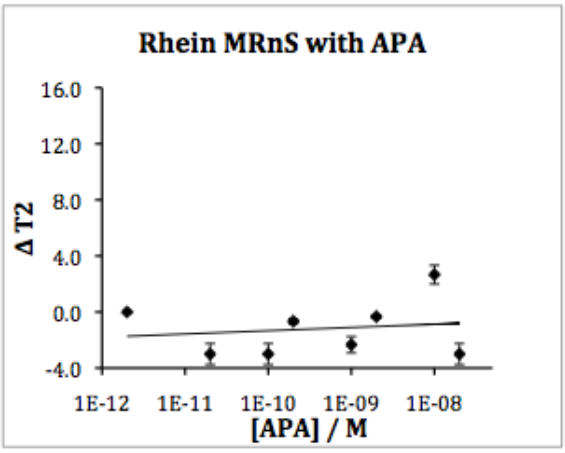

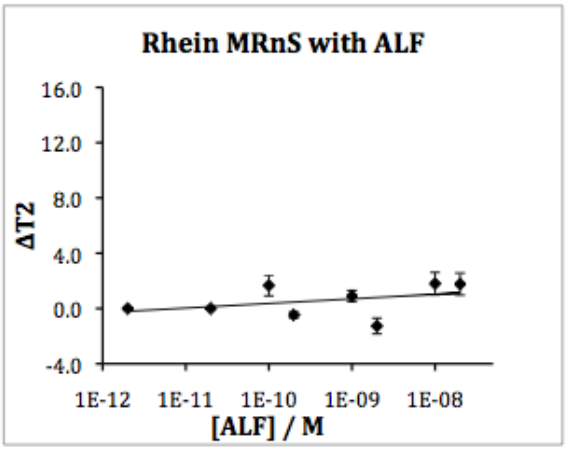

Figure 41. Studies with Rhein.
The screening of Rhein-MRnS provided negative results for both the APA and ALF. The lack of a MRnS signal with increasing concentration of either protein suggests that binding did not occur between Rhein and the components of the anthrax toxin.

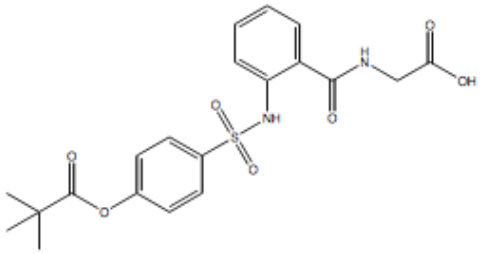

Sivelestat

Molecule Info

- Drug
- FDA approved
- **Brand Name:** Sivelestat
- **Uses:** Acute respiratory failure
- **Natural Target:** Human Neutrophil elastase.

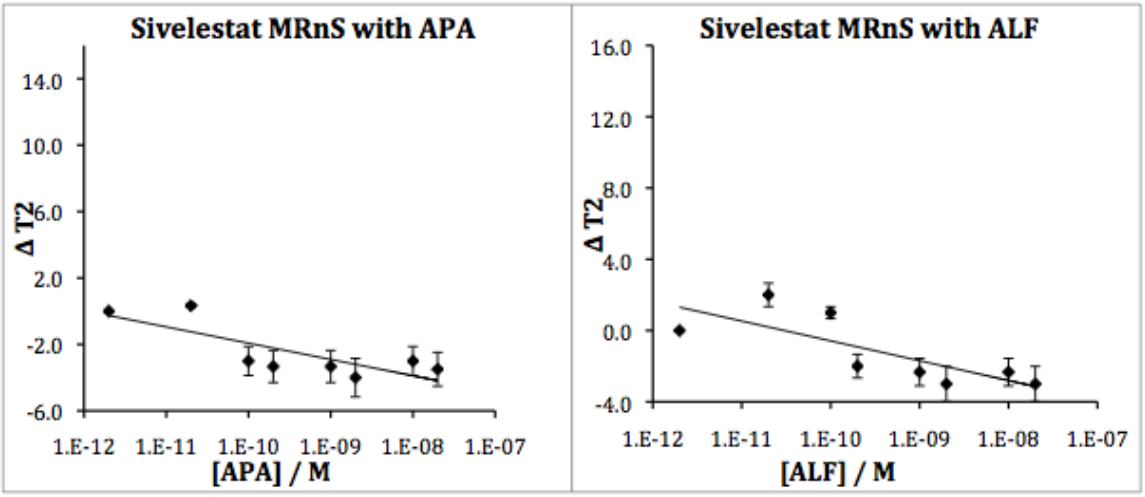

Figure 42. Studies with Sivelestat.
The screening of Sivelestat-MRnS provided negative results for both the APA and ALF. The lack of a MRnS signal with increasing concentration of either protein suggests that binding did not occur between Sivelestat and the components of the anthrax toxin.

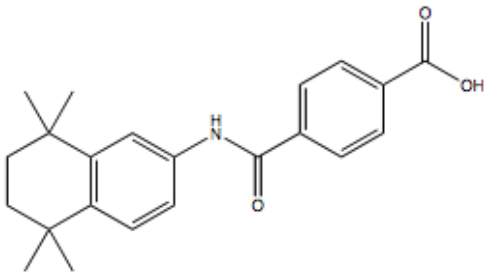

Tamibarotene

Molecule Info

- Drug
- Clinical trials Phase 2
- **Brand Name:** Tamibarotene
- **Uses:** Non-Small-Cell Lung Cancer, Acute Myeloid Leukemia
- **Natural Target:** Retinoic acid receptor

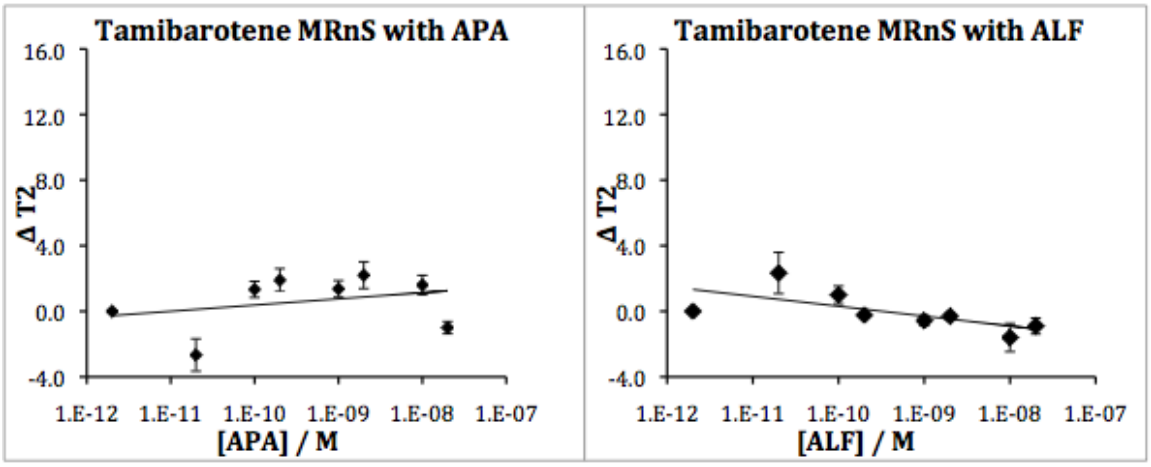

Figure 43. Studies with Tamibarotene.
The screening of Tamibarotene-MRnS provided negative results for both the APA and ALF. The lack of a MRnS signal with increasing concentration of either protein suggests that binding did not occur between Tamibarotene and the components of the anthrax toxin.

Table 4. Summary of the screening of the Small Molecules against APA and ALF.

	Small Molecule Library	Anthrax Protective Antigen (PA)	Anthrax Lethal Factor (LF)
1	Sulindac	K_d= 3.34 µM	K_d= 2.8 µM
2	Ketoprofen	K_d= 7.70 µM	-
3	Ibuprofen	K_d= 50.8 µM	-
4	Naproxen	-	K_d= 10.8 µM
5	Fusaric Acid	-	K_d= 4.5 µM
6	3-Iodo-L-tyrosine	Insoluble	Insoluble
7	Acemetacin	-	-
8	Aristolochic Acid I	-	-
9	Bezafibrate	-	-
10	Bumetanide	-	-
11	Ceterizine HCL	-	-
12	Deoxycholate	Insoluble	Insoluble
13	Doxorubicin	-	-
14	Enoxacin	Insoluble	Insoluble
15	Etodolac	-	-
16	Furosemide	-	-
17	GW9508	-	-
18	Homovanilic Acid	-	-
19	Indometacin	-	-
20	L-Mimosine	-	-
21	Lipoic Acid	-	-
22	Mefenamic Acid	-	-
23	Mycophenolic acid	No Reaction	No Reaction
24	N-Hippuryl-His-Leu	-	-
25	Nalidixic Acid	-	-
26	NS3694	-	-
27	Oxaprozin	-	-
28	R(+)-IAA-94	-	-
29	Raltiterexed	-	-
30	Rebamipide	-	-
31	Retinoic Acid	-	-
32	Rhein	-	-
33	Sivelestat	-	-
34	Tamibarotene	-	-

Molecules shaded in gray were not screened since the necessary chemical modifications were not feasible or their solubility did not allow for reactions to occur.

Conclusions

- We have assembled a small-molecule library composed of commercially available molecules, most of them being FDA approved drugs.
- We assembled a small-molecule-MRnS library by coupling each of the small molecules on the surface of MRnS using click chemistry.
- Thirty small-molecule-MRnS were screened for binding against the Anthrax Protective Antigen and Anthrax Lethal Factor using magnetic relaxation as the detectable signal.
- Three molecules, sulindac, ketoprofen and ibuprofen were identified to bind the APA with concentrations in the micromolar range.
- Three molecules, sulindac, naproxen and fusaric acid were identified to bind the ALF with concentrations in the low micromolar range.
- The results from screening the library provided five new sensitive magnetic probes that can be used to detect the anthrax toxins into the nanomolar range.

Discussion

The lack of toxin-targeted therapeutics together with the devastating consequences that bacterial toxins have on their hosts, have created a need for drugs that directly target and inhibit bacterial toxins. With the emergence of antibiotic-resistant bacteria and the increasing threat of bacteriological weapons over the last decade, there have been increasing interests in the development of therapeutics that can treat toxins. Yet, the lack of incentive for pharmaceutical companies due to the expenses associated

with the development and government-mandated review process of a new drug have hampered the development of any toxin therapeutic. Several approaches have been investigated but none of them have progressed farther than preliminary animal studies in a laboratory setting. Specifically in the case of Anthrax, a rapidly progressing disease that kills by the release of potent toxins, several toxin inhibitors have been identified but have not moved forward to clinical use.

With the purpose of filling this void in toxin therapeutics, we came up with a system to find currently available and FDA approved drugs that can be used to treat and detect bacterial toxin pathogenesis. Using drugs that are currently used to treat other diseases will lessen the time and expenses required for the FDA to approve these drugs for the treatment of the anthrax toxin since it makes the approval process less stringent. In order to achieve this task, we decided to screen a library of small molecules against two protein components of the anthrax toxins (ALF and APA). The anthrax toxin was chosen as a model system due to its rapid and devastating progress as well as its potential to infect a large number of individuals due to its development as a biological weapon. In order to evaluate the interactions between the small molecules and the proteins we resorted to magnetic relaxation nanosensors (MRnS), a system that has been traditionally used to sensitively and accurately detect several pathogens in the past. By conjugating each of the small molecules to the surface of a MRnS we created a small molecule-MRnS library that was screened for binding to both the Anthrax Protective Antigen (APA) and the Anthrax Lethal Factor (ALF). Upon completion of the screening, we identified 5 commonly available molecules that bound either the APA, ALF or both. Furthermore, we measured the dissociation constant between these small molecules and the proteins

yielding strong affinities in the micromolar range. One interesting fact is that four of these molecules are non-steroidal anti-inflammatory drugs that can currently be purchased at any pharmacy.

Even though the screening identified 5 small molecules that can bind to the components of the anthrax toxin, work is still needed to evaluate whether they can inhibit the toxin. The proteins screened play a crucial role in the development of Anthrax, specifically APA is responsible for introducing the Edema Factor and the ALF into the cells, while ALF is the one responsible for killing the cell. Studies in mice have shown that ALF is a necessary component for cell death, therefore finding inhibitors for this specific protein it of outmost importance when trying to stop the damage of the anthrax toxin. Overall, our screening system proved useful for finding interactions between toxins and small molecules. By changing to other ligands on the surface of the MRnS, this system can be used for the screening of other bacterial toxins providing a virtually unlimited platform for the screening of bacterial toxins.

CHAPTER IV: AUTOMATED DOCKING STUDIES OF THE SMALL-MOLECULE LIGANDS WITH THE ALF AND APA

Introduction

The anthrax toxin is composed of three virulent factors: (i) anthrax protective antigen (APA), (ii) anthrax lethal factor (ALF), and (iii) anthrax edema factor (AEF) that work in harmony to effectuate the lethality associated with the disease[7]. Upon release from the bacterial spores, APA is responsible for introducing both the AEF and ALF into macrophages. A zinc-dependent metalloproteinase, ALF causes cell death by targeting and cleaving the N-terminus of Mitogen Activate Protein Kinase Kinase (MAPKK) within the cells. This results in the inability of the MAPKK to phosphorylate its substrate Mitogen Activated Protein Kinase (MAPK), which consequently leads to a downstream altered signaling pathway that results in apoptosis of macrophages and dendritic cells[84, 85]. The exact mechanism by which ALF kills the cells remains unknown and it is believed that ALF inhibition of macrophages' MAPKK ultimately helps to establish infection since it essentially destroys the cells (macrophages) responsible for removing the damaged cells in the lungs. Structurally, anthrax lethal factor is composed of four domains (**Figure 44**)[86]. Domain I plays a crucial role in the toxin because it contains the biding site for the APA. It is through this domain that ALF binds to APA, a vital step in the internalization into the target cell. Domain II of the protein does not have any special roles and it acts more as a connecting structure between the other domains. Domain III is composed of α-helical bundle that create a hydrophobic surface with Domain IV, strictly

restricting access to the active site of other potential substrates. Domain IV contains the catalytic site where Zinc is located. This is the domain that is responsible for the enzymatic activity of the protein against MAPKK and therefore is a target for inhibitors of the ALF.

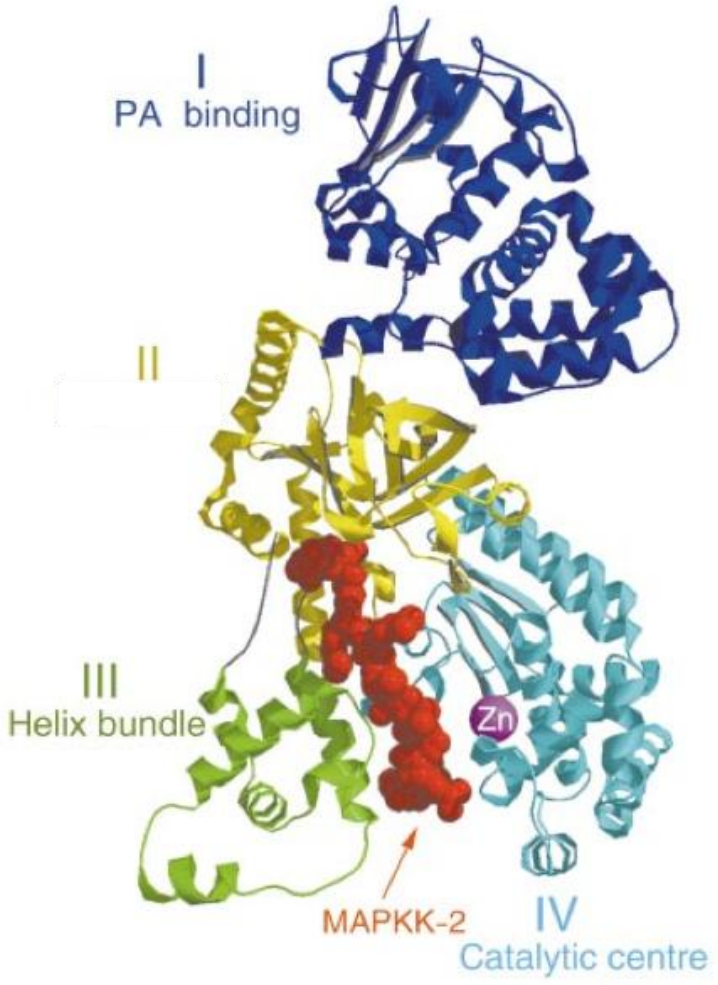

Figure 44. X-Ray structure of the Anthrax Lethal Factor colored by domain.
Structure depicting the four domains of ALF. MAPKK-2 is shown in red at the catalytic pocket.[86]

Although the Anthrax Protective Antigen does not directly kill macrophages, it is responsible in the internalization of the other two factors (**Figure 45**)[83]. In order to achieve this, the APA must go through some structural changes that will transform it into

a pore-forming protein. In its original state, the Protective Antigen is an 83 kDa (PA_{83}) protein that binds to either of the two known Anthrax Toxin Receptors (ANTXR1/2) on the surface of the cells. Upon binding, PA_{83} is activated by a furin protease that results in the cleavage of a 20 kDA fragment (PA_{20}) from the N-terminus of PA_{83}. The newly created 63 kDa piece (PA_{63}) heptamerizes with other PA_{63}s to form a ring shaped heptameric complex, known as the prepore. This prepore can then bind up to three molecules of ALF and/or Anthrax Edema Factor (AEF), which are consequently internalized into the cytosol.

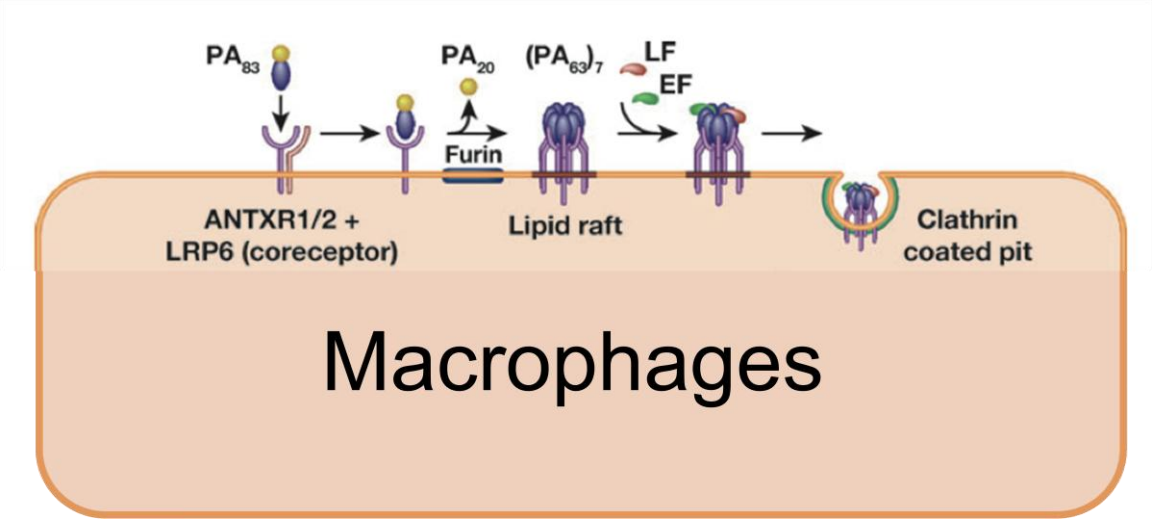

Figure 45. Function of the APA in the role of the Anthrax Toxin.
Upon binding to the ANTXR the APA is proteolytically activated by a member of the furin proteases. This allows the formation of the prepore which results in the internalization of the ALF and AEF into the target cell.[83]

Structurally, the APA is also comprised of four domains (**Figure 46**)[87]. In Domain I is where the furin cleavage occurs resulting in the formation of PA_{63}. Domain II is essential in the formation of the transmembrane pore that is used to introduce ALF and

AEF into the cytosol. It is believed that Domain III's role is to mediate the self-association of PA_{63} into the heptamer, thus having an important role in the protein's oligomerization. The last piece of this protein, domain IV, is mostly secluded from the rest of the protein and it its role is to bind the ANTXR cellular receptors.

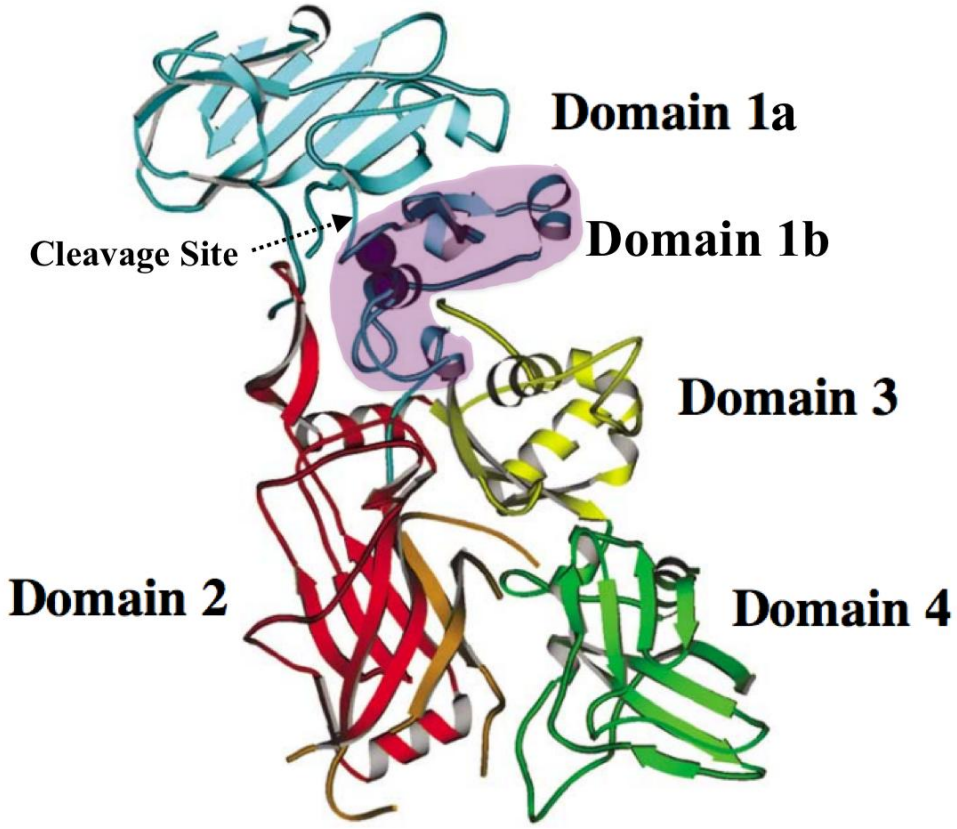

Figure 46. Structure of the Protective Antigen colored by domain.
Structure of the APA and its four domains. Domain I is divided into a and indicating the 20 kDa fragment that is displaced after furin-mediated cleavage. The purple-shaded region indicates the piece of Domain I that stay as part of PA_{63}. The two purple spheres within the purple shaded region represent calcium atoms.[87]

Detailed knowledge of protein-ligand interactions is essential when predicting binding sites on proteins. Computational molecular docking methods are continually evolving in order to provide accurate descriptions of the interactions between protein and

ligands at the atomic level[88]. Technically, molecular docking is the computational technique of placing a small molecule (ligand) into the pocket of a protein (receptor) in order to estimate its binding affinity. With modern software and advanced computers, these methods are capable of predicting molecular interactions under a broad range of conditions and constrains with impressive assertiveness[89]. However, these capabilities are often accompanied by a great technical difficulty when it comes to operating the software that often require expensive and complex supercomputer clusters.

Introduced in 1998 by the Olson's laboratory at the Scripps Research Institute, AutoDock[90] is a program that allows the study of molecular docking with relative ease. Its ability to run across different platforms and in low-budget computers along with its effectiveness makes it the most cited docking software in the research community. An effective tool capable of quickly and accurately predicting bound conformations and binding energies between ligands and receptors, Autodock played a role in the development of the first clinically approved HIV integrase inhibitor[91]. The program is capable of predicting where a ligand is going to fit into the large conformational space around a protein by using a grid-based method. A three-dimensional grid that covers all the surfaces and atoms of the protein is used to evaluate the binding energies of the trial conformations to every point in the grid. In order to search for the best conformation, Autodock uses a Lamarckian genetic algorithm[90]. This algorithm allows the conformation to mutate and compete in a manner similar to biological evolution, consequently selecting the conformation with the lowest binding energies.

One specific feature that makes Autodock useful is that it allows for blind-docking studies. Under these kinds of studies, the software predicts the binding sites of

small molecules on proteins by searching for locations through out the entire structure. This is of particular importance because it allows researchers to predict where a ligand is binding to a receptor on a newly discovered interaction. In the case of the work being presented in this thesis it will allow us to predict and evaluate the binding sites on the Anthrax Lethal Factor and Anthrax Protective Antigen of the previously discovered interactions.

Materials and Methods

Materials

AutoDock 4.2 and AutoDockTools 1.5.4 were downloaded from the Scripps Research Institute's website (http://autodock.scripps.edu). The ligand structure of sulindac, sulindac sulfide, sulindac sulfone, ibuprofen, and naproxen were downloaded from the protein data bank's ligand expo (http://ligand-expo.rcsb.org). Ketoprofen and Fusaric Acid were drawn in ChemDraw as mol format files imported into Autodock. The ALF (1J7N) and APA (1ACC) structure were downloaded from the protein data bank.

Blind Docking Studies

Blind docking studies were performed using the default parameters in AutoDock 4.2. Briefly, a three-dimensional grid that covered all the atoms of either protein was prepared. For the ALF this cubed shaped grid measured 126,90,114 points in the xyz planes and had a spacing of 0.78611 Å. The grid for APA measured 126, 104, 72 points in the xyz plane and had a spacing of 0.825 Å. After the affinity maps were generated from each of the grids, the docking search was performed using AutoDock's Lamarckian

genetic algorithm on its default settings. The logs containing the results from the docking experiments were analyzed and visualized using AutoDockTools.

Results

Docking studies with Anthrax Lethal Factor

Sulindac:

Our experimental results suggest the possible binding of sulindac to ALF. As we had seen in Chapter 3, magnetic relaxation studies involving sulindac-MRnS conjugate and ALF revealed that sulindac was binding to ALF. Therefore using computational docking studies, we investigated, which area on ALF would most preferably bind sulindac. The docking studies predicted that different sulindac conformations bound to different sites around ALF. Predominantly, we observed different interactions within domain III and IV with two of the conformations binding around or to the enzymatic pocket (**Figure 47, A**). Due to its hydrophobicity it is expected that sulindac will bind to places within the highly hydrophobic domain III. From these predictions we selected the conformation with the lowest binding energy, which predicted that sulindac would preferentially bind to the catalytic site with a binding energy of -9.0 kcal/mol (**Figure 47, B**). The binding of sulindac to the catalytic site suggests that sulindac would be capable of inhibiting ALF. Upon close analysis of this interaction we were able to evaluate the interacting residues with the parts of the small molecule (**Figure 47, C**). According to AutoDock, residues GLN642 and GLN646 interact directly with the oxygen atom and the from the sulfoxide group. The oxygen from HIS645 is interacting with the terminal alkyl groups leading off from the sulfoxide. On the other side of the molecule, PRO661,

LEU658, TYR659, and HIS690 are interacting with the fluoro-indene moiety of sulindac, while the Zn^{2+} atom on ALF is interacting with the carbonyl group from the carboxylic acid group. These multiple interactions along with its hydrophobicity make sulindac an ideal candidate for an inhibitor of ALF.

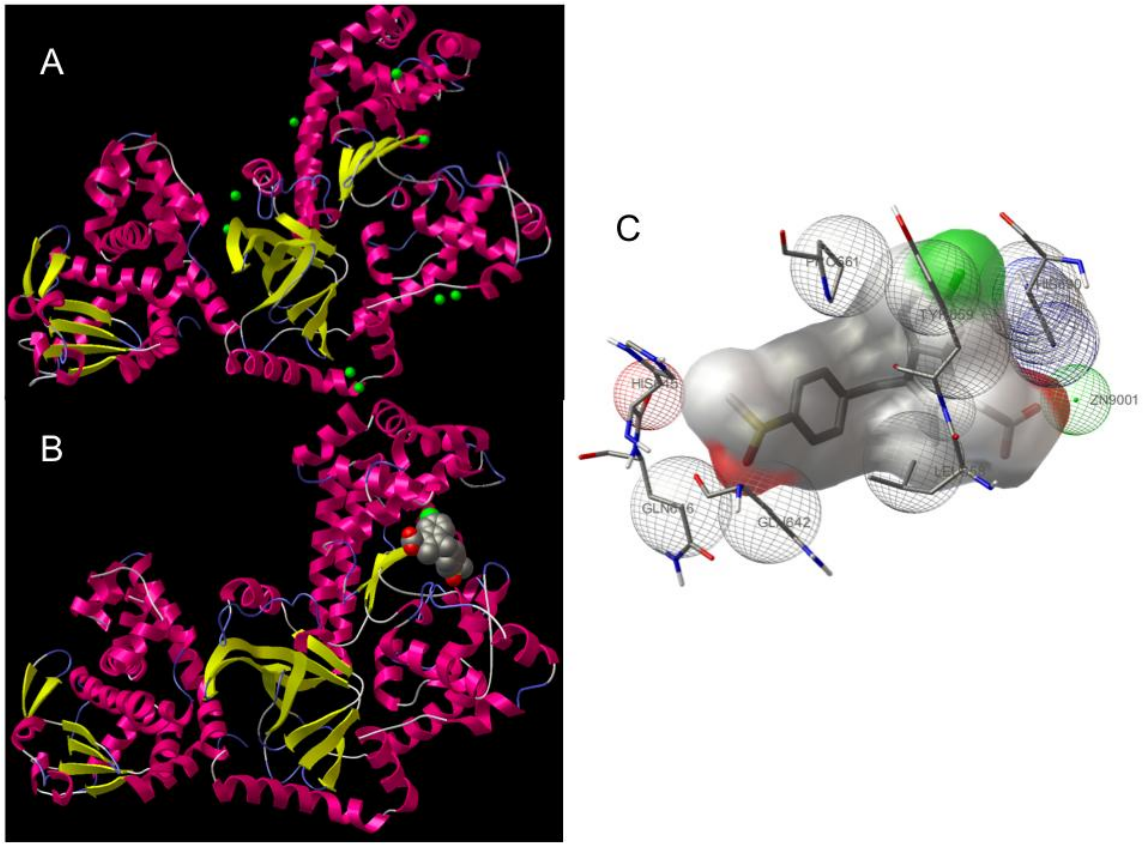

Figure 47. Results from docking studies between sulindac and ALF.
Structures of sulindac bound to ALF. **A:** The green dots represent possible binding sites for sulindac on ALF. **B:** The conformation with the lowest binding energy was observed to bind at the catalytic site of ALF. C: Sulindac interacting with the different residues at the catalytic site. This image shows how sulindac directly interacts with Zn (green dot) and other residues of the enzymatic pocket. The spheres represent the atomic interactions between the residues and sulindac.

Sulindac Sulfide and Sulindac Sulfone:

The results from Sulindac-ALF docking studies prompted us to further study this interaction. It is known that sulindac the non-steroidal anti-inflammatory drug (NSAID) is a sulfoxide prodrug that upon oral administration is transformed by the liver into two forms; the reduced sulfide analog and the oxidized sulfone analog. Its sulfide form is the active COX 1/2 inhibitor while the sulfone has no anti-inflammatory activity[92-95]. Specifically, sulindac is converted in the liver to a sulfide that is excreted in the bile and reabsorbed by the intestines[96]. This metabolized form is the active drug that remains in circulation and binds to its natural target the COX 1/2 enzymes. Since we are considering sulindac as a potential inhibitor of ALF and because of the metabolic modifications inherent to this drug, we therefore also performed docking experiments between the sulindac metabolites and ALF. Experiments with Sulindac Sulfide revealed similar results to those of sulindac with an even greater number of binding conformations at enzymatic pocket (**Figure 48, A**). After examining the most favorable binding conformation, we observed that sulindac sulfide preferably binds to the catalytic site with a binding energy of -9.3 kcal/mol (**Figure 48, B**). Upon close inspection of this interaction, we observed several residues such as LEU658, TYR659, and HIS690 interacting with the fluoro-indene moiety as were also observed with sulindac (**Figure 48, C**). The lower binding energy along with the multiple but congregated interactions observed between sulindac sulfide and ALF, suggest that this primary metabolite of sulindac can potentially be a stronger inhibitor of ALF than sulindac. Furthermore experiments with sulindac sulfone provided very similar results to those observed with both sulindac and sulindac sulfide. Most of the possible binding sites for sulindac sulfone

in ALF can be found on the enzymatic pocket and the hydrophobic domain III (**Figure 49, A**). Examination of the conformation with the lowest binding energy revealed that Sulindac sulfone prefers to bind to the catalytic pocket as well as its analogs (**Figure 49, B**). The predicted binding energy for this interaction was of -8.3 kcal/mol, a higher amount than that of both of its analogs. Close examination of the binding residues revealed that LEU658, TYR659, and HIS690 are also the main residues interacting with the fluoro-indene moiety as it was observed with sulindac and sulindac sulfide (**Figure 49, C**). As well as with sulindac and sulindac sulfide these results suggest that sulindac sulfone can also potentially inhibit ALF.

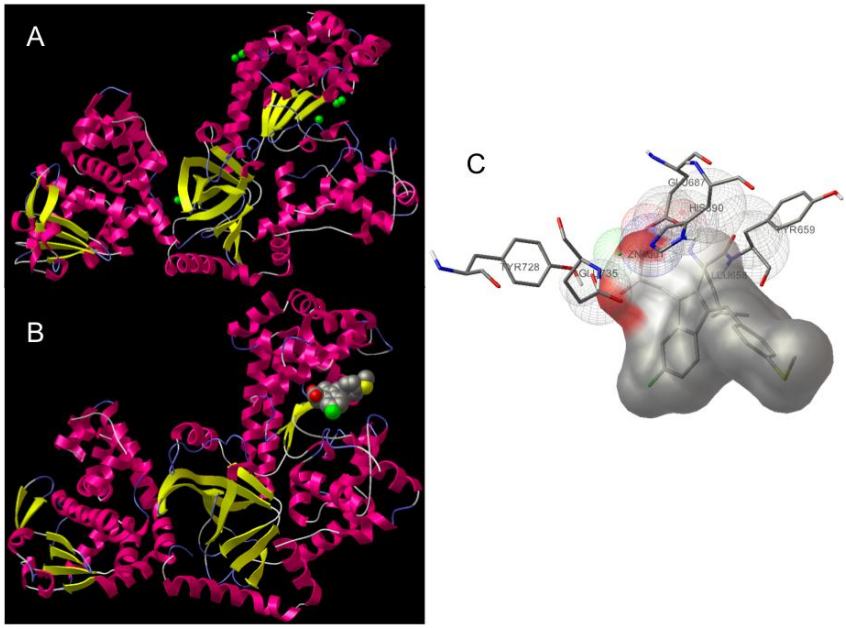

Figure 48. Results from docking studies between sulindac sulfide and ALF.
Structures of sulindac sulfide bound to ALF. **A:** The green dots represent possible binding sites for sulindac sulfide on ALF. **B:** The conformation with the lowest binding energy was observed to bind at the catalytic site of ALF. **C**: Sulindac sulfide interacting with the different residues at the catalytic site.

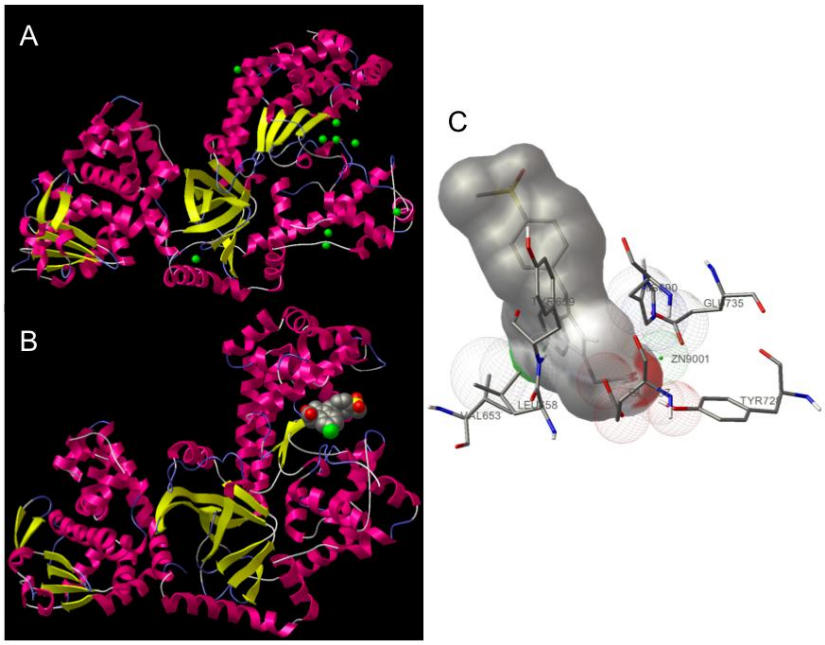

Figure 49. Results from docking studies between sulindac sulfone and ALF.
Structures of sulindac sulfone bound to ALF. **A:** The green dots represent possible binding sites for sulindac sulfone on ALF. **B:** The conformation with the lowest binding energy was observed to bind at the catalytic site of ALF. **C**: Sulindac sulfone interacting with the different residues at the catalytic site.

Fusaric Acid:

Next, we studied fusaric acid, which was also identified to bind the ALF via magnetic relaxation. The blind docking studies predicted that this molecule also bound to the enzymatic pocket in domain IV. Additionally, a great number of conformations bound in the space between domains I and II (**Figure 50, A**). The conformation with the most favorable binding was observed at the catalytic centre in domain IV with a binding energy of -6.2 kcal/mol (**Figure 50, B**). Examination of the residues predicted to bind fusaric acid revealed that VAL660, LEU658 and TYR659 interacted with the butyl chain leading off the pyridine at the center of the molecules. Also, TYR728, GLU35 and the Zn interacted with the carboxylic acid end of fusaric acid (**Figure 50, C**). Although not a

particular strong interaction between ALF and fusaric acid was predicted, the results suggest that fusaric acid can potentially inhibit ALF.

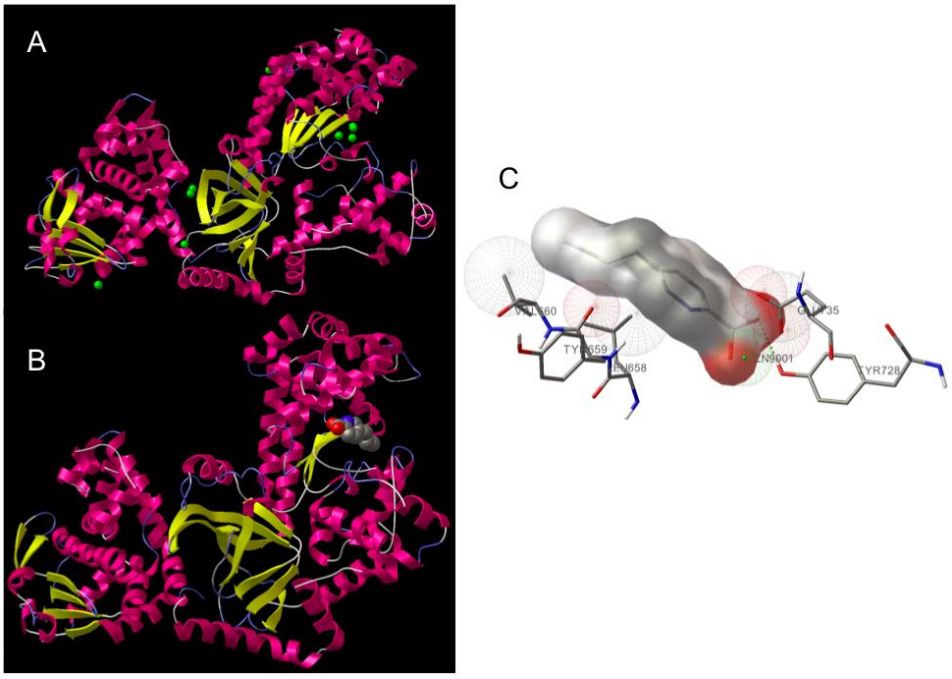

Figure 50. Results from docking studies between fusaric acid and ALF.
Structures of fusaric acid bound to ALF. **A:** The green dots represent possible binding sites fusaric acid on ALF. **B:** The conformation with the lowest binding energy was observed to bind at the catalytic site of ALF. **C**: Fusaric acid interacting with the different residues at the catalytic site.

Naproxen:

The last molecule that was evaluated for binding to ALF was naproxen. Results form the AutoDock studies predicted that naproxen bound to several locations on the ALF, with a concentrated population in the space between domains I and II. Interestingly, naproxen also bound to parts of the APA binding domain (**Figure 51, A**). This is a crucial observation since binding to this site could potentially inhibit ALF from binding to APA, ultimately stopping ALF from entering the cell. The conformation with the strongest

interaction was observed in the space between domains I and II and had a binding energy of -4.3 kcla/mol (**Figure 51, B**). Although, the binding of naproxen to the PA binding domain suggest a possible inhibitory mechanism, the high binding energies do not make this interaction a favorable one therefore reducing the possibility that naproxen may inhibit the binding of ALF to APA.

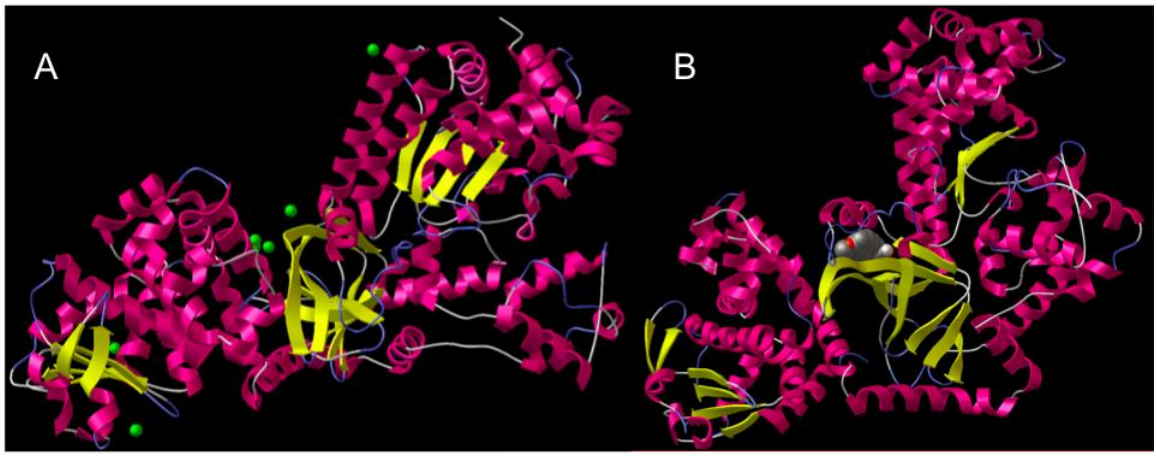

Figure 51. Results from docking studies between naproxen and ALF.
Structures of naproxen bound to ALF. **A:** The green dots represent possible binding sites naproxen on ALF. **B:** The conformation with the lowest binding energy was observed to bind at the space between domains I and II.

Docking studies with Anthrax Protective Antigen.

For our second set of experiments we studied the docking possibilities between the anthrax protective antigen and the three molecules identified to bind it in Chapter III. According to the magnetic relaxation studies, all three molecules sulindac, ibuprofen and ketoprofen bound to APA. This resulted in a decrease in the ΔT_2 that was observed in the magnetic relaxation studies.

The first experiment of this set studied the docking of sulindac to APA. Results from the docking predictions showed that sulindac was binding to different sites throughout APA. Specifically, we observed a greater population of conformations that bound between domains I and II/III very close to the furin-mediated cleavage site on domain I (**Figure 52, A**). Further examination of these binding predictions revealed that the most favorable conformation with the lowest binding energy, -6.13 kcal/mol, binds near the cleavage site, an indication that sulindac can be a potential inhibitor of the furin-mediated cleavage of APA (**Figure 52, B**). Similarly, the studies with ketoprofen and APA revealed very analogous results with most of the conformations binding at domain I around the cleavage site (**Figure 53, A**). For this particular interaction the conformation with the lowest binding energy, -5.48 kcal/mol, occurred between domains I and II below the furin-mediated binding site (**Figure 53, B**). The prediction that other conformations bind at that site could suggest that ketoprofen may also inhibit the furin-mediated cleavage of APA.

Figure 52. Results from docking studies between sulindac and APA.
Structures of sulindac bound to APA **A:** The green dots represent possible binding sites of sulindac on APA. **B:** The conformation with the lowest binding energy was observed to bind at the furin-mediated cleavage site of domain I.

Figure 53. Results from docking studies between ketoprofen and APA.
Structures of ketoprofen bound to APA **A:** The green dots represent possible binding sites of ketoprofen on APA. **B:** The conformation with the lowest binding energy was observed to bind between domains I and II.

Lastly, we studied the interaction between Ibuprofen and APA. Results from these studies indicated that Ibuprofen binds to different sites on the APA (**Figure 54, A**). Particularly, these bindings were grouped around domains II and III, with the strongest interaction measuring -5.86 kcal/mol at the bottom of domain III (**Figure 54, A**).

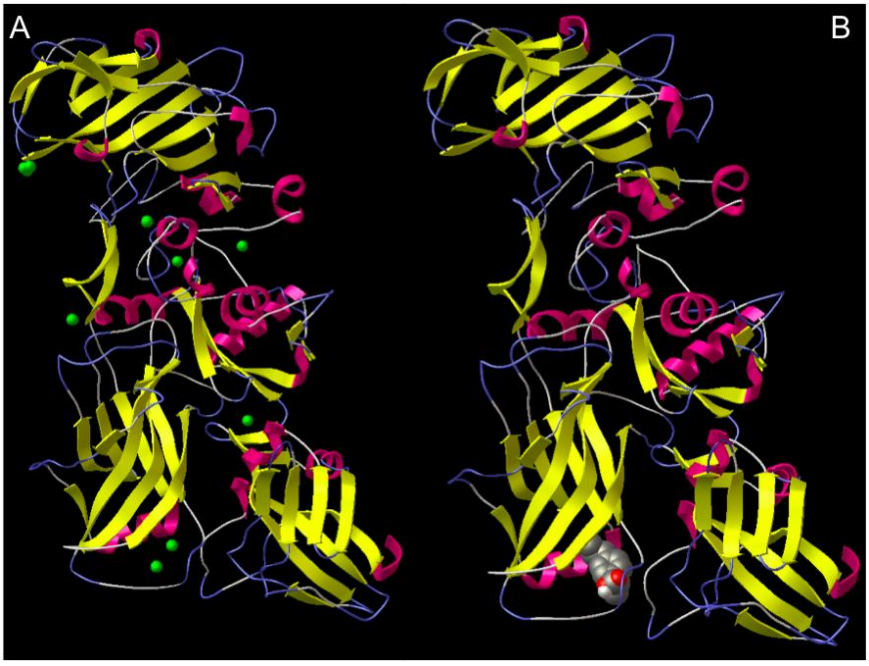

Figure 54. Results from docking studies between ibuprofen and APA.
Structures of ibuprofen bound to APA **A:** The green dots represent all the possible binding sites of ibuprofen on APA. **B:** The conformation with the lowest binding energy was observed to bind at the bottom of domain III.

Conclusions

- Studies with ALF suggested that sulindac, sulindac sulfide, sulindac sulfone and fusaric acid may be inhibitors of ALF due to their predicted binding at the catalytic site.
- Results form the APA studies suggest that sulindac and ketoprofen have the potential to inhibit the furin-mediated cleavage of domain I on APA.

Discussion

With the advancement of computers and the development scientific computational methods, scientists have gained a valuable tool that allows them to carry out an experiment without ever stepping into the lab. Experiments "in-silico" are carried out theoretically on a computer and can cover a broad range of applications. More commonly, these experiments focus on docking studies that predict with accuracy where a ligand (small molecule) binds to a receptor (protein or macromolecule). These types of experiments have proven crucial on the development of new drugs for diseases and even when investigating newly discovered interactions between ligands and receptors. In the previous chapter we screened a small molecule library for binding to the anthrax lethal factor and protective antigen via magnetic relaxation. We discovered five molecules that successfully bound to the surface of either/both proteins. Consequently, due to the experimental complexity associated with elucidating the binding site of a molecule on a protein, we relied on computational docking studies to predict these locations.

Using Autodock 4.2 to search for the most favorable binding conformation we were able to carry out blind docking studies of the small molecules and the components

to the anthrax toxin. Specifically, we focused on the ALF studies as this protein contains an enzymatic role that is devastating to target cells. Our computational docking results indicated that sulindac and fusaric acid both bind to the enzymatic pocket of ALF, suggesting that these molecules may inhibit its activity. Furthermore, because sulindac is a prodrug that is activated in the liver, we also conducted studies involving its metabolites: sulindac sulfide, the reduced form and sulindac sulfone, the oxidized form. Results with sulindac's metabolites indicated that both forms also bind to the catalytic site, suggesting that they could inhibit ALF's protease activity. Taken together, these results make sulindac the ideal candidate for a potential inhibitor of ALF, thus further experiments that test the ability of sulindac to inhibit ALF are needed.

The other protein studied, APA, is also critical for the development of the disease as its role is cellular recognition and transportation of the other two toxin fragments into the cytosol. Computational docking studies with APA revealed that as with ALF, the small molecules bind to the different sites throughout the protein. Particularly, sulindac and ketoprofen bind around a cleavage site that is crucial for the furin-mediated activation of APA. Upon cleavage at this site, the APA is able to assemble into a heptamer complex that allows the translocation of ALF and AEF into the cells. Further experiments that test the ability of sulindac and ketoprofen to inhibit this cleavage are needed in order to confirm their inhibitory potential.

CHAPTER V: INHIBITING THE ANTHRAX LETHAL FACTOR, DETERMINATION OF THE INHIBITION POTENTIAL OF SULINDAC, ITS DERIVATIVES AND FUSARIC ACID

Introduction

The anthrax lethal factor (ALF) in one of the three virulent factors released by the anthrax bacterium upon infection of a host. Together with the anthrax edema factor (EDF) these virulent factors are responsible for damaging healthy macrophages. Out of the two damaging factors, ALF has been identified to play a critical role in cell death. Studies in animals have shown that mice infected with an anthrax strain lacking ALF survive [97]. Furthermore, administration of ALF in conjunction with the anthrax protective antigen (APA) in animals induces vascular collapse similar to that observed during anthrax infections, results that point to the lethal effects of ALF[98]. After entering the cytosol via APA, ALF cause damage to the healthy cell by cleaving the N-terminus of mitogen-activated protein kinase kinase (MAPKK) preventing the phosphorylation of downstream MAPK.[99, 100] This alteration modifies the MAPK signal pathways and eventually leads to cell death by an unknown mechanism.[101, 102]

In the last decade since the anthrax attacks of 2001, very little has been elucidated about the role that ALF plays within the macrophage to induce cell death. Yet, very recently, studies from the Moayeri lab at the National Institute of Allergy and Infectious Diseases have revealed that ALF induces the caspase-1-dependent rapid programmed cell death (pyroptosis) of mouse and rat macrophages through activation of the NOD-like receptor (NLR) Nlrp1 inflammasome. In these studies LT (APA+ALF) cleaves rat Nlrp1

and this cleavage is required for toxin-induced inflammasome activation, IL-1 b release, and macrophage pyroptosis. This discovery is of critical biological relevance since it sheds light into the reason behind the rapid pathogenesis of ALF in cells[103-106].

Although the current treatment for anthrax infections is antibiotic treatments, modern medicine faces some critical limitations when combating infections. Antibiotics have proven very efficient in eliminating the bacterial infection but they lack the ability to destroy or inhibit the virulent factors released by the bacteria. Specifically, ALF can remain active in the body for days after the infection is eliminated with no way of inhibiting its destructive effects. In order to address this problem, several inhibitors of the enzymatic activity of ALF have been identified over the last decade. In order to identify inhibitors of ALF a variety of screening approaches such as library screenings, Mass Spectroscopy- based screenings and scaffold based NMR screening have been used[82]. Results from these screening have yielded mainly small molecules that can inhibit ALF in low micromolar to nanomolar concentrations. Yet, although valuable, these results have very little significance with regards to these molecules being used as actual therapeutics. There is a large expense associated with the governmental approval process that new drugs are required to undergo in order to become FDA approved. Additionally, the low occurrence of anthrax infections further discourages the interest of pharmaceutical companies since the expected return on investment is minimal. Therefore it will be crucial to be able to identify currently approved FDA drugs that are already being used in the clinics that can also inhibit ALF.

In order to achieve this undertaking, in Chapter 3 we screened a small-molecule library of mostly FDA approved drugs for their binding to ALF. This resulted in three

molecules sulindac, fusaric acid, and naproxen that were identified to bind ALF. Further computational docking studies predicted that sulindac and fusaric acid both bind to the enzymatic pocket, while naproxen did not. Herein, we will further investigate whether or not sulindac and fusaric acid are able to inhibit ALF. We will measure the enzymatic activity of ALF using a fluorogenic inhibition assay sold by Calbiochem that uses a substrate that upon cleavage by ALF is able to report a fluorescence signal (**Figure 55**)[107]. This fluorescence reporter is dependent on the amount of ALF present and therefore will allow us to calculate the 50 % inhibition concentrations at (IC_{50}) of our small molecules against ALF.

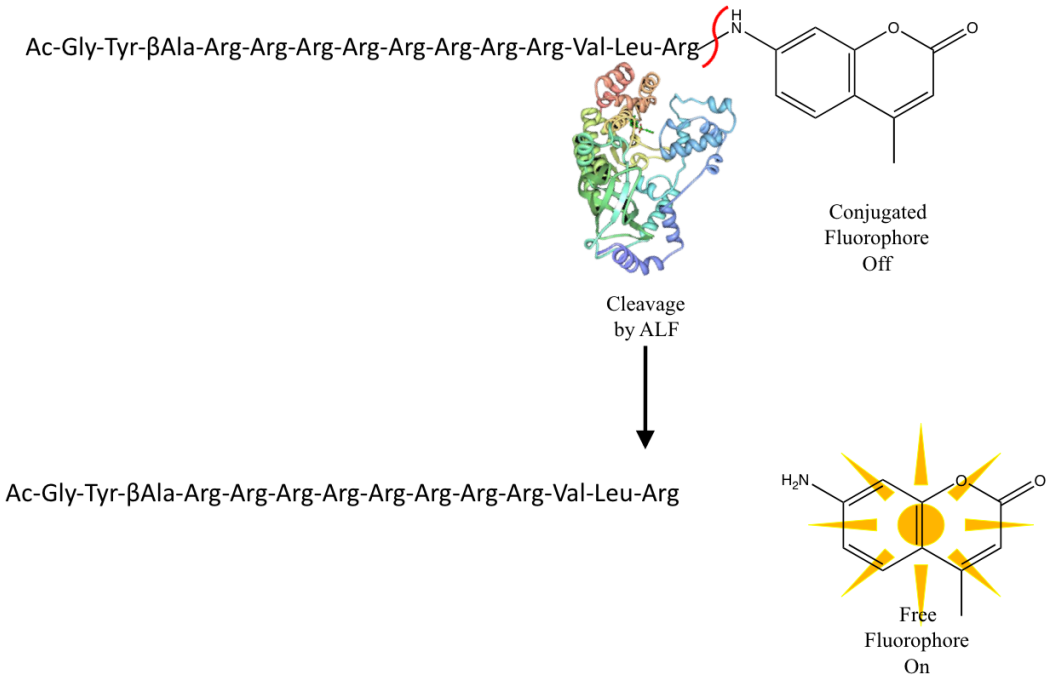

Figure 55. Schematic representation of the fluorogenic inhibition assay.
Upon cleavage of the N-terminal of the substrate by ALF, AMC is hydrolyzed and de-quenched.

Materials and Methods

Reagents.

Sulindac, Sulindac Sulfide, sulindac sulfone, fusaric acid, naproxen, HEPES, TWEEN 20, calcium chloride, and DMSO were obtained from Sigma-Aldirch. Anthrax lethal factor and anthrax protective antigen were obtained from List Biological Laboratories, INC. The anthrax lethal factor protease substrate III, fluorogenic was obtained from Calbiochem.

Anthrax Lethal Factor Protease Inhibition Assay, General Procedure.

In a florescence (black) 96-well plate, samples (100 µL) containing ALF (2 nM ALF) in a 40 mM HEPES at pH 7.2, 100 µM $CaCl_2$, 0.05 % (v/v) buffer and different concentrations of inhibitors (**Table 5**) were prepared and incubated for 30 minutes. After the incubation period, 0.5 µL of fluorogenic anthrax lethal factor protease substrate III (470 µM, DMSO) was added to each sample and the fluorescence was measured every 10 minutes for an hour. Fluorescence measurements were carried out using a Tecan infinite M200 pro at a 355 nm excitation and 460 nm emission. IC_{50} concentrations were calculated from the data collected.

Table 5. Concentration range of the inhibitors used for the ALF protease inhibition assay.

Inhibitors	Concentration Range
Sulindac	0.005 – 5 mM
Sulindac on MRnS conjugate	0.053 – 5.3 µM
Sulindac Sulfide	0.010 – 1 mM
Sulindac Sulfone	0.010 – 1 mM
Fusaric Acid	0.1 – 10 mM
Naproxen	0.1 – 10 mM

Results

In our first set of experiments we investigated whether sulindac could inhibit the proteolytic activity of ALF. In order to achieve this task we used a fluorogenic ALF substrate (Calbiochem) capable of emitting fluorescence after cleavage by ALF. Specifically, this ALF substrate III peptide (**Ac-Gly-Tyr-βAla-Arg-Arg-Arg-Arg-Arg-Arg-Arg-Arg-Val-Leu-Arg-AMC**) is a N-acetylated, C-7-amido-4-methylcoumarin (AMC) derivative of Mitogen-Activated Protein Kinase Kinase 2 (MAPKK2), which is the natural target for ALF. In the presence of ALF, the quenched substrate is cleaved at the N-terminal between the arginine residue and the C-7-amido-4-methylcoumarin derivative, restoring the proper conjugation to the chromophore and thus producing a readable fluorescence signal that is dependent on the amount of ALF present. On the other hand, if ALF is inhibited, the lack of protease activity does not cleave the substrate, causing it to remain in a quenched state. For this study we incubated different concentrations of sulindac with ALF (2 nM) for 30 minutes before adding the fluorogenic substrate (2.35 μM). Time-course florescence measurements revealed that sulindac was inhibiting ALF in a concentration-dependent manner with complete inhibition observed below 1 mM of Sulindac (**Figure 56**).

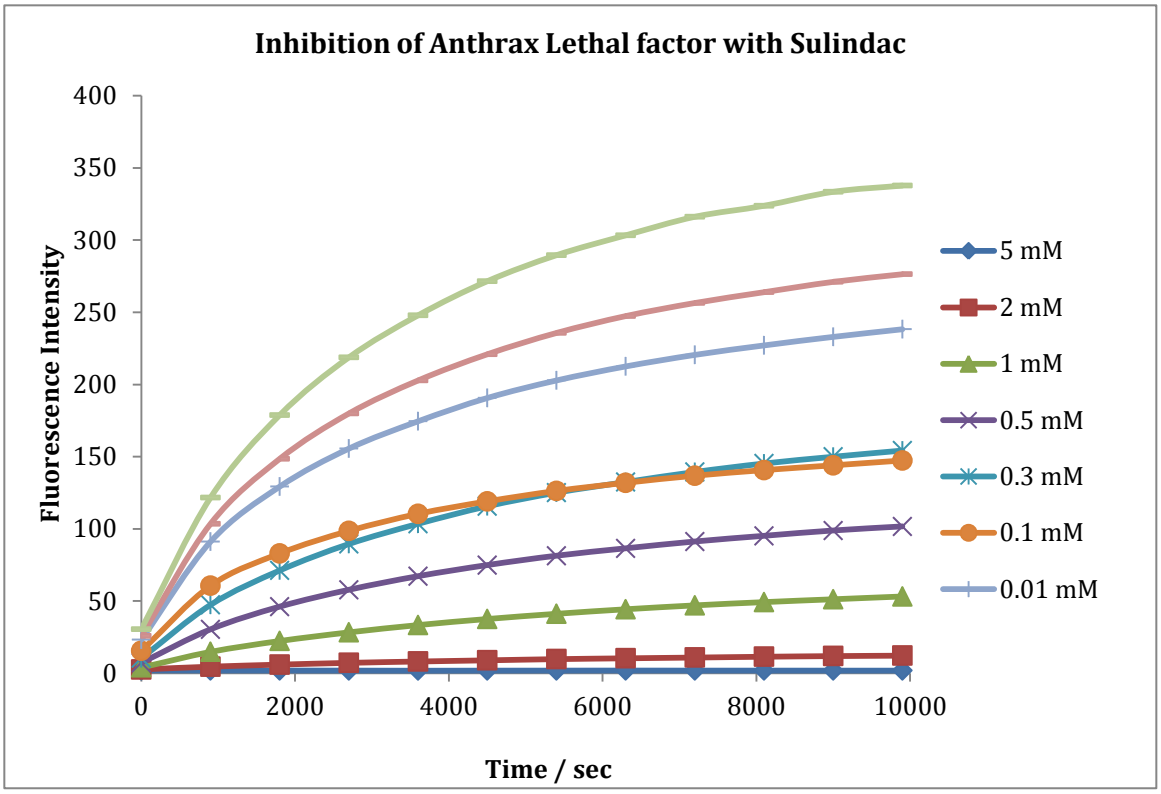

Figure 56. Inhibitory profile of sulindac against ALF.
Upon incubation of ALF (2 nM) with various concentrations of sulindac (0.005 – 5 mM), time-course experiments revealed that sulindac is capable of inhibiting ALF. Since the lower fluorescence intensity represents a higher inhibition, a concentration of 1 mM is enough to completely inhibit ALF. The control represents no sulindac added.

Additionally, using a similar experiment but using the data collected at 50 minutes after the addition of the fluorogenic substrate we were able to compute the inhibitory concentration at 50% (IC_{50}) of sulindac against ALF, which was calculated to be 173 µM (**Figure 57, A**). These results provide evidence that sulindac is in fact binding to the catalytic site of ALF as predicted in the computational studies of Chapter 4. Next, we decided to investigate the inhibitory potential of the Sulindac-MRnS conjugate. Since, low concentrations of sulindac are binding to the catalytic site of ALF, we therefore hypothesized that the lower amount of sulindac on the surface of the nanoparticles would

be capable of binding to the pocket as well. Using the same inhibitory assay, we evaluated the inhibitory potential of Sulindac-MRnS, which produced a lower IC_{50} (230 nM sulindac on the surface of the MRnS) than sulindac alone (**Figure 57, B**). This observed reduction in the IC_{50} might be attributed to the nanoparticle blocking the enzymatic pocket of ALF. Based on the computational studies of Chapter 4, this can be expected if a sulindac molecule that is attached to the nanoparticle binds the catalytic site, which will cause the nanoparticle to position itself in the opening of the binding pocket, thus blocking its entrance and inhibiting that ALF unit. A lower IC_{50} is observed when using the sulindac-MRnS conjugate as opposed to sulindac alone because just a few sulindac molecules on the surface of the MRnS are enough to position the nanoparticle at the opening of the enzymatic pocket. Additionally, with an IC_{50} of 230 nM, the Sulindac-MRnS conjugate is more effective at inhibiting ALF than sulindac alone, a discovery that suggest that the nanoparticle conjugate could be a more effective therapy against ALF than the small molecule alone.

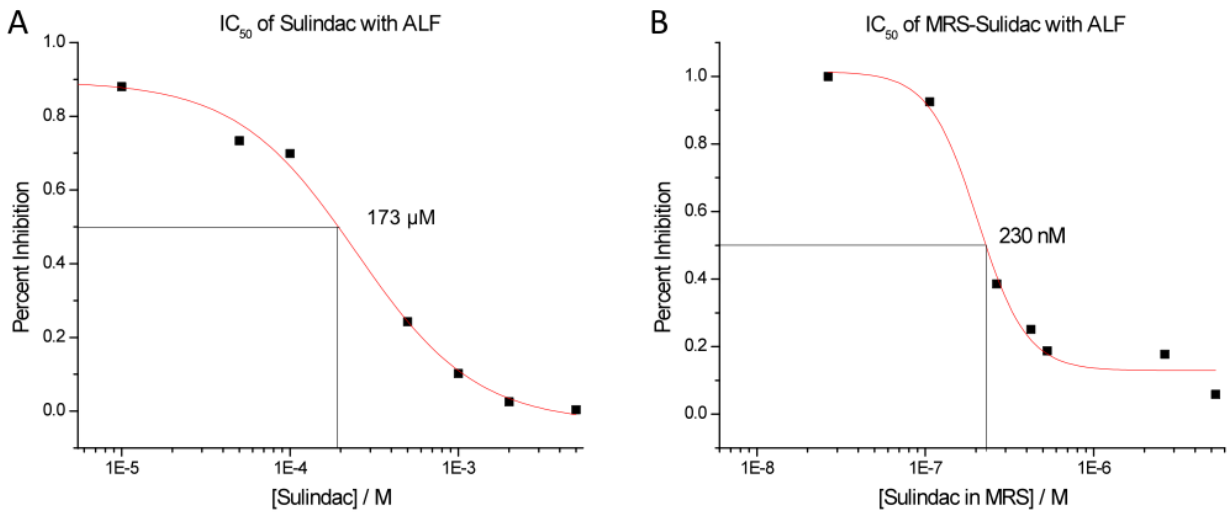

Figure 57. IC_{50} calculations of sulindac and sulindac-MRnS against ALF.
A: A concentration of 173 µM inhibits 50% of the enzymatic activity of ALF. B: Whereas, when sulindac is attached to a MRnS, the IC_{50} is significantly reduced to 230 nM.

Since sulindac is a prodrug, we also investigated the inhibitory potential of its metabolites sulindac sulfide (reduced form) and sulindac sulfone (oxidized form). These two molecules are metabolic derivatives of sulindac their ability to inhibit ALF is of great importance if sulindac is one day used to treat ALF pathogenesis. Upon ingestion, sulindac is metabolized into sulindac sulfide (the active COX 1/2 inhibitor) with a very small portion of it being metabolized into sulindac sulfone (inactive). Since, the majority of sulindac is converted to sulindac sulfide, the ability of sulindac sulfide to inhibit ALF must be evaluated. Using our fluorogenic inhibition assay with different concentrations of sulindac sulfide (10 µM – 1 mM), revealed that the reduced form of sulindac is capable of inhibiting ALF at an even lower concentrations that sulindac itself. Our experiment concluded that sulindac is able to inhibit ALF with an IC_{50} of 19.1 µM (**Figure 58, A**).

Additionally, we also evaluated the inhibitory potential of sulindac sulfone. These experiments revealed that sulindac sulfone (10 µM – 1 mM) was able to inhibit ALF at a concentration above that of its parent molecule sulindac with an IC_{50} of 185 µM (**Figure 58, B**). Taken together, these results show significant promise for the future use of sulindac as a treatment for ALF. Not only is sulindac capable of inhibiting ALF, but also its metabolic products strongly inhibit ALF with concentrations in the µM range.

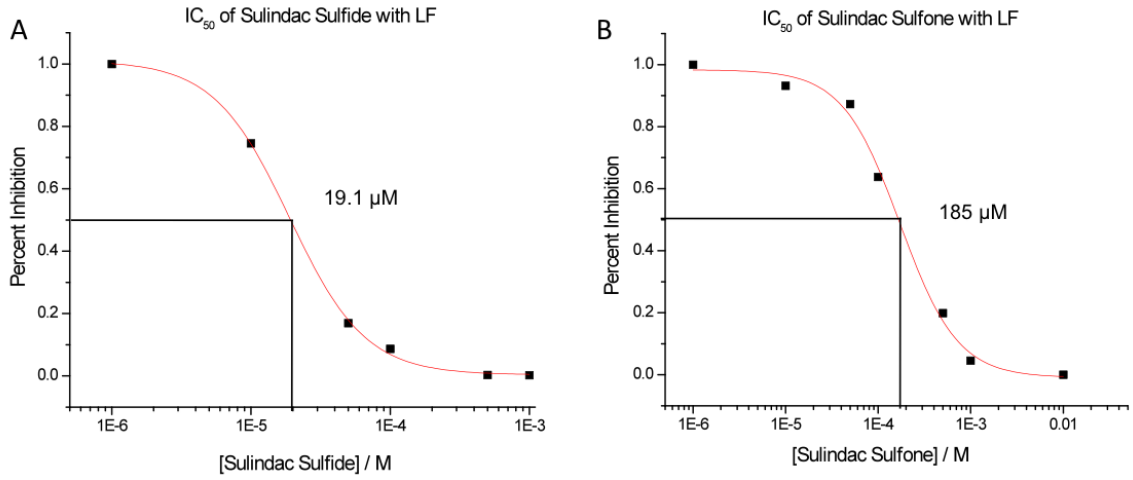

Figure 58. IC_{50} calculations of the metabolic derivatives of sulindac against ALF.
A: Out of the two metabolites, sulindac sulfide produces the highest inhibition of ALF with an IC_{50} of 19.1 µM. B: Sulindac sulfone is also able to inhibit ALF but at a higher IC_{50} of 185 µM.

After evaluating the inhibitory capacity of sulindac and its derivatives, we concentrated on fusaric acid, the other molecule that was predicted to bind at the catalytic site by computational docking studies. Using different fusaric acid concentrations (100 µM – 10 mM) for our inhibition assay, we were able to determine the inhibitory potential of this small molecule. With an IC_{50} of 530 µM, fusaric acid was able to inhibit ALF with a lower capability than sulindac and its derivatives (**Figure 59, A**). Furthermore, we

carried out inhibition experiments with naproxen (100 µM – 10 mM). Even though computational docking studies did not predict the binding of naproxen to the enzymatic pocket, we wanted to investigate whether this small molecule could affect ALF's activity (**Figure 59, B**). Our studies revealed that naproxen failed to inhibit ALF, even at high concentrations (10 mM). Since naproxen failed to inhibit ALF, these results suggest that naproxen does not bind to the toxin's enzymatic pocket as predicted by the computational studies of Chapter 4.

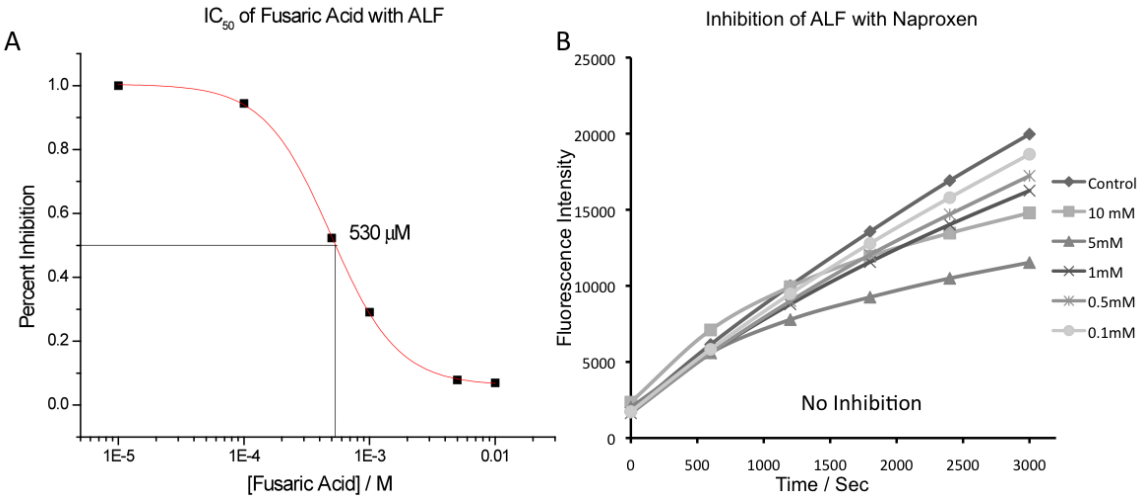

Figure 59. Inhibitory capacity of fusaric acid and naproxen against ALF.
A: Fusaric acid inhibits ALF with an IC_{50} of 530 µM. B: Even at concentrations as high as 10 mM naproxen does not inhibit ALF. The control in this graph represent no naproxen added.

Conclusions

- The inhibitory potential of sulindac and its metabolites sulindac sulfide and sulindac sulfone was assessed revealing that sulindac, sulindac sulfide and sulindac sulfone are capable of inhibiting ALF in the micromolar range.
- After evaluating fusaric acid and naproxen for the inhibition of ALF, fusaric acid was able to inhibit ALF while naproxen was not.
- These results confirmed the computational docking studies from Chapter 4 which predicted that sulindac, sulindac sulfide, sulindac sulfone, and fusaric acid bind to the enzymatic pocket while naproxen does not.

Discussion

The treatment for bacterial infections has traditionally focused on using antibiotics to eliminate the infectious pathogen. The emergence of multidrug resistance bacteria along with the evolutionary strengthening that have developed these organisms into more effective killers, has forced modern medicine to look for alternative therapies when dealing with bacterial infections. An approach that could potentially be beneficial is to treat the toxins that bacteria release, as these powerful toxins are solely responsible for damaging and killing healthy tissue. The fact that even after the organisms are eliminated bacterial toxins remain in circulation for a long time, makes this therapeutic approach desirable as it inhibits the disease from further damaging the host. Very few treatments currently exist that target bacterial toxins. This is due to an outdated culture of

pharmaceutical companies that avoid investing in the development of new drugs for diseases that are "partially" treatable by existing medicines.

In the case of inhalation anthrax, the only way of treating this deadly disease is by antibiotic therapy. This in itself is a big drawback because the toxins released by the bacterium are very toxic and can stay active in circulation for days after the elimination of the organism. Specifically, the anthrax lethal factor, one of the components of the anthrax toxin, has been shown to cause death in animals after a couple of hours of injection into the blood stream. For this reason the need for a drug that is able to inhibit the effect of the virulent factor is highly desirable. Although since the anthrax attacks of 2001, many inhibitors of ALF have been identified, the low occurrence of inhalation anthrax together with the high cost of developing a new drug has placed treatment of ALF at a low priority of pharmaceutical companies.

In order to circumvent these drawbacks we looked for currently available drugs that could inhibit ALF. After identifying possible candidates by binding studies, we study the capability of these drugs to inhibit ALF. Particularly, we identified a currently available non-steroidal anti-inflammatory drug (NSAID) that strongly inhibited ALF. Sulindac, marketed as Clinoril, is a prodrug that is currently used to treat a wide range of inflammatory conditions. Our studies revealed that this molecule and its metabolic derivatives were able to inhibit ALF in micromolar concentrations. This discovery is of great importance because it shows that a currently available FDA approved drug can be used treat the pathogenesis of a very deadly bacterial infection. Furthermore, this study serves as an example to follow since there may be many other bacterial toxins that can potentially be inhibited with currently available drugs.

LIST OF REFERENCES

1. Taubes, G., The bacteria fight back. *Science* **2008,** *321* (5887), 356-61.

2. Boerlin, P.; Reid-Smith, R. J., Antimicrobial resistance: its emergence and transmission. *Anim Health Res Rev* **2008,** *9* (2), 115-26.

3. DeLisle, S.; Perl, T. M., Vancomycin-resistant enterococci: a road map on how to prevent the emergence and transmission of antimicrobial resistance. *Chest* **2003,** *123* (5 Suppl), 504S-18S.

4. Taiwo, S. S., Methicillin resistance in Staphylococcus aureus: a review of the molecular epidemiology, clinical significance and laboratory detection methods. *West Afr J Med* **2009,** *28* (5), 281-90.

5. Goonetilleke, A.; Harris, J. B., Clostridial neurotoxins. *J Neurol Neurosurg Psychiatry* **2004,** *75 Suppl 3*, iii35-9.

6. Bouzianas, D. G., Current and future medical approaches to combat the anthrax threat. *J Med Chem* **2010,** *53* (11), 4305-31.

7. Sweeney, D. A.; Hicks, C. W.; Cui, X.; Li, Y.; Eichacker, P. Q., Anthrax infection. *Am J Respir Crit Care Med* **2011,** *184* (12), 1333-41.

8. Doganay, M.; Metan, G.; Alp, E., A review of cutaneous anthrax and its outcome. *J Infect Public Health* **2010,** *3* (3), 98-105.

9. Passalacqua, K. D.; Bergman, N. H., Bacillus anthracis: interactions with the host and establishment of inhalational anthrax. *Future Microbiol* **2006,** *1* (4), 397-415.

10. Arias, C. A.; Murray, B. E., The rise of the Enterococcus: beyond vancomycin resistance. *Nat Rev Microbiol* **2012,** *10* (4), 266-78.

11. Schmitt, C. K.; Meysick, K. C.; O'Brien, A. D., Bacterial toxins: friends or foes? *Emerg Infect Dis* **1999,** *5* (2), 224-34.

12. Marks, J. D., Medical aspects of biologic toxins. *Anesthesiol Clin North America* **2004,** *22* (3), 509-32, vii.

13. Middlebrook, J. L.; Dorland, R. B., Bacterial toxins: cellular mechanisms of action. *Microbiol Rev* **1984,** *48* (3), 199-221.

14. Morgan, M., Treatment of MRSA soft tissue infections: an overview. *Injury* **2011,** *42 Suppl 5*, S11-7.

15. Zhao, Q. J.; Xie, J. P., Mycobacterium tuberculosis proteases and implications for new antibiotics against tuberculosis. *Crit Rev Eukaryot Gene Expr* **2011,** *21* (4), 347-61.

16. Lo Vecchio, A.; Zacur, G. M., Clostridium difficile infection: an update on epidemiology, risk factors, and therapeutic options. *Curr Opin Gastroenterol* **2011,** *28* (1), 1-9.

17. Beierlein, J. M.; Anderson, A. C., New developments in vaccines, inhibitors of anthrax toxins, and antibiotic therapeutics for Bacillus anthracis. *Curr Med Chem* **2011,** *18* (33), 5083-94.

18. Ter Meulen, J., Monoclonal antibodies in infectious diseases: clinical pipeline in 2011. *Infect Dis Clin North Am* **2011,** *25* (4), 789-802.

19. Chitlaru, T.; Altboum, Z.; Reuveny, S.; Shafferman, A., Progress and novel strategies in vaccine development and treatment of anthrax. *Immunol Rev* **2011,** *239* (1), 221-36.

20. Kobayashi, S. D.; Malachowa, N.; Whitney, A. R.; Braughton, K. R.; Gardner, D. J.; Long, D.; Bubeck Wardenburg, J.; Schneewind, O.; Otto, M.; Deleo, F. R., Comparative analysis of USA300 virulence determinants in a rabbit model of skin and soft tissue infection. *J Infect Dis* **2011,** *204* (6), 937-41.

21. Wahome, P. G.; Robertus, J. D.; Mantis, N. J., Small-molecule inhibitors of ricin and Shiga toxins. *Curr Top Microbiol Immunol* **2012,** *357*, 179-207.

22. Mabry, R.; Brasky, K.; Geiger, R.; Carrion, R., Jr.; Hubbard, G. B.; Leppla, S.; Patterson, J. L.; Georgiou, G.; Iverson, B. L., Detection of anthrax toxin in the serum of animals infected with Bacillus anthracis by using engineered immunoassays. *Clin Vaccine Immunol* **2006,** *13* (6), 671-7.

23. Rucker, V. C.; Havenstrite, K. L.; Herr, A. E., Antibody microarrays for native toxin detection. *Anal Biochem* **2005,** *339* (2), 262-70.

24. Homola, J.; Dostalek, J.; Chen, S.; Rasooly, A.; Jiang, S.; Yee, S. S., Spectral surface plasmon resonance biosensor for detection of staphylococcal enterotoxin B in milk. *Int J Food Microbiol* **2002,** *75* (1-2), 61-9.

25. Ezzell, J. W., Jr.; Abshire, T. G., Serum protease cleavage of Bacillus anthracis protective antigen. *J Gen Microbiol* **1992,** *138* (3), 543-9.

26. Medina, M. B., Development of a fluorescent latex microparticle immunoassay for the detection of staphylococcal enterotoxin B (SEB). *J Agric Food Chem* **2006,** *54* (14), 4937-42.

27. Carol, J.; Gorseling, M. C.; de Jong, C. F.; Lingeman, H.; Kientz, C. E.; van Baar, B. L.; Irth, H., Determination of denaturated proteins and biotoxins by on-line size-

exclusion chromatography-digestion-liquid chromatography-electrospray mass spectrometry. *Anal Biochem* **2005,** *346* (1), 150-7.

28. Kawano, Y.; Ito, Y.; Yamakawa, Y.; Yamashino, T.; Horii, T.; Hasegawa, T.; Ohta, M., Rapid isolation and identification of staphylococcal exoproteins by reverse phase capillary high performance liquid chromatography-electrospray ionization mass spectrometry. *FEMS Microbiol Lett* **2000,** *189* (1), 103-8.

29. Pierotti, M. A.; Lombardo, C.; Rosano, C., Nanotechnology: going small for a giant leap in cancer diagnostics and therapeutics. *Tumori* **2008,** *94* (2), 191-6.

30. Kaittanis, C.; Santra, S.; Perez, J. M., Emerging nanotechnology-based strategies for the identification of microbial pathogenesis. *Adv Drug Deliv Rev* **2010,** *62* (4-5), 408-23.

31. Rosi, N. L.; Mirkin, C. A., Nanostructures in biodiagnostics. *Chem Rev* **2005,** *105* (4), 1547-62.

32. Thaxton, C. S.; Georganopoulou, D. G.; Mirkin, C. A., Gold nanoparticle probes for the detection of nucleic acid targets. *Clin Chim Acta* **2006,** *363* (1-2), 120-6.

33. Byers, R. J.; Hitchman, E. R., Quantum dots brighten biological imaging. *Prog Histochem Cytochem* **2011,** *45* (4), 201-37.

34. Santra, S.; Kaittanis, C.; Perez, J. M., Aliphatic hyperbranched polyester: a new building block in the construction of multifunctional nanoparticles and nanocomposites. *Langmuir* **2010,** *26* (8), 5364-73.

35. Jain, K. K., Nanotechnology in clinical laboratory diagnostics. *Clin Chim Acta* **2005,** *358* (1-2), 37-54.

36. Perez, J. M.; Josephson, L.; O'Loughlin, T.; Hogemann, D.; Weissleder, R., Magnetic relaxation switches capable of sensing molecular interactions. *Nat Biotechnol* **2002,** *20* (8), 816-20.

37. Santra, S.; Kaittanis, C.; Grimm, J.; Perez, J. M., Drug/dye-loaded, multifunctional iron oxide nanoparticles for combined targeted cancer therapy and dual optical/magnetic resonance imaging. *Small* **2009,** *5* (16), 1862-8.

38. Kaittanis, C.; Santra, S.; Perez, J. M., Role of nanoparticle valency in the nondestructive magnetic-relaxation-mediated detection and magnetic isolation of cells in complex media. *J Am Chem Soc* **2009,** *131* (35), 12780-91.

39. Kaittanis, C.; Santra, S.; Santiesteban, O. J.; Henderson, T. J.; Perez, J. M., The assembly state between magnetic nanosensors and their targets orchestrates their magnetic relaxation response. *J Am Chem Soc* **2011,** *133* (10), 3668-76.

40. Kaittanis, C.; Banerjee, T.; Santra, S.; Santiesteban, O. J.; Teter, K.; Perez, J. M., Identification of molecular-mimicry-based ligands for cholera diagnostics using magnetic relaxation. *Bioconjug Chem* **2011,** *22* (2), 307-14.

41. Thompson, L. A.; Ellman, J. A., Synthesis and Applications of Small Molecule Libraries. *Chem Rev* **1996,** *96* (1), 555-600.

42. Bannwarth, L.; Goldberg, A. B.; Chen, C.; Turk, B. E., Identification of exosite-targeting inhibitors of anthrax lethal factor by high-throughput screening. *Chem Biol* **2012,** *19* (7), 875-82.

43. Wei, D.; Bu, Z.; Yu, A.; Li, F., Identification of a lead small-molecule inhibitor of anthrax lethal toxin by using fluorescence-based high-throughput screening. *BMB Rep* **2011,** *44* (12), 811-5.

44. Wilson, W. D., Tech.Sight. Analyzing biomolecular interactions. *Science* **2002,** *295* (5562), 2103-5.

45. Bornhop, D. J.; Latham, J. C.; Kussrow, A.; Markov, D. A.; Jones, R. D.; Sorensen, H. S., Free-solution, label-free molecular interactions studied by back-scattering interferometry. *Science* **2007,** *317* (5845), 1732-6.

46. Gaster, R. S.; Xu, L.; Han, S. J.; Wilson, R. J.; Hall, D. A.; Osterfeld, S. J.; Yu, H.; Wang, S. X., Quantification of protein interactions and solution transport using high-density GMR sensor arrays. *Nat Nanotechnol* **2011,** *6* (5), 314-20.

47. Mammen, M.; Choi, S. K.; Whitesides, G. M., Polyvalent interactions in biological systems: Implications for design and use of multivalent ligands and inhibitors. *Angewandte Chemie-International Edition* **1998,** *37* (20), 2755-2794.

48. MacBeath, G.; Schreiber, S. L., Printing proteins as microarrays for high-throughput function determination. *Science* **2000,** *289* (5485), 1760-1763.

49. Hulme, E. C.; Trevethick, M. A., Ligand binding assays at equilibrium: validation and interpretation. *Br J Pharmacol* **2010,** *161* (6), 1219-37.

50. Ladbury, J. E., Calorimetry as a tool for understanding biomolecular interactions and an aid to drug design. *Biochem Soc Trans* **2010,** *38* (4), 888-93.

51. Perozzo, R.; Folkers, G.; Scapozza, L., Thermodynamics of protein-ligand interactions: history, presence, and future aspects. *J Recept Signal Transduct Res* **2004,** *24* (1-2), 1-52.

52. Frey, K. A.; Albin, R. L., Receptor binding techniques. *Curr Protoc Neurosci* **2001,** *Chapter 1*, Unit1 4.

53. Crayton, S. H.; Tsourkas, A., pH-Titratable Superparamagnetic Iron Oxide for Improved Nanoparticle Accumulation in Acidic Tumor Microenvironments. *ACS Nano* **2011,** *5* (12), 9592-601.

54. Thorek, D. L.; Weisshaar, C. L.; Czupryna, J. C.; Winkelstein, B. A.; Tsourkas, A., Superparamagnetic iron oxide-enhanced magnetic resonance imaging of neuroinflammation in a rat model of radicular pain. *Mol Imaging* **2011,** *10* (3), 206-14.

55. Livnah, O.; Bayer, E. A.; Wilchek, M.; Sussman, J. L., Three-dimensional structures of avidin and the avidin-biotin complex. *Proc Natl Acad Sci U S A* **1993,** *90* (11), 5076-80.

56. Li, H.; Zhou, D.; Browne, H.; Balasubramanian, S.; Klenerman, D., Molecule by molecule direct and quantitative counting of antibody-protein complexes in solution. *Anal Chem* **2004,** *76* (15), 4446-51.

57. Akerstrom, B.; Bjorck, L., A physicochemical study of protein G, a molecule with unique immunoglobulin G-binding properties. *J Biol Chem* **1986,** *261* (22), 10240-7.

58. Liang, F.; Pan, T.; Sevick-Muraca, E. M., Measurements of FRET in a glucose-sensitive affinity system with frequency-domain lifetime spectroscopy. *Photochem Photobiol* **2005,** *81* (6), 1386-94.

59. Russell, R. B.; Eggleston, D. S., New roles for structure in biology and drug discovery. *Nat Struct Biol* **2000,** *7 Suppl*, 928-30.

60. Grisshammer, R.; Buchanan, S. K., *Structural Biology of Membrane Proteins*. RSC Publishing: 2006.

61. White, S. H., Biophysical dissection of membrane proteins. *Nature* **2009,** *459* (7245), 344-6.

62. Ebel, W.; Routhier, E. L.; Foley, B.; Jacob, S.; McDonough, J. M.; Patel, R. K.; Turchin, H. A.; Chao, Q.; Kline, J. B.; Old, L. J.; Phillips, M. D.; Nicolaides, N. C.; Sass, P. M.; Grasso, L., Preclinical evaluation of MORAb-003, a humanized monoclonal antibody antagonizing folate receptor-alpha. *Cancer Immun* **2007,** *7*, 6.

63. Ruf, P.; Gires, O.; Jager, M.; Fellinger, K.; Atz, J.; Lindhofer, H., Characterisation of the new EpCAM-specific antibody HO-3: implications for trifunctional antibody immunotherapy of cancer. *Br J Cancer* **2007,** *97* (3), 315-21.

64. Wang, X.; Shen, F.; Freisheim, J. H.; Gentry, L. E.; Ratnam, M., Differential stereospecificities and affinities of folate receptor isoforms for folate compounds and antifolates. *Biochem Pharmacol* **1992,** *44* (9), 1898-901.

65. Parker, N.; Turk, M. J.; Westrick, E.; Lewis, J. D.; Low, P. S.; Leamon, C. P., Folate receptor expression in carcinomas and normal tissues determined by a quantitative radioligand binding assay. *Anal Biochem* **2005,** *338* (2), 284-93.

66. Sudimack, J.; Lee, R. J., Targeted drug delivery via the folate receptor. *Adv Drug Deliv Rev* **2000,** *41* (2), 147-62.

67. Cosman, M.; Lightstone, F. C.; Krishnan, V. V.; Zeller, L.; Prieto, M. C.; Roe, D. C.; Balhorn, R., Identification of novel small molecules that bind to two different sites on the surface of tetanus toxin C fragment. *Chem Res Toxicol* **2002,** *15* (10), 1218-28.

68. Lightstone, F. C.; Prieto, M. C.; Singh, A. K.; Piqueras, M. C.; Whittal, R. M.; Knapp, M. S.; Balhorn, R.; Roe, D. C., Identification of novel small molecule ligands that bind to tetanus toxin. *Chem Res Toxicol* **2000,** *13* (5), 356-62.

69. Tsai, C. S.; Yu, T. B.; Chen, C. T., Gold nanoparticle-based competitive colorimetric assay for detection of protein-protein interactions. *Chem Commun (Camb)* **2005,** (34), 4273-5.

70. Watanabe, S.; Yoshida, K.; Shinkawa, K.; Kumagawa, D.; Seguchi, H., Thioglucose-stabilized gold nanoparticles as a novel platform for colorimetric bioassay based on nanoparticle aggregation. *Colloids Surf B Biointerfaces* **2010,** *81* (2), 570-7.

71. Nordmann, B. D., Issues in biosecurity and biosafety. *Int J Antimicrob Agents* **2010,** *36 Suppl 1*, S66-9.

72. Jernigan, J. A.; Stephens, D. S.; Ashford, D. A.; Omenaca, C.; Topiel, M. S.; Galbraith, M.; Tapper, M.; Fisk, T. L.; Zaki, S.; Popovic, T.; Meyer, R. F.; Quinn, C. P.; Harper, S. A.; Fridkin, S. K.; Sejvar, J. J.; Shepard, C. W.; McConnell, M.; Guarner, J.; Shieh, W. J.; Malecki, J. M.; Gerberding, J. L.; Hughes, J. M.; Perkins, B. A., Bioterrorism-related inhalational anthrax: the first 10 cases reported in the United States. *Emerg Infect Dis* **2001,** *7* (6), 933-44.

73. Bann, J. G., Anthrax toxin protective antigen--insights into molecular switching from prepore to pore. *Protein Sci* **2011,** *21* (1), 1-12.

74. Collier, R. J., Membrane translocation by anthrax toxin. *Mol Aspects Med* **2009,** *30* (6), 413-22.

75. Collier, R. J., Mechanism of membrane translocation by anthrax toxin: insertion and pore formation by protective antigen. *J Appl Microbiol* **1999,** *87* (2), 283.

76. CDC Fact Sheet: Anthrax Information for Health Care Providers. http://www.bt.cdc.gov/agent/anthrax/anthrax-hcp-factsheet.asp.

77. Irenge, L. M.; Gala, J. L., Rapid detection methods for Bacillus anthracis in environmental samples: a review. *Appl Microbiol Biotechnol* **2012,** *93* (4), 1411-22.

78. Bouzianas, D. G., Medical countermeasures to protect humans from anthrax bioterrorism. *Trends Microbiol* **2009,** *17* (11), 522-8.

79. Kaittanis, C.; Boukhriss, H.; Santra, S.; Naser, S. A.; Perez, J. M., Rapid and sensitive detection of an intracellular pathogen in human peripheral leukocytes with hybridizing magnetic relaxation nanosensors. *PLoS One* **2012,** *7* (4), e35326.

80. Kaittanis, C.; Nath, S.; Perez, J. M., Rapid nanoparticle-mediated monitoring of bacterial metabolic activity and assessment of antimicrobial susceptibility in blood with magnetic relaxation. *PLoS One* **2008,** *3* (9), e3253.

81. Panchal, R. G.; Hermone, A. R.; Nguyen, T. L.; Wong, T. Y.; Schwarzenbacher, R.; Schmidt, J.; Lane, D.; McGrath, C.; Turk, B. E.; Burnett, J.; Aman, M. J.; Little, S.; Sausville, E. A.; Zaharevitz, D. W.; Cantley, L. C.; Liddington, R. C.; Gussio, R.; Bavari, S., Identification of small molecule inhibitors of anthrax lethal factor. *Nat Struct Mol Biol* **2004,** *11* (1), 67-72.

82. Forino, M.; Johnson, S.; Wong, T. Y.; Rozanov, D. V.; Savinov, A. Y.; Li, W.; Fattorusso, R.; Becattini, B.; Orry, A. J.; Jung, D.; Abagyan, R. A.; Smith, J. W.; Alibek, K.; Liddington, R. C.; Strongin, A. Y.; Pellecchia, M., Efficient synthetic inhibitors of anthrax lethal factor. *Proc Natl Acad Sci U S A* **2005,** *102* (27), 9499-504.

83. Young, J. A.; Collier, R. J., Anthrax toxin: receptor binding, internalization, pore formation, and translocation. *Annu Rev Biochem* **2007,** *76*, 243-65.

84. Alileche, A.; Squires, R. C.; Muehlbauer, S. M.; Lisanti, M. P.; Brojatsch, J., Mitochondrial impairment is a critical event in anthrax lethal toxin-induced cytolysis of murine macrophages. *Cell Cycle* **2006,** *5* (1), 100-6.

85. Alileche, A.; Serfass, E. R.; Muehlbauer, S. M.; Porcelli, S. A.; Brojatsch, J., Anthrax lethal toxin-mediated killing of human and murine dendritic cells impairs the adaptive immune response. *PLoS Pathog* **2005,** *1* (2), e19.

86. Pannifer, A. D.; Wong, T. Y.; Schwarzenbacher, R.; Renatus, M.; Petosa, C.; Bienkowska, J.; Lacy, D. B.; Collier, R. J.; Park, S.; Leppla, S. H.; Hanna, P.; Liddington, R. C., Crystal structure of the anthrax lethal factor. *Nature* **2001,** *414* (6860), 229-33.

87. Nguyen, T. L., Three-dimensional model of the pore form of anthrax protective antigen. Structure and biological implications. *J Biomol Struct Dyn* **2004,** *22* (3), 253-65.

88. Yuriev, E.; Agostino, M.; Ramsland, P. A., Challenges and advances in computational docking: 2009 in review. *J Mol Recognit* **2011,** *24* (2), 149-64.

89. Morris, G. M.; Huey, R.; Lindstrom, W.; Sanner, M. F.; Belew, R. K.; Goodsell, D. S.; Olson, A. J., AutoDock4 and AutoDockTools4: Automated docking with selective receptor flexibility. *J Comput Chem* **2009,** *30* (16), 2785-91.

90. Morris, G. M.; Goodsell, D. S.; Halliday, R. S.; Huey, R.; Hart, W. E.; Belew, R. K.; Olson, A. J., Automated docking using a Lamarckian genetic algorithm and an

empirical binding free energy function. *Journal of Computational Chemistry* **1998,** *19* (14), 1639-1662.

91. Schames, J. R.; Henchman, R. H.; Siegel, J. S.; Sotriffer, C. A.; Ni, H.; McCammon, J. A., Discovery of a novel binding trench in HIV integrase. *J Med Chem* **2004,** *47* (8), 1879-81.

92. Mattila, J.; Mantyla, R.; Vuorela, A.; Lamminsivu, U.; Mannisto, P., Pharmacokinetics of graded oral doses of sulindac in man. *Arzneimittelforschung* **1984,** *34* (2), 226-9.

93. Reddy, B. S.; Kawamori, T.; Lubet, R. A.; Steele, V. E.; Kelloff, G. J.; Rao, C. V., Chemopreventive efficacy of sulindac sulfone against colon cancer depends on time of administration during carcinogenic process. *Cancer Res* **1999,** *59* (14), 3387-91.

94. Duggan, D. E.; Hooke, K. F.; Risley, E. A.; Shen, T. Y.; Arman, C. G., Identification of the biologically active form of sulindac. *J Pharmacol Exp Ther* **1977,** *201* (1), 8-13.

95. Piazza, G. A.; Alberts, D. S.; Hixson, L. J.; Paranka, N. S.; Li, H.; Finn, T.; Bogert, C.; Guillen, J. M.; Brendel, K.; Gross, P. H.; Sperl, G.; Ritchie, J.; Burt, R. W.; Ellsworth, L.; Ahnen, D. J.; Pamukcu, R., Sulindac sulfone inhibits azoxymethane-induced colon carcinogenesis in rats without reducing prostaglandin levels. *Cancer Res* **1997,** *57* (14), 2909-15.

96. Hucker, H. B.; Stauffer, S. C.; White, S. D.; Rhodes, R. E.; Arison, B. H.; Umbenhauer, E. R.; Bower, R. J.; McMahon, F. G., Physiologic disposition and metabolic fate of a new anti-inflammatory agent, cis-5-fluro-2-methyl-1-(p-(methylsulfinyl)-benzylidenyl)-indene-3-acetic acid in the rat, dog, rhesus monkey, and man. *Drug Metab Dispos* **1973,** *1* (6), 721-36.

97. Johnson, S. L.; Chen, L. H.; Barile, E.; Emdadi, A.; Sabet, M.; Yuan, H.; Wei, J.; Guiney, D.; Pellecchia, M., Structure-activity relationship studies of a novel series of anthrax lethal factor inhibitors. *Bioorg Med Chem* **2009,** *17* (9), 3352-68.

98. Moayeri, M.; Leppla, S. H., Cellular and systemic effects of anthrax lethal toxin and edema toxin. *Mol Aspects Med* **2009,** *30* (6), 439-55.

99. Pellizzari, R.; Guidi-Rontani, C.; Vitale, G.; Mock, M.; Montecucco, C., Anthrax lethal factor cleaves MKK3 in macrophages and inhibits the LPS/IFNgamma-induced release of NO and TNFalpha. *FEBS Lett* **1999,** *462* (1-2), 199-204.

100. Vitale, G.; Bernardi, L.; Napolitani, G.; Mock, M.; Montecucco, C., Susceptibility of mitogen-activated protein kinase kinase family members to proteolysis by anthrax lethal factor. *Biochem J* **2000,** *352 Pt 3*, 739-45.

101. Turk, B. E.; Wong, T. Y.; Schwarzenbacher, R.; Jarrell, E. T.; Leppla, S. H.; Collier, R. J.; Liddington, R. C.; Cantley, L. C., The structural basis for substrate and inhibitor selectivity of the anthrax lethal factor. *Nat Struct Mol Biol* **2004,** *11* (1), 60-6.

102. Agrawal, A.; Lingappa, J.; Leppla, S. H.; Agrawal, S.; Jabbar, A.; Quinn, C.; Pulendran, B., Impairment of dendritic cells and adaptive immunity by anthrax lethal toxin. *Nature* **2003,** *424* (6946), 329-34.

103. Levinsohn, J. L.; Newman, Z. L.; Hellmich, K. A.; Fattah, R.; Getz, M. A.; Liu, S.; Sastalla, I.; Leppla, S. H.; Moayeri, M., Anthrax lethal factor cleavage of Nlrp1 is required for activation of the inflammasome. *PLoS Pathog* **2012,** *8* (3), e1002638.

104. Moayeri, M.; Sastalla, I.; Leppla, S. H., Anthrax and the inflammasome. *Microbes Infect* **2012,** *14* (5), 392-400.

105. Moayeri, M.; Crown, D.; Newman, Z. L.; Okugawa, S.; Eckhaus, M.; Cataisson, C.; Liu, S.; Sastalla, I.; Leppla, S. H., Inflammasome sensor Nlrp1b-dependent resistance to anthrax is mediated by caspase-1, IL-1 signaling and neutrophil recruitment. *PLoS Pathog* **2012,** *6* (12), e1001222.

106. Newman, Z. L.; Crown, D.; Leppla, S. H.; Moayeri, M., Anthrax lethal toxin activates the inflammasome in sensitive rat macrophages. *Biochem Biophys Res Commun* **2010,** *398* (4), 785-9.

107. Tonello, F.; Seveso, M.; Marin, O.; Mock, M.; Montecucco, C., Screening inhibitors of anthrax lethal factor. *Nature* **2002,** *418* (6896), 386.